

**Selected problems in Earth
and related environmental sciences
2022**

Editors:

**Magdalena Mieloszyk
Sławomir Sagan**

Gdańsk 2024

Pod redakcją/ Editors:

dr hab. inż. Magdalena Mieloszyk, prof. IMP PAN

dr hab. Sławomir Sagan, prof. IO PAN

Projekt okładki:

Mirosław Sawczak

Skład komputerowy LaTeX, łamanie, adjustacja:

Paweł Kudela, Katarzyna Majewska, Magdalena Mieloszyk

© Copyright by Instytut Maszyn Przepływowych
im. Roberta Szwalskiego PAN, Gdańsk 2024, Wydanie I

All Rights Reserved. Wszelkie prawa zastrzeżone.

Żadna część niniejszej publikacji nie może być reprodukowana ani rozpowszechniana bez pisemnej zgody posiadacza praw autorskich.

ISBN 978-83-66928-10-7



WYDAWNICTWO INSTYTUTU MASZYN PRZEPŁYWOWYCH PAN

Instytut Maszyn Przepływowych im. Roberta Szwalskiego

Polskiej Akademii Nauk

ul. Fiszera 14, 80-231 Gdańsk

tel. (+48) 58-52-25-141; fax (+48) 58-341-61-44

e-mail: redakcja@imp.gda.pl <https://www.imp.gda.pl/wydawnictwo>

Recenzenci monografii/ Reviewers of the monograph:

*Instytut Geofizyki Polskiej Akademii Nauk/
Institute of Geophysics, Polish Academy of Sciences*
dr hab. Mateusz Moskalik, prof. IGF PAN

*Instytut Oceanologii Polskiej Akademii Nauk/
Institute of Oceanology, Polish Academy of Sciences*
prof. dr hab. Zygmunt Klusek
prof. dr hab. Piotr Kuklinski
prof. dr hab. Ksenia Pazdro
dr hab. Karol Kuliński, prof. IO PAN
dr Piotr Bałazy
dr Agnieszka Beszczyńska-Möller

Politechnika Gdańska/ Gdańsk University of Technology
dr hab. inż. Marek Moszyński, prof. PG

Uniwersytet Gdański/ University of Gdańsk
dr hab. Adam Sokołowski, prof. UG
dr hab. Agata Weydmann-Zwolicka, prof. UG

Uniwersytet Warszawski/ University of Warsaw
dr hab. Zofia Dubicka, prof. UW

Contents

Przedmowa	vii
Preface	ix
1 The proxy tools to determine the paleoproductivity in the marine environment: An overview	1
DHANUSHKA DEVENDRA	
1.1 Introduction	2
1.2 Paleoproductivity proxies and their applications . . .	4
1.2.1 Organic geochemistry	5
1.2.2 Phytoplankton derived alkenones	8
1.2.3 Foraminifera	9
1.2.4 Foraminiferal geochemistry: Stable carbon isotope ($\delta^{13}\text{C}$)	11
1.3 Summary	13
2 The application of underwater optical imagery for a long-term experiment in Arctic coastal shallows – A comparison of technical specifications, settings and outputs	23
BERNABÉ MORENO	
2.1 Introduction	24
2.2 Scientific and technical background	25
2.2.1 Studying change in marine benthic assemblages	25
2.2.2 Parameters when using underwater photography as a tool for ecological research	25

2.3	Methodical considerations	29
2.3.1	Experimental design	29
2.3.2	Underwater optical imagery	30
2.3.3	Image acquisition	32
2.3.4	Image processing pipeline	32
2.3.5	Image analysis pipeline	38
2.4	Summary	41
3	Ancient environmental genomics: An introduction	48
	NGOC-LOI NGUYEN	
3.1	Introduction	49
3.2	Ancient <i>e</i> DNA and environmental metagenomics	49
3.3	The problem of environmental ancient DNA	50
3.4	How to study ancient metagenomic	51
3.4.1	Metabarcoding and its limitations	53
3.4.2	Shotgun sequencing and Whole Genome Sequencing	54
3.4.3	Bioinformatics considerations	56
3.4.4	Applications of ancient environmental metagenomics	57
3.5	Summary	58
4	The Arctic carbon cycle: Main factors and winter-summer variability	72
	KAMIL REGINIA	
4.1	Introduction	73
4.2	Characteristics of the Arctic Ocean	74
4.2.1	Water circulation in the Arctic Ocean	77
4.3	The Carbon Cycle in the Arctic	80
4.4	Differences between the winter and summer seasons of the selected factors in the carbon cycle	86
4.5	Conclusion	91

5 The seasonal variations in the thermohaline structure of the Arctic Fjords in a changing climate: A comparison between Kongsfjorden, Isfjorden and Hornsund **104**

PAVANI VITHANA MADUGETA VIDANAMESTRIGE

5.1	Introduction	105
5.2	Locations and characteristic features of fjords	106
5.2.1	Kongsfjorden	107
5.2.2	Isfjorden	108
5.2.3	Hornsund	109
5.2.4	Comparison of Kongsfjorden, Isfjorden and Hornsund	111
5.3	Seasonal trends in the thermohaline structure of the Arctic fjords	112
5.3.1	Internal and external factors affecting the ther- mohaline structure	112
5.3.2	Characteristic features of the thermohaline structure of the West Spitsbergen Fjords	114
5.3.3	Comparison of seasonal variations of the ther- mohaline structure in Kongsfjorden, Isfjorden and Hornsund	124
5.4	Kongsfjorden, Isfjorden and Hornsund in a warming climate: current observation and future perspectives	125

6 The behaviour of fish (*Baltic herring*) with particular emphasis on spatial orientation in various conditions **134**

ALEKSANDER ŻYTKO

6.1	Introduction	135
6.2	Herring swimming patterns and buoyancy	136
6.3	Diel variation	138
6.3.1	Schooling behaviour during day – impact on fish orientation	138
6.3.2	Night-time shoaling behaviour – impact on fish orientation	139
6.3.3	Diel vertical migration	140

6.4	Diel variation in behaviour – measurements of herring orientation angles	140
6.4.1	Research methodologies	140
6.4.2	Measuring tilt angles – results	141
6.5	Disturbances in fish behaviour	145
6.5.1	Predator avoidance behaviour	145
6.5.2	Vessel avoidance	145
6.6	Vessel avoidance – measurements of herring orientation angles	148
6.6.1	Research methodologies	148
6.6.2	Measuring tilt angles – results	149
6.7	Discussion	150
6.7.1	Comparison of various methodologies for measuring fish orientation	150
6.7.2	Fish orientation and their behaviour – comparison	152

Przedmowa

W 2019 roku została utworzona Trójmiejska Szkoła Doktorska Polskiej Akademii Nauk (TSD PAN) prowadzona wspólnie przez:

- Instytut Maszyn Przepływowych PAN (IMP PAN),
- Instytut Budownictwa Wodnego PAN (IBW PAN),
- Instytut Oceanologii PAN (IO PAN).

Szkoła Doktorska oferuje kształcenie w ramach trzech dyscyplin: inżynierii mechanicznej, inżynierii lądowej, geodezji i transportu oraz nauki o Ziemi i środowisku.

Mam ogromną przyjemność przedstawić Państwu monografię będącą podsumowaniem aktywności naukowej kolejnego roku działalności TSD PAN zawierającą prace naukowe zaproponowane przez doktorantów Szkoły Doktorskiej.

Niniejsza monografia zawiera zbiór prac z dyscypliny nauki o Ziemi i środowisku. Ich krótkie podsumowanie doktoranci TSD PAN zaprezentowali w ramach *III Seminarium Naukowego TSD PAN*, które odbyło się w dniach 13-14 czerwca 2022 r. Wydarzenie to jest kontynuacją cyklu corocznych otwartych seminariów naukowych, na których doktoranci Szkoły Doktorskiej prezentują swoje osiągnięcia naukowe.

dr hab. inż. Magdalena Mieloszyk, profesor IMP PAN
Dyrektor TSD PAN

Preface

In 2019 the Tricity Doctoral School of the Polish Academy of Sciences (TSD PAN) was established, which is run jointly by:

- Institute of Fluid-Flow Machinery PAS (IMP PAN),
- Institute of Hydro-Engineering PAS (IBW PAN),
- Institute of Oceanology PAS (IO PAN).

The Doctoral School offers education in three disciplines: mechanical engineering, civil engineering, geodesy and transport as well as Earth and environmental science.

It is my great pleasure to present you a monograph which is a summary of the next year of TSD PAN scientific activity, including scientific papers proposed by PhD students of the Doctoral School.

This monograph contains a collection of papers from the discipline of Earth and related environmental sciences. Their short summaries were presented by PhD students during the *3rd Scientific Seminar of TSD PAN*, which took place on June 13th-14th, 2022. This event is a continuation of a series of annual open scientific seminars where PhD students of the Doctoral School present their scientific achievements.

dr hab. inż. Magdalena Mieloszyk, profesor IMP PAN
Director of TSD PAN,

Chapter 1

The proxy tools to determine the paleoproductivity in the marine environment: An overview

DHANUSHKA DEVENDRA

Institute of Oceanology, Polish Academy of Sciences,
Powstańców Warszawy 55, 81-712 Sopot, Poland

1.1 Introduction

A firm knowledge of how current ecosystems have evolved and their long-term natural variability is necessary to comprehend our current environment better and forecast future changes. In order to achieve this, we'll need to rely on environmental archives like marine sediments, which store paleoenvironmental information in the form of physical, chemical, and biological proxy records. A large number of analytical methods have been developed last few decades, providing further insight to achieve these records. Despite the many methods, further development of proxies and their analytical methods is still required to obtain a detailed understanding of paleoenvironmental changes. This is especially true for the newly developing proxies such as ancient sedimentary DNA [1, 2] and also for classical microfossil proxies, where the ecological preferences of some individual species are still unknown [3, 4].

Paleoproductivity is a prominent topic of paleoceanographic studies because it accurately traces the significant variations of ancient ocean circulation, and nutrient distributions, as well as the history of the oceanic carbon cycle and carbon burial. The modifications of ocean circulation resulted in a change in the vertical burst of carbon and nutrients and caused a limitation of primary productivity in both the surface waters and the deep ocean [5–7]. As the deep ocean is the largest reservoir of CO_2 , variations in ocean circulation and changes in primary productivity lead to an imbalance in atmospheric CO_2 concentration on the glacial/interglacial time scale [8].

Organic productivity is a critical determinant of ecological dynamics, environmental redox conditions, and the cycling of carbon, nitrogen, phosphorus, and other nutrient components in all marine environments. Single-celled phytoplankton is the dominant primary producer in the modern open ocean in the uppermost mixed layer. Several modern studies explained the complexity of the influx of organic matter from the surface organic production to the deep ocean which varies both seasonally and geographically [9–11]. The particle flux, also known as the biological pump, is a key player in the biogeochemical cycles of many elements, including carbon. It also serves as the primary food source for life in the ocean's interior

and, to some extent, regulates the ocean's uptake of atmospheric carbon dioxide and the spatial patterns of ocean primary productivity. Primary and export productivity may be high in places with intense vertical mixing. However, biological pumping to sediments may be limited because microbial action and grazing lead to the remineralization of organic materials in the water column. The biological pump regulates the quantity of organic carbon that can be sequestered into sediments from the atmosphere-ocean system [12] (Fig. 1.1). The amount of organic matter that is available to be buried as organic carbon in the sediment is a function of the rate of production and bottom export, and further, the dominating type of microbial degradation and its duration relative to sediment burial rate. Furthermore, the organic matter has a relatively short retention time in the water column, and the relative proportion of output that is reaching the sediment surface is high. However, it is well known that about 10% of total surface productivity leaves the euphotic zone and is transported to the bottom sediments [13].

Subsequent studies used marine sediment cores to address past productivity changes in the oceans. Deep marine sediments contain various biological and geochemical proxies, which have been extensively used to reconstruct the paleoproductivity, including methods based on C and N isotopes, organic biomarkers, trace metal abundances, and indicator foraminifera species [13, 14] (Fig. 1.2). Though, a variety of environmental factors affect each proxy, including temperature, redox conditions, and ocean circulation, as well as elements that influence the composition of marine ecosystems [13]. Therefore, estimating paleoproductivity using various proxies is generally recommended.

Paleoproductivity in the Nordic Seas differs from the tropical and temperate regions. Nordic Seas are mostly colder, some parts covered with sea ice, which furthers the under-ice algae bloom development. It is also a frontal zone where Atlantic and Arctic water meet, and there is always a productivity hotspot at the border sites. The melting glacier (Greenland Ice Sheet now, e.g., Svalbard-Barents Ice Sheet in the geological past) and icebergs release nutrients (e.g., iron and phosphorus), boosting the surface water primary

production. This chapter provides a short review of reliable proxies to estimate past surface productivity, widely used in Nordic Seas during the last few decades.

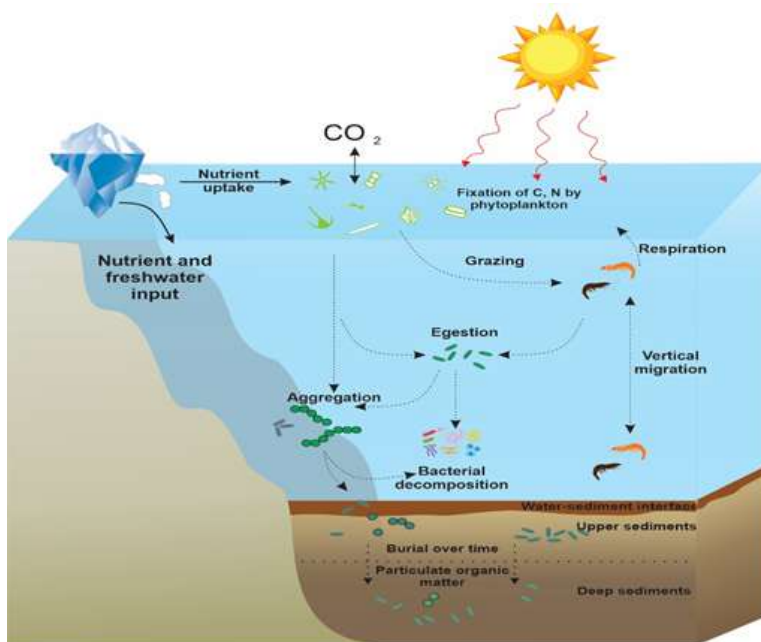


Fig. 1.1: Schematic illustration of the biological pump in the ocean water column. The pump moves organic carbon into deep water layers and buries the sediments from primary production.

1.2 Paleoproductivity proxies and their applications

Investigating components that reflect nutrient changes is a typical indirect method to reconstruct paleoproductivity. However, due to the difficulties of discovering primary producers that have decomposed throughout the depositional process, primary paleoproductivity can only be estimated using a few reliable proxies. Hence, we have focused on the following major proxies which are used to estimate paleoproductivity accurately in the Nordic Seas.

1.2.1 Organic geochemistry

Total Organic Carbon (TOC)

Organic carbon, the single most abundant component in organic matter, is the most direct indicator of productivity [15–17]. The majority of organic carbon in sediments comes from sinking organic material produced on the surface ocean, with a small amount of terrestrial organic carbon in some coastal marine environments [18]. However, in most marine environments, a huge amount of organic carbon is decomposed by bacterial activity (respiration), significantly reducing the amount of organic materials reaching the bottom [18, 19]. Canfield [16] and Müller and Suess [20] estimated that about 0.1% to 10% of surface production survived to be reached the sediment-water interface and was further lost by anaerobic respiration at the bottom.

TOC has been used in several presents and ancient marine sediment studies to reconstruct primary productivity [21–23]. Low TOC is regarded as a direct result of low paleoproductivity, whereas high TOC is thought to be associated with high paleoproductivity. The use of TOC as a paleoproductivity proxy depends on a predominantly marine supply of organic matter and favorable circumstances for sediment preservation. However, the TOC content of the sediments is a function of surface productivity, the preservation of organic carbon in the water column and sediments, and the dilution of organic carbon from biogenic materials within the sediments [16]. Because organic carbon is typically a small component of marine sediments and only a small fraction of primary production is preserved, small changes in organic carbon preservation can significantly impact the sediment's TOC concentration [24]. Even if surface water primary productivity is high, TOC in the sediment may be low due to aerobic bacterial respiration within the water column and oxygen-rich sediments [25].

Also, TOC accumulation rates are highly used to reconstruct the paleoproductivity. In many aerobic and anaerobic environments, TOC accumulation rates may be a better proxy to estimate primary productivity as it is more independent from sedimentation rates.

$$\begin{aligned}
 \text{TOC accumulation rate} &= \text{TOC content} \times \\
 &\times \text{Linear sedimentation rate} \times \text{Dry bulk sediment density}
 \end{aligned}
 \tag{1.1}$$

Barium (Barite and biogenic Barium)

In seawater residence time of the barium is relatively short (about 10 kyr). The profile of barium in seawater closely resembles that of silica. The river runoff is the principal source of Ba in the marine environment, and the primary sink of Ba in marine sediments is burial as barite (BaSO_4). Sinking organic materials transports a significant portion of the barite burial influx to the sediment-water interface, resulting in local Ba enrichment of the sediment. Dymond, Suess [26] used sediment trap data to show a strong correlation between Ba fluxes and organic carbon. Thus, this is referred to as biogenic barium, where the Ba is associated with sinking organic matter flux [26].

The significant correlation between the production of authigenic barite and the degradation of organic matter in contact with seawater, which is the source of biogenic Ba, is attributed to the utility of biogenic Ba as a productivity proxy [27]. The mineral barite is relatively resistant to dissolving and has a high burial efficiency under oxic to suboxic conditions, making it an ideal proxy for calculating export production in non-reducing paleoenvironment. Furthermore, even in reducing conditions where barite retention is comparatively low, the substantial flux of biogenic Ba to the sediment-water interface can serve as a useful paleoproductivity proxy. Therefore, barite and biogenic Ba have been extensively used to reconstruct the paleoproductivity for different periods, including the modern, Quaternary, Paleogene, and Cretaceous. However, the use of Ba as a proxy for paleoproductivity estimation has its limitations. Hydrothermal overprinting can affect Ba contents in sediments, leading to false paleoproductivity interpretations.

Organic phosphorus

Phosphorus is a structural and functional component of all organisms, making it essential for marine phytoplankton growth [28]. The majority of phosphorus in marine sediments comes from organic materials, while detrital phosphorus (terrigenous) accounts for around 20% of total phosphorus [29]. Phosphorus burial records in marine sediments have been used in many studies as direct indications of paleoproductivity and climatic implications through the nutrient and CO₂ relationship. In the modern oxygenated Ocean, a large fraction of burial organic phosphorus to sediment is remineralized. A considerable fraction of both organic and element-bound phosphorus is released to sediment pore waters, the majority of which diffuses back into the water column [30].

The phosphorus accumulation rate has been used as an excellent proxy to reconstruct the paleo export productivity and organic carbon burial into the sediment [31] (Fig. 2). Many studies have also discovered that the rate of phosphorus accumulation in modern oceans is closely related to underlying export productivity and organic carbon burial in newly deposited sediments [32].

In most upwelling regions, Sulfur-oxidizing bacteria utilize some of the pore water phosphorus under anoxic conditions, resulting in the formation of phosphorites. Therefore, phosphorites in the sediment record are associated with high organic carbon levels and have been connected to high-productivity areas like upwelling zones. However, on the other hand, physical sedimentary processes can produce and increase phosphorite availability in the sediments. Therefore, it has been suggested that for the paleoproductivity interpretations, phosphorus must be used with the other proxies to reconstruct paleoproductivity accurately. According to Szymczak-Żyła, Krajewska [33], phosphorus is one of the most reliable and extensively used productivity proxies.

Organic biomarkers

Biomarkers have been widely used to reconstruct paleoproductivity changes since they are produced by specific organisms and are well

preserved during sedimentation and early diagenesis [33]. The rate of accumulation of chloropigments, for example, has been employed as a molecular indication of overall [34]. This technique is based on the fact that chlorophyll-a, one of the photosynthesis pigments, is found in all photosynthetic organisms (aerobic) and is the most common chlorophyll type in the ecosystem. The pigment content in sediments is influenced by a variety of factors, including primary production, sedimentation, post-depositional processes, and pigment stability. Due to depletion during water column transformation and diagenesis within the sediment, less than 1% of chlorophyll production is generally preserved in marine sediments [35]. Hence, early consideration of chloropigments as a proxy to estimate paleoproductivity was narrow due to this uncertainty. However, some studies reveal that the pigment is an excellent proxy for reconstructing paleoproductivity, as pigment accumulation rates correlate well with productivity indicators [34]. Thus, chloropigments have been applied for reconstructing paleoproductivity [33, 36].

Lipid biomarker distributions in sediments can reveal important details about the origin and transport routes of organic matter OM as well as oceanographic conditions [37]. Depending on the nutrition levels of the surface waters, different phytoplankton groups contribute lipids to the primary produced OM [37]. Because of their strong resistance to degradation and diversity of molecular structures, sterols are an excellent lipid biomarker that might be used to detect organic matter sources [38]. In different marginal seas, the contents and quantities of certain sterols in sediment cores have been frequently employed to show temporal changes in paleoproductivity and phytoplankton community structure.

1.2.2 Phytoplankton derived alkenones

The efficiency of the biological pump was controlled by phytoplankton, which is a major contribution to marine primary productivity. Alkenones are formed from the Prymnesiophyceae class of marine phytoplankton; in cold, polar seas, they are only found in the coccolithophorid *Emiliania huxleyi* [39]. *E. huxleyi* adjusts the chemical composition of its cell membranes in response to changes in water

temperature. Because more of the C_{37:4} alkenone and less of the C_{37:2} are synthesized in colder temperatures, the percent C_{37:4} index can be used to qualitatively reconstruct the extent of the past Arctic Water mass. Furthermore, total C₃₇ alkenone concentration (measured as C₃₇ alkenone per gram in sediment) corresponds with other sea productivity indicators (e.g., TOC) and will be utilized as a qualitative proxy for reconstructing the marine paleoproductivity. The use of alkenones as paleoproductivity markers, like TOC and many other lipids and pigments, depends on the consistency of preservation conditions during the study period. Alkenones are useful indicators for this purpose because of their strong resistance to degradation compared to other lipids.

1.2.3 Foraminifera

Benthic foraminifera indicator species

Foraminifera are the most prevalent benthic microorganisms preserved in the fossil record, and they dominate present meiobenthic communities [40]. In the faunal pattern of benthic foraminifera, accurate information about environmental changes is recorded. Benthic foraminifera faunas have been extensively used to reconstruct environmental changes in the geological past [7, 41–43]. Despite the number of factors that influence the abundance and distribution of benthic foraminifera, the quality and quantity of organic matter, mainly originating from surface production, is considered a major factor. Because different benthic foraminifera species have different preferences for food availability (Tab. 1.1), their ecology is broadly used to reconstruct past productivity. As an example, Mackensen, Fu [44], and Lutze and Coulbourn [45] explained the term "high productive groups" of species observed in highly productive areas along the continental margins. Furthermore, because foraminiferal biomass is strongly tied to organic matter inputs from surface productivity, the overall abundance of benthic foraminifera can be applied to reconstruct paleoproductivity [46].

Tab. 1.1: The distinctive species assemblages are typically found in areas with different conditions of organic matter (OM) inputs.

Species	OM preferences	Reference
<i>Bulimina aculeata</i>	Limited input of phytodetritus, an intermittent flux of organic carbon	[47]
<i>Cassidulina laevigata</i>	High organic matter input	[48]
<i>Cibicidoides wuellerstorfi</i>	A reduced flux of organic matter to the ocean bottom	[44, 49, 50]
<i>Melonis barleeanum</i>	Adapted to degraded organic matter	[51, 52]
<i>Alabaminella weddellensis</i>	More continuous aggregates of phytodetritus input	[53]
<i>Epistominella exigua</i>	More continuous aggregates of phytodetritus input	[53]
<i>Uvigerina peregrina</i>	The continuous flux of organic carbon; High surface productivity	[45]
<i>Nonionellina labradorica</i>	Known to feed on fresh phytodetritus and is indicative of high-productivity environments	[54, 55]
<i>Islandiella spp.</i>	High surface productivity at oceanographic fronts	[56]
<i>Cassidulina reniforme</i>	High surface productivity at oceanographic fronts	[56]

Benthic foraminifera accumulation rate (BFAR)

BFAR has been used as a reliable proxy for estimating past carbon fluxes (export productivity) to the seafloor from surface production [57–59]. Organic compounds produced in the photic zone and exported to the sediments are consumed by benthic foraminifera on the bottom. In sediments deposited above the lysocline, the number of benthic foraminifera produced per unit of space and time depends on the water depth and the supply of organic carbon [60].

Planktic foraminifera and calcareous fossils dissolve at depths below the carbonate compensation depth, benthic foraminiferal counts per gram of bulk sediment increase, and benthic foraminifera become relatively abundant. Moreover, carbonate compensation depth in most oceans is over 5000 m [61], and most benthic calcareous foraminifera dissolution is excluded. The use of BFAR as a productivity proxy is based on the concept that the availability of organic carbon influences the quantity of benthic foraminifera generated per unit area and unit time to the seafloor and organic carbon is a reflection of photic zone production [62].

BFAR [$\text{N}/(\text{cm}^2 \cdot \text{yr})$] can be calculated for counted samples using benthic foraminifera number (BFN) [N/g], linear sedimentation rate (LSR) [cm/yr], and dry bulk density (DBD) [g/cm^3].

$$BFAR = BFN * LSR * DBD \quad (1.2)$$

Planktonic foraminifera

Some planktonic foraminiferal species have been identified mainly in high-productivity areas, but others avoid or cannot thrive in bloom environments. Some species have been identified as high productivity indicators [63, 64]. In higher latitudes, left-coiling *Neogloboquadrina pachyderma* indicates productive upwelling cold water [65]. In low latitudes, common productivity indicator species include *Neogloboquadrina dutertrei*, *Globigerina bulloides*, and *Globorotalia tumida*, while *Turborotalita quinqueloba* indicates high productivity in temperate latitudes. Thus, the percentage abundance of productivity-indicating species provides insight into variations in surface productivity changes at the time of sedimentation.

1.2.4 Foraminiferal geochemistry: Stable carbon isotope ($\delta^{13}\text{C}$)

Carbon, which exists in two stable forms, ^{12}C and ^{13}C , is essential for all life on Earth. The carbon isotope ratio ($^{13}\text{C}/^{12}\text{C}$) of foraminifera tests is defined as $\delta^{13}\text{C}$ in ‰ PDB units. The $\delta^{13}\text{C}$ in the water is controlled by a complex process of CO_2 exchange with the atmosphere, removal of carbon in solids by primary production, and resupply to the water by degradation and decomposition at the subsurface and bottom waters. Photosynthesis removes the ^{12}C by converting it to organic carbon, and ^{13}C tends to be left behind. Thus, during the highly productive seasons, $\delta^{13}\text{C}$ values in the surface water are more positive and accurately recorded in the planktonic foraminiferal tests [66, 67]. Hence, planktonic $\delta^{13}\text{C}$ is widely used as a proxy for past surface water productivity (Devendra *et al.*, under review). More positive $\delta^{13}\text{C}$ values in planktonic tests reflect high surface productivity, as the enrichment in ^{13}C due to rapid use of ^{12}C through the photosynthesis on the sea surface.

The organic matter rained down from the surface and underwent degradation and decomposition processes at deeper depths. Con-

sequently, ^{12}C at the bottom increased, resulting in lower $\delta^{13}\text{C}$ values in bottom waters. Therefore, more negative values of $\delta^{13}\text{C}$ in benthic foraminifera (mostly *Cibicidoides wuellerstorfi*) tests indicate enhanced organic matter input from surface production [68]. Thus, foraminiferal $\delta^{13}\text{C}$ can be used as an excellent proxy to reconstruct the changes in paleoproductivity [69].

$$\delta^{13}\text{C} \text{ ‰} = \frac{\text{Ratio}(\text{sample}) - \text{Ratio}(\text{standard})}{\text{Ratio}(\text{standard})} \times 1000 \quad (1.3)$$

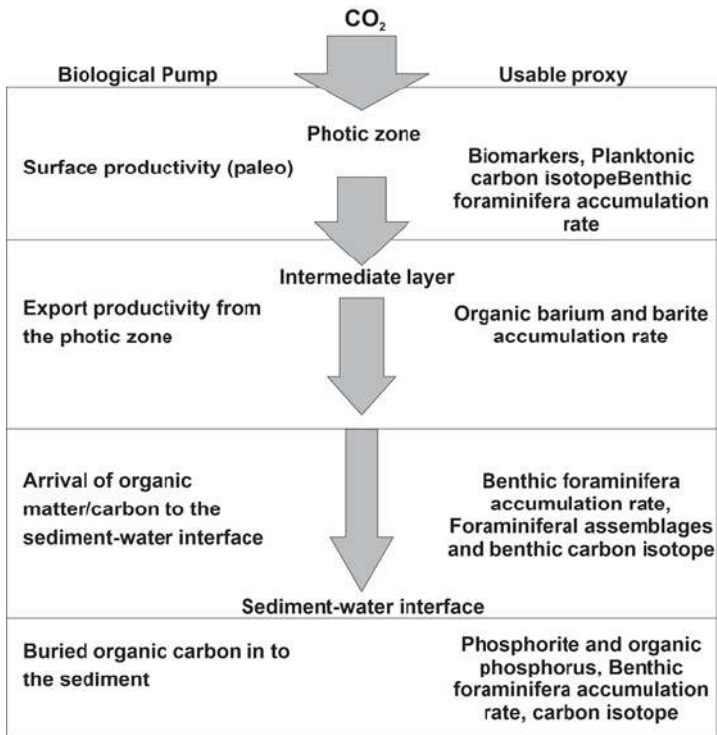


Fig. 1.2: Schematic diagram of the stages of the biological pump and usable paleoproductivity indicator proxies as described in the text.

1.3 Summary

Organic matter (OM) concentrations in sediments represent only a small portion of the total primary productivity in ocean surface waters. Export productivity refers to the portion of phytoplankton biomass that manage to survive from the water column's generally efficient recycling system (organic C sinking flux). Following further degradation during passage through the water column, this substance is delivered to the sediment-water contact. Only around 10% of total productivity leaves the euphotic zone in normal oceanic environments.

Several novel proxies for reconstructing paleoproductivity conditions in the global ocean have been created in the last few decades. Some classical proxies, such as TOC and carbon isotope of foraminifera provide direct information about surface water productivity. However, some novel proxies (e.g. alkenone and lipid pigments) have been fit specifically higher latitudes, but the majority of paleoproductivity proxies have been successfully corrected to the higher latitudes after the important calibrations.

Acknowledgement

The research work at the Institute of Oceanology was financially supported by the Norwegian Financial Mechanism for 2014-2021, project No. 2019/34/H/ST10/00682. The author would like to thank supervisors Prof. Marek Zajęzkowski and Dr. Magdalena Łącka for their encouragement, advice, and ideas.

Bibliography

- [1] L.H. Armbricht, M.J. Coolen, F. Lejzerowicz, S.C. George, K. Negandhi, and Y. Suzuki. Ancient dna from marine sediments: precautions and considerations for seafloor coring, sample handling and data generation. *Earth-Science Reviews*, 2019.
- [2] J. Pawlowska, F. Lejzerowicz, P. Esling, W. Szczucinski, M. Zajaczkowski, and J. Pawlowski. Ancient dna sheds new light on the svalbard foraminiferal fossil record of the last millennium. *Geobiology*, 12(4):277–88, 2014.
- [3] A.J. Pienkowski, N.K. Gill, M.F. Furze, S.M. Mugo, F. Marret, and A. Perreaux. Arctic sea-ice proxies: Comparisons between biogeochemical and micropalaeontological reconstructions in a sediment archive from arctic canada. *The Holocene*, 27(5):665–82, 2017.
- [4] M. Oksman, S. Juggins, A. Miettinen, A. Witkowski, and K. Weckstrom. The biogeography and ecology of common diatom species in the northern north atlantic, and their implications for paleoceanographic reconstructions. *Marine Micropaleontology*, 148:1–28, 2019.
- [5] M. Sarnthein and K. Winn. *Reconstruction of low and middle latitude export productivity, 30,000 years BP to present: implications for global carbon reservoirs*. Springer, Climate-Ocean Interaction, 1990.
- [6] B. Schneider and A. Schmittner. Simulating the impact of

- the panamanian seaway closure on ocean circulation, marine productivity and nutrient cycling. *Earth and Planetary Science Letters*, 246(3-4):367–80, 2006.
- [7] M. Lacka, M. Zajaczkowski, M. Forwick, and W. Szczucinski. Late weichselian and holocene palaeoceanography of storfjordrenna, southern svalbard. *Climate of the Past*, 11(3):587–603, 2015.
- [8] D.M. Sigman and E.A. Boyle. Glacial/interglacial variations in atmospheric carbon dioxide. *Nature*, 407(6806):859–69, 2000.
- [9] R.B. Rivkin and L. Legendre. Biogenic carbon cycling in the upper ocean: effects of microbial respiration. *Science*, 291(5512):2398–400, 2001.
- [10] P. Boyd and T. Trull. Understanding the export of biogenic particles in oceanic waters: Is there consensus? *Progress in Oceanography*, 72(4):276–312, 2007.
- [11] K.O. Buesseler, C.H. Lamborg, P.W. Boyd, P.J. Lam, T.W. Trull, and R.R. Bidigare. *et al. Revisiting carbon flux through the ocean’s twilight zone. science*, 316(5824):567–70, 2007.
- [12] E. Seibold and W. Berger. *Productivity of the Ocean and Implications*. Springer, The Sea Floor, 2017.
- [13] N. Tribovillard, T.J. Algeo, T. Lyons, and A. Riboulleau. Trace metals as paleoredox and paleoproductivity proxies: an upyear. *Chemical geology*, 232(1-2):12–32, 2006.
- [14] S. Calvert and T. Pedersen. Chapter fourteen elemental proxies for palaeoclimatic and palaeoceanographic variability in marine sediments: interpretation and application. *Developments in marine geology*, 2007.
- [15] T. Pedersen and S. Calvert. Anoxia vs. productivity: what controls the formation of organic-carbon-rich sediments and sedimentary rocks? *Aapg Bulletin*, 74(4):454–66, 1990.

- [16] D.E. Canfield. Factors influencing organic carbon preservation in marine sediments. *Chemical geology*, 114(3-4):315–29, 1994.
- [17] K.A. Zonneveld, G.J. Versteegh, S. Kasten, T.I. Eglinton, K.-C. Emeis, and C. Huguet. Selective preservation of organic matter in marine environments; processes and impact on the sedimentary record. *Biogeosciences*, 7(2):483–511, 2010.
- [18] S. Opsahl and R. Benner. Distribution and cycling of terrigenous dissolved organic matter in the ocean. *Nature*, 386(6624):480–2, 1997.
- [19] Werner G Deuser. Organic-carbon budget of the black sea. In *Deep Sea Research and Oceanographic Abstracts*, volume 18, pages 995–1004. Elsevier, 1971.
- [20] P.J. Muller and E. Suess. Productivity, sedimentation rate, and sedimentary organic matter in the oceans—i. organic carbon preservation. *Deep Sea Research Part A Oceanographic Research Papers*, 26(12):1347–62, 1979.
- [21] S. Aagaard-Sorensen, K. Husum, M. Hald, and J. Knies. Paleooceanographic development in the sw barents sea during the late weichselian-early holocene transition. *Quaternary Science Reviews*, 29(25-26):3442–56, 2010.
- [22] K. Sztybor and T.L. Rasmussen. Late glacial and deglacial paleooceanographic changes at vestnesa ridge, fram strait: Methane seep versus non-seep environments. *Palaeogeography, Palaeoclimatology, Palaeoecology*, 476:77–89, 2017.
- [23] M.M. Kuypers, R.D. Pancost, I.A. Nijenhuis, and J.S. Sinninghe Damste. Enhanced productivity led to increased organic carbon burial in the euxinic north atlantic basin during the late cenomanian oceanic anoxic event. *Paleoceanography*, 17(4):3–1, 2002.
- [24] R. Tyson. The” productivity versus preservation” controversy: cause, flaws, and resolution. *Special Publication-SEPM*, 82(17), 2005.

- [25] R.A. Berner. Sedimentary pyrite formation: an upyear. *Geochimica et cosmochimica Acta*, 48(4):605–15, 1984.
- [26] J. Dymond, E. Suess, and M. Lyle. Barium in deep-see sediment: A geochemical proxy for paleoproductivity. *Paleoceanography*, 7(2):163–81, 1992.
- [27] A. Paytan and E.M. Griffith. Marine barite: Recorder of variations in ocean export productivity. deep sea research part ii. *Topical Studies in Oceanography*, 54(5-7):687–705, 2007.
- [28] A.C. Redfield. The biological control of chemical factors in the environment. *American scientist*, 46(3), 1958.
- [29] T.J. Algeo and E. Ingall. Sedimentary corg: P ratios, paleocean ventilation, and phanerozoic atmospheric po₂. *Palaeogeography, Palaeoclimatology, Palaeoecology*, 256(3-4):130–55, 2007.
- [30] C.R. Benitez-Nelson. The biogeochemical cycling of phosphorus in marine systems. *Earth-Science Reviews*, 51(1-4):109–35, 2000.
- [31] T. Goldhammer, V. BrÄlchert, T.G. Ferdelman, and M. Zabel. Microbial sequestration of phosphorus in anoxic upwelling sediments. *Nature Geoscience*, 3(8):557–61, 2010.
- [32] K.L. Faul, A. Paytan, and M.L. Delaney. Phosphorus distribution in sinking oceanic particulate matter. *Marine Chemistry*, 97(3-4):307–33, 2005.
- [33] M. Szymczak-Zyla, M. Krajewska, M. Witak, T.M. Ciesielski, M.V. Ardelan, and B.M. Janssen. Present and past-millennial eutrophication in the gulf of gdaÅsk (southern baltic sea. *Paleoceanography and Paleoclimatology*, 34(2):136–52, 2019.
- [34] P. Harris, M. Zhao, A. Rosell-Mele, R. Tiedemann, M. Sarnthein, and J. Maxwell. Chlorin accumulation rate as a proxy for quaternary marine primary productivity. *Nature*, 383(6595):63–5, 1996.

- [35] A.M. Shankle, R. Goericke, P.J. Franks, and L.A. Levin. Chlorin distribution and degradation in sediments within and below the arabian sea oxygen minimum zone. *Deep Sea Research Part I: Oceanographic Research Papers*, 49(6):953–69, 2002.
- [36] M.J. Higginson. *Chlorin pigment stratigraphy as a new and rapid palaeoceanographic proxy in the quaternary*. University of Bristol, 2000.
- [37] M.H. Conte, G. Eglinton, and L.A. Madreira. Origin and fate of organic biomarker compounds in the water column and sediments of the eastern north atlantic. *Philosophical Transactions of the Royal Society of London Series B: Biological Sciences*, 348(1324):169–78, 1995.
- [38] E. Schefuss, G.J.M. Versteegh, J.H.F. Jansen, and J.S. Sinninghe Damste. Lipid biomarkers as major source and preservation indicators in se atlantic surface sediments. *Deep Sea Research Part I: Oceanographic Research Papers*, 51(9):1199–228, 2004.
- [39] J. Bendle and A. Rosell-Mele. Distributions of uk37and uk37â€¸ in the surface waters and sediments of the nordic seas: Implications for paleoceanography. *Geochemistry, Geophysics, Geosystems*, 5(11), 2004.
- [40] A.J. Gooday, L.A. Levin, P. Linke, and T. Heeger. *The role of benthic foraminifera in deep-sea food webs and carbon cycling. Deep-sea food chains and the global carbon cycle*. Springer, 1992.
- [41] T.L. Rasmussen and E. Thomsen. Warm atlantic surface water inflow to the nordic seas 34-10 calibrated ka b.p. *Paleoceanography*, 23(1), 2008.
- [42] A.E. Jennings and G. Helgadottir. Foraminiferal assemblages from the fjords and shelf of eastern greenland. *J Foramin Res*, 24(2):123–44, 1994.

- [43] M.M. Telesinski, J.E. Przytarska, B. Sternal, M. Forwick, W. Szczucinski, and M. Lacka. Palaeoceanographic evolution of the sw svalbard shelf over the last 14 000 years. *Boreas*, 47(2):410–22, 2018.
- [44] A. Mackensen, D. Fu, H. Grobe, and G. Schmiedl. Benthic foraminiferal assemblages from the eastern south atlantic polar front region between 35 and 57 s: Distribution, ecology and fossilization potential. *Marine Micropaleontology*, 22(1-2):33–69, 1993.
- [45] G. Lutze and W. Coulbourn. Recent benthic foraminifera from the continental margin of northwest africa: community structure and distribution. *Marine Micropaleontology*, 8(5):361–401, 1984.
- [46] J.C. Herguera and W. Berger. Paleoproductivity from benthic foraminifera abundance: Glacial to postglacial change in the west-equatorial pacific. *Geology*, 19(12):1173–6, 1991.
- [47] C. Cauille, K.A. Koho, M. Mojtahid, G.-J. Reichart, and F.J. Jorissen. Live (rose bengal stained) foraminiferal faunas from the northern arabian sea: faunal succession within and below the omz. *Biogeosciences*, 11(4):1155–75, 2014.
- [48] S.B. Suhr and D. Pond. Antarctic benthic foraminifera facilitate rapid cycling of phytoplankton-derived organic carbon. deep sea research part ii. *Topical Studies in Oceanography*, 53(8-10):895–902, 2006.
- [49] G. Lutze and H. Thiel. Epibenthic foraminifera from elevated microhabitats; cibicidoides wuellerstorfi and planulina ariminensis. *The Journal of Foraminiferal Research*, 19(2):153–8, 1989.
- [50] D.S. Murgese and P. Deckker. The late quaternary evolution of water masses in the eastern indian ocean between australia and indonesia, based on benthic foraminifera faunal and carbon isotopes analyses. *Palaeogeography, Palaeoclimatology, Palaeoecology*, 247(3-4):382–401, 2007.

- [51] B.H. Corliss. Microhabitats of benthic foraminifera within deep-sea sediments. *Nature*, 314(6010):435–8, 1985.
- [52] M.H. Caralp. Size and morphology of the benthic foraminifer *melonis barleeanum*; relationships with marine organic matter. *The Journal of Foraminiferal Research*, 19(3):235–45, 1989.
- [53] A.J. Gooday. A response by benthic foraminifera to the deposition of phytodetritus in the deep sea. *Nature*, 332(6159):70–3, 1988.
- [54] M. Lacka and M. Zajaczkowski. Does the recent pool of benthic foraminiferal tests in fjordic surface sediments reflect interannual environmental changes? the resolution limit of the foraminiferal record. *Annales Societatis Geologorum Poloniae*, 2015.
- [55] L. Polyak and V. Mikhailov. Post-glacial environments of the southeastern barents sea: foraminiferal evidence. *Geological Society, London, Special Publications*, 111(1):323–37, 1996.
- [56] Alix G Cage, Anna J Pieńkowski, Anne Jennings, Karen Louise Knudsen, and Marit-Solveig Seidenkrantz. Comparative analysis of six common foraminiferal species of the genera *casidulina*, *paracassidulina*, and *islandiella* from the arctic–north atlantic domain. *Journal of Micropalaeontology*, 40(1):37–60, 2021.
- [57] J.E. Wollenburg, J. Knies, and A. Mackensen. High-resolution paleoproductivity fluctuations during the past 24 kyr as indicated by benthic foraminifera in the marginal arctic ocean. *Palaeogeography, Palaeoclimatology, Palaeoecology*, 204(3-4):209–38, 2004.
- [58] E. Thomas, L. Booth, M. Maslin, and N. Shackleton. North-eastern atlantic benthic foraminifera during the last 45,000 years: changes in productivity seen from the bottom up. *Paleoceanography*, 10(3):545–62, 1995.

- [59] L. Diester-Haass and R. Zahn. Paleoproductivity increase at the eocene-oligocene climatic transition: ODP/DSDP sites 763 and 592. *Palaeogeography, Palaeoclimatology, Palaeoecology*, 172(1-2):153–70, 2001.
- [60] J.C. Herguera. Deep-sea benthic foraminifera and biogenic opal: glacial to postglacial productivity changes in the western equatorial pacific. *Marine Micropaleontology*, 19(1-2):79–98, 1992.
- [61] E.M. Emelyanov. Calcium carbonate compensation depth (ccd). *The Barrier Zones in the Ocean*, 2005:345–61.
- [62] P.D. Naidu and B.A. Malmgren. Do benthic foraminifer records represent a productivity index in oxygen minimum zone areas? an evaluation from the oman margin, arabian sea. *Marine Micropaleontology*, 26(1-4):49–55, 1995.
- [63] W. Prell and W. Curry. Faunal and isotopic indices of monsoonal upwelling-western arabian sea. *Oceanologica Acta*, 4(1):91–8, 1981.
- [64] E. Vincent and W. Berger. Planktonic foraminifera and their use in paleoceanography. *The sea*, 7:1025–119, 1981.
- [65] J. Giraudeau. Planktonic foraminiferal assemblages in surface sediments from the southwest african continental-margin. *Marine Geology*, 110(1-2):47–62, 1993.
- [66] D. Devendra, R. Xiang, F. Zhong, Y. Yang, and L. Tang. Palaeoproductivity and associated changes in the north-eastern indian ocean since the last glacial: Evidence from benthic foraminifera and stable isotopes. *Journal of Asian Earth Sciences*, 2019.
- [67] D. Devendra, L.-L. Zhang, X. Su, A. Hewa Bandulage, V. Thilakanayaka, and F.-C. Zhong. Late quaternary deep and surface water mass evolution in the northeastern indian ocean inferred from carbon and oxygen isotopes of benthic and planktonic foraminifera. *Palaeoworld*, 29(4):807–18, 2020.

- [68] J. Duplessy, N. Shackleton, R. Fairbanks, L. Labeyrie, D. Oppo, and N. Kallel. Deepwater source variations during the last climatic cycle and their impact on the global deepwater circulation. *Paleoceanography*, 3(3):343–60, 1988.
- [69] M. Lacka, M. Cao, A. Rosell-Mele, J. Pawłowska, M. Kucharska, and M. Forwick. Postglacial paleoceanography of the western barents sea: Implications for alkenone-based sea surface temperatures and primary productivity. *Quaternary Science Reviews*, 224:105973–86, 2019.

Chapter 2

The application of underwater optical imagery for a long-term experiment in Arctic coastal shallows – A comparison of technical specifications, settings and outputs

BERNABÉ MORENO

Institute of Oceanology, Polish Academy of Sciences,
Powstańców Warszawy 55, 81-712 Sopot, Poland

2.1 Introduction

One of the first applications of underwater photography was for scientific purposes. This goes back to the French zoologist and marine engineer Louis Boutan who at the end of 1890s designed a series of apparatuses specifically for either long-exposure or instant underwater photographs, at depths down to 7 m [1, 2]. Much has changed since then, when both the photography apparatus and the diving suit (i.e., Denayrouze Charles Petit Modele 1889 diving helmet) were incredibly heavy and cumbersome [3]. Current technologies enable marine scientists to access a bewildering array of equipment, methods, software, and certainly, depths; hence, the resulting approaches are numerous. Moreover, in recent decades most technological development has focused on the deep sea (>500 m) [4], meanwhile sampling efforts operated by divers in the shallows are assessed with relatively less intensity [5].

Long-term underwater experiments are valuable, *inter alia*, for the capacity of normalising the influence of cyclical variability patterns on natural systems (e.g., seasonal, and decadal oscillations). Monitoring efforts collect archive information of indisputable value, especially when assessed from the endpoint [6, 7]. However, analysing archive ecological information requires robust and repeatable processing protocols and well-designed downstream analyses. Available technology for automation processes is rapidly developing and constantly evolving, and although establishing the workflow may require trial–error feedbacks, it can be a more efficient process in the long run. In this sense, marine scientist opting for the latter rely on technology both for input acquisition (photography gear and its specs), and during the process (image processing pipeline).

The aim of the present chapter is to assess preliminary outputs and to provide a comparative insight of the optical imagery specifications and settings used to monitor a specific underwater experiment throughout 12 years. This is part of the first stage’s (image processing) quality assessment of a project dealing with the marine succession in a rapidly changing environment in the high-Arctic shallows (78°N).

2.2 Scientific and technical background

2.2.1 Studying change in marine benthic assemblages

Many processes across Earth systems are changing at unprecedented rates attributable to climate change. The Arctic is considered as the most rapidly warming region globally [8]. Biological responses to disturbances depend on several interacting factors, therefore, it is key to evaluate them at the proper spatiotemporal scale and compare it to baseline knowledge. Ecological and biological long-term monitoring serves to recognise natural variability from other changes in the biocoenosis. Shallow hard-bottom habitats are both relatively accessible and suitable for examining interactions between, and responses of the assemblages to the surrounding physical environment [9]. For benthic assemblages, dispersal of larvae, recruitment, competition, facilitation, and predation integrate an intertwined and complex process [10]. Here, recruitment is fundamental since it determines the establishment, diversity (either inhibit or facilitate the settlement of other species), and persistence during the whole process of ecological succession in benthic assemblages [11]. To study this, artificial settlement panels have been widely used in different marine regions since the second half of the last century [7, 12–14]. Until recently, polar regions have been comparatively less studied in such way.

Photo and videography are being increasingly used to study marine habitats at wide latitudinal and bathymetrical ranges [4]. However, the infralittoral and shallow circalittoral zones are the most accessible to divers to undertake direct observations/annotations, conduct sampling and acquire optical imagery. Furthermore, photographing panels underwater can arguably be considered a less invasive approach for long-term study of epibenthic assemblages [15].

2.2.2 Parameters when using underwater photography as a tool for ecological research

In underwater photography, the reduction of water column volume between the sensor and the object is most desirable. However, there are fundamental interacting parameters that influence on the res-

ulting optical image, most of which can be modified by the photographer to obtain a 'good' light exposure (Fig. 2.1).

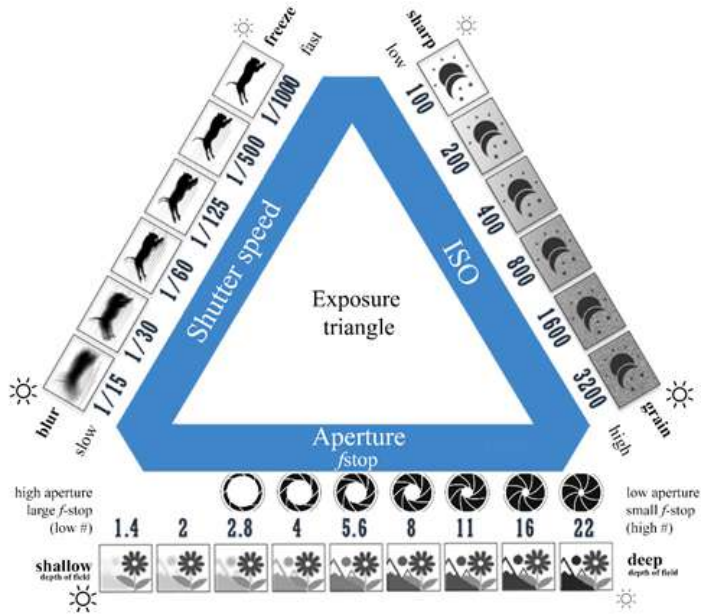


Fig. 2.1: The light-exposure triangle showing the fundamental interacting parameters in photography. Common terminologies are shown on spectra ends, the effects on the output are shown in bold together with the influence on light intensity (☼ symbol size). Adapted from BrentMail Photography (<https://brentmailphotography.com/>).

Prioritising one parameter means a trade-off between the others. The following three parameters can be modified on site, depending on the light availability.

- Aperture/ f -stop (and depth-of-field). The f -stop or f -number stands for the relation between the aperture (ϕ) and the focal length of the lens [16], so that $f22$ means that $\phi = 1/22$ of the lens focal length (in mm). The most depth-of-field is achieved (i.e., more 'layers' in focus) at the lowest apertures (small f -stop, e.g., $f22$) (Fig. 2.1). However, smaller

diaphragm aperture also means less light reaching the sensor, therefore artificial lighting is required to achieve better results. Furthermore, the sharpness (i.e., resolving power, the smallest detail that can be detected) is not uniform at all apertures. The aperture at which the sharpness is the highest is commonly known as the lens 'sweet spot' and this is usually two- or three-stops from the maximum aperture (e.g., $f5.6$ is the sweet spot for a $f2.8$ lens, Fig. 2.1).

- Shutter speed. This refers to the length of time for which the shutter remains open and photons can reach the image sensor. Most photographs are taken at fractions of a second (e.g., '1/100 s), but long-exposures can also occur (e.g., slower than 1 s), however, these are less used in underwater photography. This parameter is important especially when using external light sources. Although video (continuous) lights are useful for both videography and photography, strobe-lights (flashes or flashguns) are the most recommended for the latter for its ability to 'freeze' motion. External strobes are connected to the camera either via optical-fibre cables or electrical cords, further, to properly synchronise the components it is required to consider that mechanical shutters have a maximum shutter speed; this is called the strobe 'sync speed'. For most cameras 1/200–1/250 s are commonly the maximum strobe sync speeds.
- ISO. It refers to the sensitivity of the digital camera sensor to light (the term derives from film-photography). ISO influences the sharpness of the photograph, so that noise (grains) increases at higher ISO. It is of common thought that the lower the ISO the better quality, nevertheless, modern cameras are being designed for low-light conditions without impacting on the output.

When shooting on Manual mode, the photographer has total control on these parameters. However, there are also Semi-manual exposure modes where the camera's internal metering system select the value of the corresponding complementary parameter to obtain a correct exposure. It can either be aperture-priority (A) or

shutter-priority (S).

In digital photography crop factor is a parameter regarding the sensor size relative to a 35 mm-film format. Therefore, cameras with full-frame sensors are not subjected to this. This is a parameter related to the final magnification ratio (see below).

The following properties are fixed to the lens model (optical component), hence cannot be modified on site.

- Focal length (FL). This refers to the distance (in mm) between the sensor and the centre of the lens. The shorter the focal length, the wider the coverage, small FL are called wide-angle lenses (35 mm or shorter), while larger FL are called telephoto lenses. The latter can be short- (85-135 mm), medium- (135-300 mm), or super-telephoto lenses (>300 mm). In the middle range, between wide-angle and tele lenses, macro lenses can be found between 30-110 mm. Lenses can also be either prime (single FL) or zoom lenses (a range of FL). Almost all macro lenses are prime lenses.
- Magnification (reproduction) ratio. Assuming the use of a full-frame sensor, macro lenses are optimal for optical-based image acquisition since the aberration is kept to a minimum and the user can be sure of the 1:1 (one-to-one) magnification ratio. Magnification refers to "the real size of the subject compared to the size at which the subject is recorded on the sensor" [16], hence macrophotography is such when the subject is either the same size ('life-size') or greater in reality than on the sensor.

In littoral zones the underwater photographer will deal also with further factors of the surrounding environment. These are related to both light penetration and suspended particles.

- Turbidity. It is the reduction of water clarity because of the presence of suspended particles scattering or absorbing light [17]. Suspended matter is often more abundant in shallow environments that are subject to the influence of tides, winds, glacier- and riverine inputs [18] and because of the onset of spring blooms in fjords [19]. The trim, balance, and propulsion of the underwater photographer are also contrib-

uting factors to avoid further resuspension of particles; thus, peak-performance buoyancy and proper kicking techniques are desirable skills.

- Backscatter. Is the lighting up by external light of the particles suspending in the water column between the subject(s) of interest and the lens.

2.3 Methodical considerations

2.3.1 Experimental design

The experimental apparatus setups were deployed at two depths (6 and 12 m) and two sites (S1 and S2) in Isfjorden, the largest fjord of Spitsbergen (Fig. 2.2), to monitor ecological changes in the high-Arctic (littoral) zone.

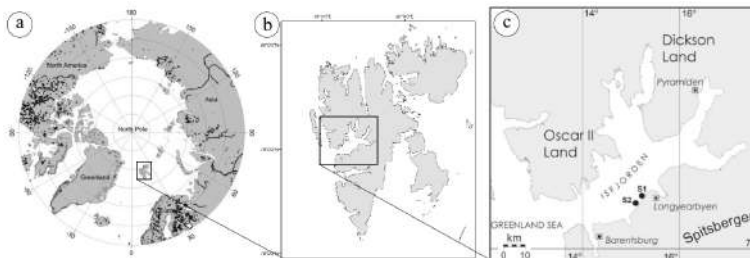


Fig. 2.2: Deployment sites of the long-term experiment. (a) Arctic realm, (b) Svalbard archipelago, (c) Isfjorden showing sites S1 and S2.

The apparatus consisted of a set of 12 High Impact Polystyrene (HIPS) panels (3 rows x 4 columns), Fig. 2.3(a); described in detail in [15]. The colonisation component of the study (short temporal scale) consisted of the removal of the three panels from the first column after 1 year. to be photographed at surface and dried for further analysis under the stereo-microscope. The remaining nine panels were periodically revisited and photographed in situ to establish the rate and mode of ecological succession over a decade, considering different starting points (i.e., seasons). Initially, the

numerical position of each one of the twelve panels was written on the bakelite holding bar with permanent pen (Fig. 2.3(d)), and this information was recorded on the logbook. The holding bar would eventually get colonised by encrusting organisms (mainly bryozoans, Fig. 2.3(d)), making it difficult to read-out the codes in situ later. Therefore, it was critical for the underwater photographer to use a standardised procedure during the whole decade of annual revisits, but at the same time use some physical markers as additional aid (e.g., plastic cable-ties and other marks, Fig. 2.3(d)). Deployment, revisits, and recovery of the experimental set ups were done using SCUBA diving.

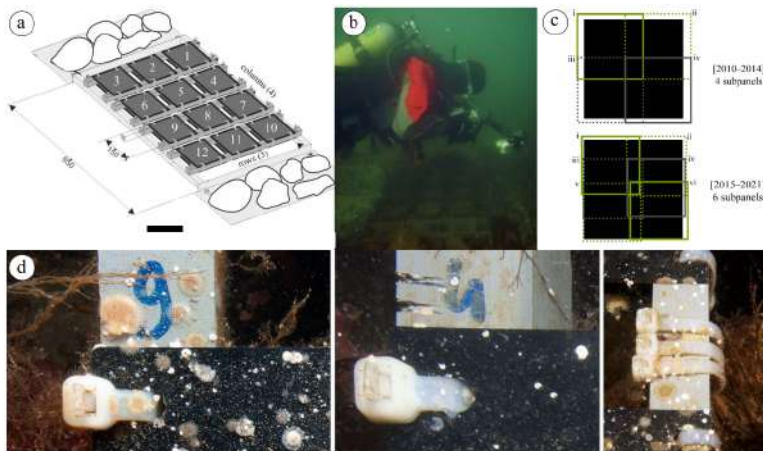




Fig. 2.3: Underwater experiment setting. (a) Codification used during the revisits (numbered panels), scale bar: 200 mm; (b) photography of the panels in situ; (c) subpanels overlapping photographs (4 or 6 depending on the period); (d) different approaches for order recognition: using the bakelite holding bar, permanent marker (left), erosion (middle), or cable-ties (right). Adapted from [15].

2.3.2 Underwater optical imagery

Technical specifications of the photography gear are shown in Tab. 2.1.

The Tokina AT-X M35 35 mm is a 9-elements macro lens; aperture range from $f2.8$ to $f22$; minimum focusing distance at surface: 14 cm. This 35 mm focal length multiplied by the magnification factor of APS-C sensors (1.5) gives an equivalent of 52.5 mm in a full-frame sensor. The Nikon NIKKOR 60 mm features high-speed Internal Focusing (IF) mechanisms that employs a Silent Wave Motor (SWM) enabling fast and quiet autofocus performance. Minimum focusing distance at surface is 18.5 cm. Aperture range from $f2.8$ to $f32$.

Tab. 2.1: Technical specifications of the underwater camera sets used throughout the experiment. Image sensor sizes are also represented in colour-filled rectangles for size comparison purposes.

		Time period	
Descriptor		2010-2014	2015-2021
Camera	Camera model	Nikon D200	Nikon D810
	Image sensor type	RGB CCD	CMOS
	Image sensor size	APS-C  (23.6 x 15.8 mm)	Full-frame  (35.8 x 24 mm)
	Total pixels (x10 ⁶)	10.92	37.09
	Effective pixels (x10 ⁶)	10.2 (93.4%) (3.872 x 2.592)	36.3 (97.8%) (7.36 x 4.912)
	Magnification ratio/factor	1.5:1	1:1
	Lenses	Tokina AT-X M35 PRO DX 35mm f/2.8, macro Tokina AT-X 107 DX AF 10-17 mm f/3.5-4.5, fish-eye	Nikon AF-S Micro NIKKOR 60 mm f/2.8G ED Lens
	Lighting	(x2) INON Z-240 underwater strobe-light	
Housing	Model	Subal ND200	Subal ND810
	Weight (kg)	2.2	3.2
	Depth rating (m)	70	80

Underwater photographs were taken using the native Nikon Electronic Format (NEF) for highest resolution and full access to metadata. In the context of software applications, 'native' refers to the file structure which the application works with during cre-

ation, edition, or publication of a file [20]. The EXIF (Exchangeable Image File) format information was accessed using Adobe Photoshop (PS) CC; the NEF file was opened in PS(*File-File Info* [or *Alt+Shift+Ctrl+I*]-*Camera Data*). Values of interest for the present work were those related with the underwater photography set (cameras and lenses), and light-exposure parameters.

2.3.3 Image acquisition

Optical imagery was acquired under challenging conditions in the Arctic fjord. Procedures, configurations, and technical aspects of the underwater operations are provided at some extent in [21, 22]. The experimental construction required to be flipped upside down to photograph the bottom panels (labelled as 'dól' or 'dol', which were preliminarily analysed in this work).

Camera position. Position of the camera is key and should be perpendicular to the seabed. Because of the task-load and the required manoeuvre of the experimental apparatus, the scientific diver opted for not using a fixed rig, which is normally recommended to obtain photoquadrats [6, 20, 23]. This implied a trade-off since it ultimately may prevent from yielding homogeneous outputs which are desired for semi-automated image calibration and further measurements and analysis. The use of 'quadropods' or 'sliding frames' (Ashton GV, *pers comm*) reduce the variability of the distance between the panel surface and the camera lens [24].

Positioning of the light source. This is a critical aspect to avoid backscattering. Backscattering can be reduced by firing the artificial light sources from behind the camera and far from the lens, using an indirect angle (light up the subject only with the edges of the light beams), and the use of light-diffusers on the strobes.

2.3.4 Image processing pipeline

The following equipment and software were used to process and assess the quality of the outputs.

- Laptop computers. Two different laptops were used during the image pre-processing which enabled a further compar-

ison between technical specifications. These are detailed on Tab. 2.2.

- Monitor. To standardise the visual assessment and imagery-derived outputs a Dell UltraSharp 27” 4K monitor (U2720Q) was used as a secondary screen (Display settings–Expand image) for all image processing. This monitor was set to the recommended resolution of 3840x2160 px (4K/UHD; ITU-T P.1204.3). The monitor was calibrated for both gamma and contrast. Gamma refers to the mathematical relationship between the colour channels (RGB) sent to display and the amount of light emitted from it. Contrast determines the clarity and level of highlights.
- Adobe Photoshop (CC 2017 and CC 2021). This is a raster digital graphics editor where different processes can be done in multiple layers. Workspaces can be saved in non-compressed formats such as TIFF (Tag Image File Format) or the native extension PSD. This software is widely used in the image industry, for either commercial or scientific purposes. It enables the installation of plug-ins.

Tab. 2.2: Comparison of technical specifications between laptops (personal computer, PC).

Descriptor	PC1	PC2
System manufacturer	Lenovo	Lenovo
Model	ThinkPad X1 Carbon 3 rd Gen (20BTS19J00)	Legion 7 16ACHg6 (82N6)
System type	x64-based PC	x64-based PC
Processor	Intel Core i7–5600U, 2.6GHz Intel HD Graphics 520, 2 cores, 4 logical processors (threads)	AMD Ryzen 7–5800H, Radeon graphics, 8 cores, 16 logical processors (threads)
Physical memory (RAM)	8 GB	32 GB (DDR4, 3200MHz)
Solid state drive (SSD)	256 GB	512 GB
Graphic card memory	Intel(R) HD Graphics 5500 0.95 Hz	GeForce RTX 3070 165 Hz 8GB GDDR6
Graphics display (screen) resolution	1920 x 1080 (Full HD)	2560 x 1600 (WQXGA)
Screen size (diagonal)	14”	16”

The proposed workflow utilised for the set of underwater photographs is detailed in Fig. 2.4. The input is described as the preparation of the photo-files prior the photomerging process (PhM) where recommendations are given for easier location and handling of the files. The output includes the photomerged images and their further handling prior the next step (i.e., image analysis pipeline, not described in the present work).

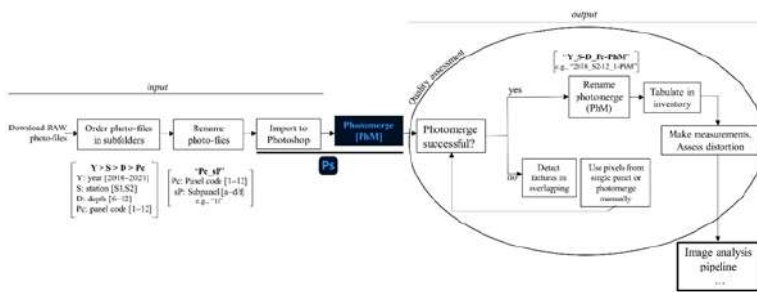


Fig. 2.4: Proposed image workflow prior the image analysis pipeline.

Spatial calibration

In digital imagery a pixel (px) is defined as the 'smallest addressable (controllable) element in a (raster) image' [25]. The number of both, the total and effective pixels, are standard for different cameras (sensors), and this is a critical value defining the specs (1 Megapixel = 106 px). Spatial calibration is a fundamental step in the image processing pipeline since it enables accurate measurement of attributes such as spatial cover [26]. Spatial calibration is a basic task most image-analysis software have (e.g., ImageJ, photoQuad, CPCe, Fovea Pro), however, most users are not aware of the calibration and measurement tools in Adobe Photoshop (PS). As mentioned in the previous section, distance from the camera operator to the object was not constant, therefore customizable calibration presets available in PS could not be applied. The quality of optical imagery outputs can also be further assessed through measurements, to this end, spatial calibration is necessary. Manual calibration

(px to mm) had to be done by the user instead, either using the bakelite holding bar (20 mm) or the HIPS panel length (150 mm) as fixed measurements for reference. Calibration was done obtaining the mm-equivalent (in px). For any measurement, Window-Measurement Log-Record Measurement command was used in PS.

Photomosaics

(Underwater) photomosaics can be built in PS [24, 27, 28]. However, none of the studies above mentioned the automation of this process. For current versions of Adobe Photoshop (Adobe Creative Cloud-CC) this is now possible with the Photomerge™ command. Photomerge is an image-transformation process which combines (merges) several photographs into a continuous image (i.e., a panorama). To void problems at the processing stage, photographs should be taken ideally using one focal length and one exposure, avoid position changes and severe tilting (oblique angles, i.e., the difference in the angle of the substratum relative to the plane of the camera lens [29]), avoid using distortion lens, and make sure there is enough overlap in selected images (Fig. 2.3(c), Fig. 2.6(a)). This command is not only useful to build panoramas, but it also enables to merge photographs with different exposition (multi-exposure high-dynamic range-HDR), if needed. Photomerge is a JavaScript (.jsx) stored as a preset in PS documentation. The software Visual Studio Code 1.65.2 was used to access the script. Photomerge is a 1230 lines-long script (see Fig. 2.5, top). To photomerge a series of photographs click File-Automate-Photomerge in PS. Once the source files (layers) and desired options are selected, the script runs through the following process: layers alignment (and vignette removal)-output generation-blend selected layers based on content-layer generation-seamless composition generation. The duration of the photomerging process will depend both on the size of the images, and the image-processing capacity of the computer (Tab. 2.2). The stitching quality was assessed by zooming-in and by (de)selecting different layers.

If the '*Geometric Distortion Correction*' box was not ticked (Fig. 2.5, bottom right) this can be done to each file when importing:

Filter-Lens Correction [or *Shift+Ctrl+R*], selecting either (or all) 'geometric distortion, chromatic aberration, vignette'; selecting the camera brand and model, and selecting the correct lens model. Distortion can be further corrected with the photomerged file: select layers to correct, go to *Edit-Transform-Distort*. Corners can be modified correspondingly, to form right angles.

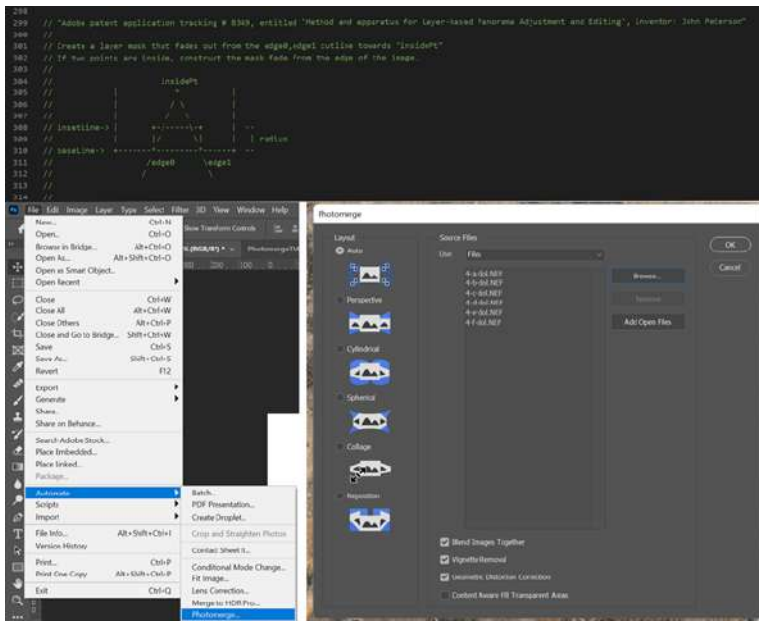


Fig. 2.5: Photomerging (PhM) in Adobe Photoshop CC (2017 or 2021). Top: comment lines (299–314) taken from *Photomerge.jsx* (JavaScript) where the layer-based panorama adjustment is described. Script visualised in Visual Studio Code software. Bottom: steps to open the Photomerge window menu (left), and selected subpanels with boxes ticked (*Blend Images Together*, *Vignette Removal* and *Geometric Distortion Correction*) prior clicking OK (which initiates the photomerging).

Image enhancement

Basic photograph editing (i.e., 'image developing') is recommended to improve visibility of features and enhance overall brightness [30], without over-editing the image. This can be done either in Adobe Lightroom or Adobe Photoshop, by using the curves and levels adjustments (*Image-Adjustments-Curves/Levels*).

Quality assessment

The registration effectiveness (ef) was calculated as the number of panels effectively photographed for all four experimental units ($100\% = 36.\text{yr}^{-1}$; i.e., nine per experimental apparatus, two stations, two depths). The photomerging success is the percentage of successfully photomerged panels (s), this value is dependent on ef . For the *succession* experiment on down-facing surfaces, around 2034 photographs were taken: 648 (31.9%) and 1386 (68.1%) for the first (2010-2014) and second (2015-2021) period, respectively. During the whole experiment duration, 393 HIPS panels were photographed between 2010 and 2021 from which 304 (77.6%) were successfully photomerged (Tab. 2.3). The ef was lower for the first period (90%) but the photomerging success was high ($s = 95\%$). For the second period, ef was higher (91.7%) but the photomerging success was considerably lower ($s = 78.3\%$). These issues may be attributable to both the conditions underwater, and the performance of the underwater photographer.

Time and processing demand. These parameters depended both on the size of the (NEF) files (which depend on the camera/sensor used), and the computer power (Tab. 2.2). When using the PC1 with files from 2010 (first period, Tab. 2.1), it would take ~ 30 min to photomerge and export (PSD, TIFF and PNG) a set of 9 panels corresponding to a single underwater apparatus; i.e., ~ 3 min per panel. Processing time was considerably higher (~ 9 min per panel) when using files from 2018 (second period). However, when using PC2, with higher graphic processing capabilities, this time was significantly reduced to 1 min per panel.

Tab. 2.3: Qualitative and quantitative assessment of the photopanel (php) image acquisition throughout the years. Single photopanel (+/-): if image of the whole panel was taken; and the numbers (#) of subpanels. Numbers in red indicate low, suboptimal values. Registration effectiveness (ef%) and photomerging success (s%) are shown per year, and per period of the study.

Year	Photopanel (php)		Registration	Photomerging
	single	# subpanels	effectiveness (ef%)	success (s%)
2010	+	4	100	100
2011	+	4	83.3	100
2012	+	4	100	94.4
2013	+	4	66.7	88.3
2014	+	4	100	91.3
2010-14 n ₁ =162			90	95
2015	+	4, 5, 6	100	50
2016	+	4	100	50
2017	-	6	100	50
2018	+ -	6	100	61.1
2019	-	6	33.3	58.3
2020	-	6	100	87.2
2021	-	6	100	94.4
2015-21 n ₂ =231			91.7	78.3
Σ Overall			n ₁₊₂ =393	77.6%

2.3.5 Image analysis pipeline

The number of images acquired during monitoring efforts can be vast, however, state-of-the-art software and technologies can be used for implementing automation, thus reducing the processing time in ecological research. This section aims to provide a brief horizon on analysis and techniques that could be further used during the image analysis pipeline (an example of automated pipeline for image processing can be found in [31]).

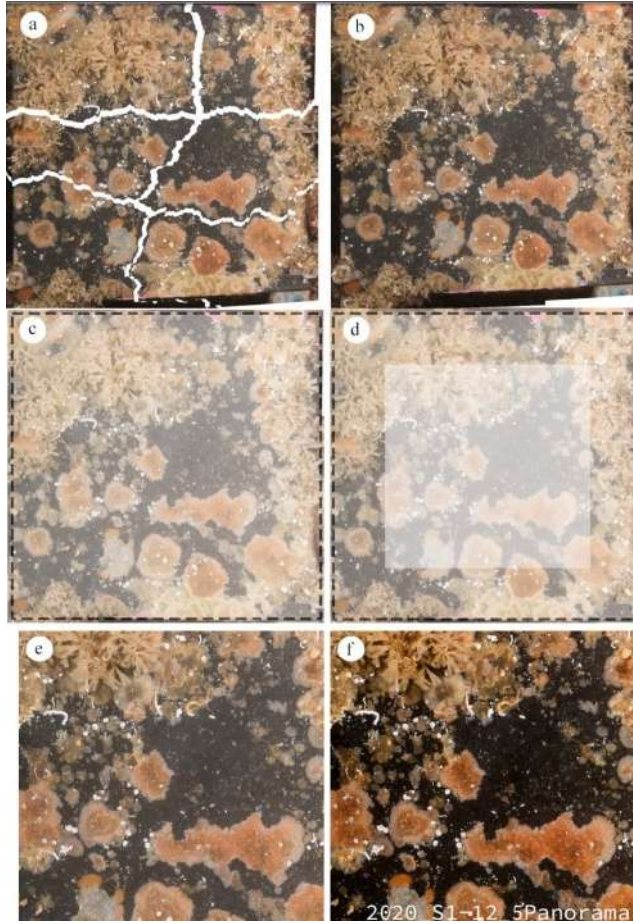


Fig. 2.6: Stepwise digital construction of a photomerged panel using the #5 at 12 m at S1 in 2020 (bottom right label: '2020_S1-12_5Panorama'). (a), (b) Photomerging output obtained from the selection of best pixels from six subpanels; (c) panel borders demarcation (150 x 150 mm); (d) internal area of interest (100 x 100 mm) for further analysis of area cover ($\text{ind.}100 \text{ cm}^{-2}$) and biological interactions (e.g., win, loss, stand-off); (e) tilt correction; and (f) image enhancement adjusting levels and curves. All steps were done in Adobe Photoshop CC 2021.

Functionalities from ImageJ (mostly used image-processing software) have been gathered from PS, such as the inclusion of plug-ins and 'macros' (i.e., "simple, custom programming scripts that automate tasks inside a large piece of software" [32]). Basic knowledge on programming (e.g., creating scripts) can boost the applicability of any software.

Scripting in Adobe Photoshop (PS). 'Scripting instead of Actions'. In PS, Actions are customised sets of commands and tools that enable the automation of repetitive tasks. Using scripts extend these benefits by adding functionality which is not available in Actions [33]. The benefits of scripting include: that are easily transferrable from one computer (or workstation) to another, are more versatile, and can be customised by the user. Scripting can be used, for example, to automatically rename, or open photo-files. PS supports scripts in AppleScript (.sct), VBScript (.vbs), and JavaScript (.jsx) languages. The latter is recommended since it works both in Mac OS and Windows platforms, and can be written in the free software Visual Studio Code.

Machine Learning (ML). ML is a promising artificial-intelligence (AI) discipline that is being implemented in marine research for its capability of dealing with large image-datasets [34–36]. ML is at the mainstay of the image analysis pipeline. To prepare the data there are some steps and concepts to cover first.

- Image enhancement. This refers to the improvement of visual quality to represent 'real colours' more accurately, compensate lighting, and facilitate the detection of certain attributes of interest. Image enhancement methods are reviewed in [4]. The degree of enhancement required depends on the question raised, and the quality of available photo-files.
- Image annotation. The process of documenting what is observed on the optical imagery to extract data. This data can be qualitative or quantitative, and it is recommended to be done by an expert (e.g., taxonomist). Image annotation is a necessary input for training the algorithm.

- Convolutional Neural Network (CNN). A routine based on neural network consisting of convolutional, pooling, and dense layers. CNN are highly effective in image recognition [37].
- TensorFlow. It is a large-scale distributed ML-platform used to express training and inference algorithms for CNN models [38].

2.4 Summary

Monitoring efforts require systematically revisiting the experimental unit; thus, it is critical for the underwater photographer to use a standard sequence when photographing the panels. Placing physical markers such as cable-ties in the bars can be used for this purpose.

For the underwater operations, the recommended photography gear consists of a full-frame sensor camera, optimally with a resolution of ≥ 36 MP, and a macro lens (1:1, one-to-one magnification ratio) protected by a metal housing; and two strobe-lights.

For the image acquisition, the use of fixed rigs (e.g., sliding frame or quadropod) is necessary to avoid variability of the distance between the panel surface and the camera lens. It is recommended to take ≥ 6 subpanel photographs considering the best combination between the spectrum of f-stop ≥ 16 ; shutter speed faster than 1/100 s, but slower than 1/250 s (or whatever the max strobe sync speed is); and ISO between 100 and 300. Additionally, lighting up the subject from behind the camera only with the edges of the light-beams of the strobes (indirect angle) will avoid backscattering, and in turn, will produce a photograph of better quality.

More overlapping subpanels increase the final resolution of the photomerged panel (panorama); however, the overall quality of the latter (e.g., photomerging success) will depend on the consistency of the underwater photographer. It is highly advised to register the whole panel in a single picture to have a reference prior photomerging, or to use its pixels in case photomerging subpanels is not entirely successful.

Although processing high-resolution images demand more from the computer (storage space, graphic and RAM memory use and time), the quality assessment has demonstrated that this is compensated by the output's resolution and yet a much better performance is achieved with sufficient computer power.

Advancements in technological tools at both ends of the workflow (i.e., better cameras and lenses and more refined image-processing tools) can be promising to further explore natural environments following a less-invasive approach and obtaining high-quality ecological information. Further steps are to work on automation processes across the image analysis pipeline: from scripting in Photoshop, to automation in the identification of species on the panels using annotation and machine-learning tools.

Acknowledgement

This work is part of the research project funded by PRELUDIUM-BIS-2 grant from National Science Centre, Poland no. 2020/39/O/NZ8/00376. All underwater photographs used in the present work were registered by the PI of this project, prof. dr hab. Piotr Kuklinski. Thanks are due to him for granting access to an optical imagery archive of immense ecological value.

Bibliography

- [1] Louis Boutan. *La photographie sous-marine et les progrès de la photographie*. 1900.
- [2] Trevor Norton. *Stars beneath the sea: the extraordinary lives of the pioneers of diving*. Century, Random House, 2000.
- [3] Dimitri Rebikoff. History of underwater photography. *Photogrammetric Engineering*, 33(8):897–904, 1967.
- [4] Jennifer M Durden, Timm Schoening, Franziska Althaus, Ariell Friedman, Rafael Garcia, Adrian G Glover, Jens Greinert, Nancy Jacobsen Stout, Daniel OB Jones, Anne Jordt, et al. Perspectives in visual imaging for marine biology and ecology: from acquisition to understanding. In *Oceanography and Marine Biology*, pages 9–80. CRC Press, 2016.
- [5] Delphine Mallet and Dominique Pelletier. Underwater video techniques for observing coastal marine biodiversity: a review of sixty years of publications (1952–2012). *Fisheries Research*, 154:44–62, 2014.
- [6] Frank Beuchel and Bjørn Gulliksen. Temporal patterns of benthic community development in an arctic fjord (kongsfjorden, svalbard): results of a 24-year manipulation study. *Polar Biology*, 31:913–924, 2008.
- [7] Jean-Pierre Féral, Thomas Saucède, Elie Poulin, Christian Marschal, Gilles Marty, Jean-Claude Roca, Sébastien Motreuil,

- and Jean-Pierre Beurier. Proteker: implementation of a submarine observatory at the kerguelen islands (southern ocean). *Underwater Technology*, 34(1):3–10, 2016.
- [8] Valérie Masson-Delmotte, Panmao Zhai, Anna Pirani, Sarah L Connors, Clotilde Péan, Sophie Berger, Nada Caud, Y Chen, L Goldfarb, MI Gomis, et al. Climate change 2021: the physical science basis. *Contribution of working group I to the sixth assessment report of the intergovernmental panel on climate change*, 2(1):2391, 2021.
- [9] Frank Beuchel, Bjørn Gulliksen, and Michael L Carroll. Long-term patterns of rocky bottom macrobenthic community structure in an arctic fjord (kongsfjorden, svalbard) in relation to climate variability (1980–2003). *Journal of Marine Systems*, 63(1-2):35–48, 2006.
- [10] Kirstin S Meyer-Kaiser, Kharis R Schrage, Wilken-Jon Von Appen, Mario Hoppmann, Normen Lochthofen, Arild Sundfjord, and Thomas Soltwedel. Larval dispersal and recruitment of benthic invertebrates in the arctic ocean. *Progress in Oceanography*, 203:102776, 2022.
- [11] David A Bowden. Seasonality of recruitment in antarctic sessile marine benthos. *Marine Ecology Progress Series*, 297:101–118, 2005.
- [12] John P Sutherland and Ronald H Karlson. Development and stability of the fouling community at beaufort, north carolina. *Ecological monographs*, 47(4):425–446, 1977.
- [13] Stephanie J Turner and Christopher D Todd. Competition for space in encrusting bryozoan assemblages: the influence of encounter angle, site and year. *Journal of the Marine Biological Association of the United Kingdom*, 74(3):603–622, 1994.
- [14] David KA Barnes. Low levels of colonisation in antarctica: the role of bryozoans in early community development. pages 19–28, 1996.

- [15] Piotr Kuklinski, Piotr Balazy, Joanne Porter, Jennifer Loxton, Marta Ronowicz, and Adam Sokołowski. Experimental apparatus for investigating colonization, succession and related processes of rocky bottom epifauna. *Continental Shelf Research*, 233:104641, 2022.
- [16] Martin Edge. *The underwater photographer*. Routledge, 2012.
- [17] JU Grobbelaar. *Turbidity*. In: *Encyclopedia of Inland Waters*. Elsevier, 2009.
- [18] M Zajaczkowski, W Szczucinski, and Ryszard Bojanowski. Recent changes in sediment accumulation rates in adventfjorden, svalbard. *Oceanologia*, 46(2), 2004.
- [19] Marlena Szeligowska, Emilia Trudnowska, Rafał Boehnke, Anna Maria Dąbrowska, Katarzyna Dragańska-Deja, Kajetan Deja, Mirosław Darecki, and Katarzyna Błachowiak-Samołyk. The interplay between plankton and particles in the isfjorden waters influenced by marine-and land-terminating glaciers. *Science of the Total Environment*, 780:146491, 2021.
- [20] Eric W Deutsch. File formats commonly used in mass spectrometry proteomics. *Molecular & cellular proteomics*, 11(12):1612–1621, 2012.
- [21] Piotr Balazy. Polar night diving—lessons learned from the past four seasons. *FOG-Freiberg Online Geoscience*, 58, 2021.
- [22] P Bałazy, P Kukliński, and M Włodarska-Kowalczyk. Scientific diving in polar regions—the example of ecological studies at the institute of oceanology, polish academy of sciences. *Polish Hyperbaric Research*, 46(1):65–84, 2013.
- [23] Gonzalo Bravo, Juan Pablo Livore, and Gregorio Bigatti. Monitoring rocky reef biodiversity by underwater geo-referenced photoquadrats. pages 17–24, 2021.
- [24] Gail V Ashton, Simon A Morley, David KA Barnes, Melody S Clark, and Lloyd S Peck. Warming by 1 c drives species and as-

- semblage level responses in antarctica's marine shallows. *Current Biology*, 27(17):2698–2705, 2017.
- [25] Google arts & culture. pixel. <https://artsandculture.google.com/entity/pixel/m05x50?hl=en>.
- [26] David A Bowden. Quantitative characterization of shallow marine benthic assemblages at ryder bay, adelaide island, antarctica. *Marine Biology*, 146:1235–1249, 2005.
- [27] Colin JM Martin and Edward A Martin. An underwater photomosaic technique using adobe photoshop™. *International Journal of Nautical Archaeology*, 31(1):137–147, 2002.
- [28] H Van Rein, David S Schoeman, CJ Brown, R Quinn, and J Breen. Development of low-cost image mosaics of hard-bottom sessile communities using scuba: comparisons of optical media and of proxy measures of community structure. *Journal of the Marine Biological Association of the United Kingdom*, 92(1):49–62, 2012.
- [29] Joseph R Pawlik, Roy A Armstrong, Stephanie Farrington, John Reed, Sara Rivero-Calle, Hanumant Singh, Brian K Walker, and Jason White. Comparison of recent survey techniques for estimating benthic cover on caribbean mesophotic reefs. *Marine Ecology Progress Series*, 686:201–211, 2022.
- [30] Chloe A Game. Weibull tone mapping for underwater imagery. In *Color and Imaging Conference*, volume 28, pages 156–161. Society for Imaging Science and Technology, 2020.
- [31] Ander Zuazo, Jordi Grinyó, Vanesa López-Vázquez, Erik Rodríguez, Corrado Costa, Luciano Ortenzi, Sascha Flögel, Javier Valencia, Simone Marini, Guosong Zhang, et al. An automated pipeline for image processing and data treatment to track activity rhythms of paragorgia arborea in relation to hydrographic conditions. *Sensors*, 20(21):6281, 2020.
- [32] Caroline A Schneider, Wayne S Rasband, and Kevin W Eliceiri. Nih image to imagej: 25 years of image analysis. *Nature methods*, 9(7):671–675, 2012.

- [33] Adobe systems incorporated. adobe photoshop cc scripting guide, 2013.
- [34] Kakani Katija, Eric Orenstein, Brian Schlining, Lonny Lundsten, Kevin Barnard, Giovanna Sainz, Oceane Boulais, Megan Cromwell, Erin Butler, Benjamin Woodward, et al. Fathomnet: A global image database for enabling artificial intelligence in the ocean. *Scientific reports*, 12(1):15914, 2022.
- [35] Simone Marini, Federico Bonofiglio, Lorenzo P Corgnati, Andrea Bordone, Stefano Schiaparelli, and Andrea Peirano. Long-term automated visual monitoring of antarctic benthic fauna. *Methods in Ecology and Evolution*, 13(8):1746–1764, 2022.
- [36] A Romero-Ramirez, A Grémare, Guillaume Bernard, Ludovic Pascal, Olivier Maire, and JC Duchêne. Development and validation of a video analysis software for marine benthic applications. *Journal of Marine Systems*, 162:4–17, 2016.
- [37] Google developers. machine learning glossary. <https://developers.google.com/machine-learning/glossar>.
- [38] Martín Abadi, Ashish Agarwal, Paul Barham, Eugene Brevdo, Zhifeng Chen, Craig Citro, Greg S Corrado, Andy Davis, Jeffrey Dean, Matthieu Devin, et al. Tensorflow: Large-scale machine learning on heterogeneous distributed systems. 2016.

Chapter 3

Ancient environmental genomics: An introduction

NGOC-LOI NGUYEN

Institute of Oceanology, Polish Academy of Sciences,
Powstańców Warszawy 55, 81-712 Sopot, Poland

3.1 Introduction

Environmental DNA (*eDNA*) obtained from ancient samples such as sediments, ice or water are valuable data sources for a wide range of disciplines in past and present biodiversity and biogeography [1–4]. Within the field of ancient metagenomics, the number of published genetic datasets has risen dramatically in recent years and have become an increasingly powerful tool to investigate wide-ranging topics [5]. However, the ancient environmental metagenomics remains many issues that should be to be addressed relating to ancient DNA (*aDNA*) such as degraded nature, incomplete reference databases, sensitivity to contamination by modern DNA [6–8]. This review aims to provide an overview of the use of ancient metagenomics in large-scale ecological and evolutionary studies of individual taxa and communities of both microbes and eukaryotes and illustrate the limitations, risks, and potentiality of this ancient *eDNA* research via high-throughput sequencing (HTS) technologies. Further, paleogenetic and paleogenomics will provide diverse insights into studying evolution and how the present world came to be.

3.2 Ancient *eDNA* and environmental metagenomics

Generally, *eDNA* was extracted from ancient samples extremely fragmented and chemically modified depending on the sample types [6]. Typically, the size of ancient *eDNA* fragments is from 70 base pairs (bp) to less than 100 bp long [9] and with ends impacted by cytosine deamination [10]. Only in a few cases, where extraordinary preservation such as Antarctic conditions, for example, 500 bp of *aDNA* were recovered from lake sediment [11], respectively. These conditions generally feature anoxic, cold and dry conditions [6]. In the context of isolating *aDNA* from environmental samples, environmental *aDNA* including sedimentary ancient DNA (or *seDNA*) is used widely and applies to DNA isolated from sedimentary deposits in lake cores [12–14], marine [15, 16], cave [17–19], ancient forest [20], permafrost [13, 21–23], tropical swamp [24],

peat [25]. However, there is potential for many other materials to provide information about the past via *a*DNA analysis as basal ice [20], glacial soil [26], silt-soaked [27]. Analysis of *a*DNA datasets, when combined with traditional proxy results, appears to complement each other, revealing a greater diversity of species than utilizing the methodologies independently [15, 28, 29]. Therefore, *a*DNA should be considered as a complementary, rather than alternative, approach to assays of more traditional established methods [3, 30].

The metagenomics of ancient environmental DNA can be broadly defined as the study of the total genetic content of samples that have degraded over time from several hundred to hundred-thousand years [5, 31]. Despite an extensive application including studies of genome reconstruction of specific microbial taxa [12, 32], host-associated microbial communities [33, 34], and environmental reconstructions using *seda*DNA [5, 24, 35], the major source of ancient *e*DNA has been almost entirely limited to inventorying taxa through time by using DNA metabarcoding approach [15, 16, 36, 37]. Recent advances of next-generation sequencing (NGS), massively parallel or deep sequencing technology, have the potential to radically change this situation, from sequencing of millions of short DNA fragments to generating datasets of genome-scale from extant and extinct species by bioinformatics analyses [12, 13, 32, 37].

3.3 The problem of environmental ancient DNA

Despite recent methodological strategies for *a*DNA extraction, Polymerase Chain Reaction (PCR) and/or sequencing, the study of *a*DNA could be negatively affected by the applicability and the outcome by several inherent technical issues. Part of the challenge is the fact that ancient samples are often rare and precious materials, such as low DNA quantities, DNA damage, high fragmentation, and contamination with modern sources [6]. In general, the ancient *e*DNA sample processing and analysis should be processed with practical recommendations for ancient DNA research to prevent contamination, reviewed in Capo *et al.*, 2021 [35] for lake sediment

cores and Armbricht *et al.*, 2019 [8] for marine sediment cores.

The current *a*DNA extraction protocols were not very different from the protocols used to obtain DNA from environmental settings including silica-based, alcoholic, and phenol-chloroform protocols [22, 38, 39]. For the molecular analyses, the yield and integrity of the recovered *a*DNA obtained will influence the reliability of subsequent results. Therefore, extraction protocols of *a*DNA should be carefully considered and adapted depending on the physical and chemical properties of sediments, DNA-substrates interaction, or target organisms [8, 15, 40, 41]. Further, quick, simple and direct DNA extraction procedures are needed for use in regular analysis of *a*DNA.

DNA damage alters the base-pairing properties of individual bases and is vastly over-represented in *a*DNA sequences. This increased rate of polymerase misincorporation errors and therefore sequencing errors by incorporating wrong nucleotides opposite modified bases [42, 43]. During PCR, DNA damages cause blocking primer binding/DNA polymerase progression, preventing the amplification of the templates, or hydrolysis of the phosphodiester bond, resulting in a single-strand break [44–46]. For instance, the majority of errors give by deamination of cytosine to uracil, which pairs up with adenine instead of guanine, leading to thymine to cytosine transitions [45–47]. However, well-characterized degradation features of *a*DNA i.e., damage patterns and high fragmentation, allow us to authenticate 'true' *a*DNA sequences.

3.4 How to study ancient metagenomic

The application of several technologies, from PCR and the earlier methods, including Sanger sequencing, to HTS, also known as Next-Generation Sequencing (NGS) [48] for short-read (shotgun) sequencing [49] or long-read sequencing, dramatically started a new revolution in ancient DNA research (Fig. 3.1). While traditional PCR methods could only amplify a small number of specific target sequences, HTS combines amplification and sequencing of up to several billions of individual DNA library templates at a time.

DNA/RNA metabarcoding approach is an extension of DNA barcoding, which relies on HTS technologies [36, 50–53]. Furthermore, HTS can sequence shorter DNA fragments – shotgun [37] and even recover whole genome sequences for the study of paleogenomics [12, 54, 55]. These technologies generate large quantities of highly accurate DNA sequences at lower costs than it was possible by using first-generation sequencing technologies.

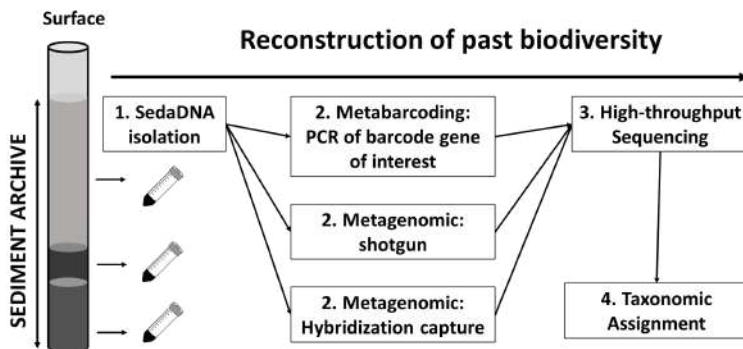


Fig. 3.1: Conceptual workflow of ancient metagenomic approach applied to DNA preserved in environmental archives (e.g., marine and freshwater sediment cores) to reconstruct the past diversity.

In brief in Fig. 3.1, two main approaches to the study of *a*DNA are metabarcoding, the taxonomic identification of the community via analysis of short DNA sequences of one or a few genes, and metagenomics, the analysis of total DNA of the community via whole-genome sequencing. For workflow of the wet laboratory, total DNA is initially isolated from the sample, for example, sediment cores. Next, the DNA metabarcoding standard steps include PCR amplification, library preparation, and sequencing followed by bioinformatic analyses. Depending on the targeted organisms, the specific primers are used to amplify DNA fragments, e.g., the mitochondrial COI region [56], foraminiferal 37f hypervariable region [57–59], and the internal transcribed spacer (ITS) region [60]. For distinguishing samples during bioinformatic processing, specific tags or indexes are added using ligation or other PCR-round. After quantification and normalization steps, the final library is then sequenced on one

of the various available sequencing platforms, e.g., Illumina, Ion Torrent, PacBio, or Oxford Nanopore. In contrast, after collecting suitable samples under the guideline of *a*DNA research, the wet lab workflow for (shotgun) metagenomics can be roughly divided into three steps: DNA extraction, library preparation, and sequencing, without PCR.

3.4.1 Metabarcoding and its limitations

To date, most paleoecological *a*DNA investigations have employed the widely used DNA metabarcoding method, usually, with a focus on a particular organismal group [61]. DNA metabarcoding represents a molecular approach to contemporary taxonomy and identification, e.g., plant [50, 62–65], fungi [60], foraminifera [57, 58], metazoan [56, 66, 67]. The PCR-metabarcoding approach uses primer pairs to target and maximize portions of the hypervariable regions of the phylogenetic marker genes. Amplicons from separate samples are then given molecular barcodes, pooled together, and sequenced by amplicon-based HTS approaches. Fragments of *a*DNA are analyzed with a bioinformatics pipeline and identified from environmental archives, by comparison, them against sequences of reference database taken from modern reference organisms [29, 36, 68, 69].

However, metabarcoding which is applied to environmental *a*DNA is complicated by its natural degradation. The PCR-based approach for sequencing can generate incorrect sequence data from *a*DNA for several reasons. The total amplified sequence count is likely to reflect the original abundance of different DNA sequences in the sample. Damages of *a*DNA could inhibit DNA polymerase progression or prevent primers from binding to templates during PCR. The *a*DNA fragments are extremely short and low-yields, while preferential random amplification is longer or requires abundant DNA molecules. As a result, a lot of PCR cycles are needed, and false-positive findings are more frequent, and heavily biased towards well-preserved or more abundant sequences, possibly from present-day DNA contamination during the first few cycles [37, 70]. It can be induced predictably biased in multi-template PCR and significantly distort the final output. To solve this problem, PCRs

can be repeated independently and increase the total number of replicates for each sample as well as using negative controls should be applied [71]. This approach makes short and rare sequences more likely to be identified than if only one replicate were used since they are likely to be missed in a single PCR but should be expected in one or more of the repeat PCRs. Further, based on using genetic markers in molecular studies of previous paleo-microbiome research, the length of taxonomic marker genes is a major cause of differential amplification resulting in a taxonomic bias in ancient reconstructions [72].

3.4.2 Shotgun sequencing and Whole Genome Sequencing

Shotgun sequencing is the untargeted (shotgun) sequencing of all genetic material (metagenomics) present in a sample, which has the potential to look for population genomic variation from multi-taxon mixtures and independent of DNA fragment size [36, 72]. Compared to metabarcoding, the shotgun approach is less subject to bias introduced by laboratory processing, ever-reducing sequencing costs. Generally, shotgun sequencing randomly breaks DNA sequences of the entire chromosome or entire genome into many small fragments and reassembles the sequences by computers via observing the overlapping sequences or regions. The shotgun approach can detect this genomic variation of the population by utilizing extensive intraspecific genomic reference datasets [73, 74] or assembling de novo genomes [75, 76]. Furthermore, the whole-genome shotgun (WGS) method entails sequencing many overlapping DNA fragments in parallel and then using a computer to assemble the small fragments into larger contigs and, eventually, chromosomes within a short period. NGS has also been used to obtain RNA and pathogen genome sequences from ancient plant remains [77]. The adoption of NGS technologies significantly expanded the range of *a*DNA studies possible, enabling the analysis of full chloroplast [54, 78], and mitochondrial and nuclear genomes [79, 80] from ancient samples. For instance, chloroplast and mitochondrial genomes of single-celled microalgae (*Nannochloropsis limnetica*) were successfully reconstruc-

ted from 20 000-year-old lake sediments [12].

Shotgun sequencing is a faster method and cheaper to carry out compared with traditional sequencing. Usefully, the advent of the shotgun approach permits statistical data analyses to detect specific substitutions that are normally present at the ends of ancient DNA fragments, therefore confirming whether a sequence or set of sequences is relatively ancient and not modern contamination, as well as improving the specificity and sensitivity of taxonomic identification [81, 82]. In some cases, as for eukaryotes in *seadDNA*, if the targeted DNA is rare compared to the total genomic DNA, producing large numbers of short sequencing reads [83] is required to recover sufficient genetic information and perform meaningful statistical analyses, particularly useful for *aDNA* analysis for its fragmentation and degradation [84]. Usefully, the ends of older sequences retrieved using a shotgun approach will show deamination damage, which can confirm whether a sequence or set of sequences is relatively ancient and not modern contamination. Although whole ancient genomes are becoming more readily accessible, mitochondrial [13, 85, 86] or chloroplast [12, 54, 78] genomes are an alternative choice in *aDNA* studies dealing with samples with high DNA degradation, and low DNA yields. Before sequencing, another alternative option applies the hybridization capture technique [78, 87]. The constraint of shotgun sequencing might be solved by using the hybridization capture approach before sequencing to enrich the DNA of the targeted species in the samples. To do this, small segments of DNA from the species and target sites of interest can be used as baits, with the matching sites of interest in ancient DNA libraries being hybridized. This technique, originally developed for modern DNA, is commonly applied in ancient DNA studies, particularly for use on single specimens [88] and with a focus on mammals, mostly using mitochondrial DNA [89, 90], chloroplast and nuclear DNA [78, 91–93], cave sediments [19], permafrost samples [22].

3.4.3 Bioinformatics considerations

Now the shotgun approach provides an alternative approach to metabarcoding for determining for taxonomic and functional profiling of metagenome-assembled genomes. The amount of genetic data has risen exponentially and vast amounts of that are mostly uploaded to and stored on public archives, for example, European Bioinformatic Institute's (EBI) European Nucleotide Archive (ENA, <https://www.ebi.ac.uk/ena/>) or the US National Center for Biotechnology Information (NCBI)'s Sequence Read Archive (SRA, <https://www.ncbi.nlm.nih.gov/sra>). However, it brings huge challenges at the stage of bioinformatics for its analysis. A vast of bioinformatics tools, protocols and studies have been introduced to improve efficiency in analyzing ancient metagenomic data. Bioinformatics tools designed for *a*DNA metagenomics as mapDamage [94–96], PyDamage [97] or open-sourced/mapping guidelines pipeline [98, 99] for estimating DNA damage, SourceTracker [100] for identifying the proportions of endogenous and contaminant signals in each sample; resolving the sequencing errors [96, 101]; MEGAN [102, 103], PIA [104] for taxonomic identification; KEGG [105], EGGnog [106], SEED [107] protein databases for functional profiles can be analysed in MEGAN, reference-free alternative approaches based on k-mer counts [108] to annotate metagenomes. However, differences between metagenomic analysis pipelines produce systematic biases [24], which will require the development of more accurate analysis pipelines for ancient DNA.

Nevertheless, several issues currently limit the shotgun sequencing approach. Cytosine deamination patterns of *seda*DNA molecules impede *de novo* assembly of contigs [10, 109]. The limitation of sufficiently curated genome-scale reference data substantially reduces the potential for success of the bioinformatic analyses with metagenomic data, for example, plants [77, 110], and eukaryotic [111, 112]. The large fraction of taxa present in the environment, but not represented in databases is still problematic. In these cases, metagenomic data can vary in content across samples from the same or similar environments. In contrast, there are more than 130 000 genome or near-complete sequences available from different phyla

that have been sequenced along with a variety of microorganisms, including archaea, fungi, and viruses [113–115]. Based on the annotated reference genomes or clade-specific [116] or universal markers [117], appropriate normalization by genome size [55], and taxon relative abundances can be estimated. This led to the development of the field of paleomicrobiology [1, 32], to the analysis of deposited microbial DNA to study microbial diversity, ecology, and evolution in environmental archives.

3.4.4 Applications of ancient environmental metagenomics

The shotgun of *seda*DNA in paleoecology from lake sediment cores combined a multi-proxy approach [14], and marine environments [37, 40], which has provided greater taxonomic resolution and extended the historical record of aquatic ecosystems to centennial or even millennial time scales. These *seda*DNA archives can be used to characterize biodiversity trends, illuminate past food web dynamics, and reconstruct long-term environmental changes in aquatic ecosystems. As ecology and paleoecology merge, both short-term and long-term trends as a consequence of human actions on aquatic ecosystems have been traced using paleogenomic research in freshwater ecosystems [118–120] and marine sediments [121, 122].

Paleogenomics is a branch of research concerned with reconstructing and analyzing genetic data from extinct organisms. Ancient genomes may be used to explore the evolution of present species in great detail by sequencing ancient DNA preserved in subfossil remains [54, 123] or environmental archives [1, 12]. By analyzing large-scale environmental DNA metagenomic study of ancient plant and mammal communities, tracking the ancient population origins, movements and interrelationships, the evolutionary genomic changes at both macro- and micro-evolutionary temporal scales of the microbiome, vegetation, animals and Homo species [12, 13], as well as identification of phenotypic features over large temporal and geographical scales [89, 90, 124]. For example, a study on DNA retrieved from Arctic permafrost and lake sediment samples by Wang *et al.* [13] demonstrated that steppe-tundra flora dom-

inated the Arctic during the Last Glacial Maximum, followed by the regional divergence of vegetation during the Holocene epoch. The extinction of several now-extinct megafauna species enabled the survival of some ancient plants and animals. Moreover, analysis of mammoth environmental DNA reveals a previously unsampled mitochondrial lineage. Additionally, the genetic material preserved in sedimentary archives offers a unique way to uncover the role of microorganisms in past ecosystems and their responses to environmental perturbations. Genomic reconstruction of historical and present microbial communities from ancient permafrost samples in Siberian broadened our understanding of biogeochemical changes [32]. Furthermore, this study provides insights into microorganisms' long-term survival strategies from the past paleoenvironment to present-day freezing-temperature conditions.

3.5 Summary

The fields of *a*DNA are increasingly turning to the environmental archives and provide great potential for entire paleoecosystems and paleoclimate reconstructions. As technology advances and procedures are optimized, metagenomic-based approaches, from metabarcoding (amplicon-based) to shotgun and true ancient metagenomics, are part of the next breakthrough in paleogenetic, offering the potential for better species identification and quantitative estimations of their abundances in large-scale biodiversity comparisons over both time and place. Importantly, further basic studies are needed to use a full understanding of its potential and limitations for applications of the use of metagenomics for ancient *e*DNA.

Acknowledgement

The research was financially supported by the Norwegian Financial Mechanism for 2014-2021, project No. 2019/34/H/ST10/00682, full title: "Sedimentary ancient DNA – a new proxy to investigate the impact of environmental change on past and present biodiversity in Nordic Seas".

Bibliography

- [1] E. Capo. Environmental paleomicrobiology: using dna preserved in aquatic sediments to its full potential. *Environmental Microbiology*, 2022.
- [2] J. Pawlowski. Environmental dna for biomonitoring. *Molecular Ecology*, 30(13):2931–2936, 2021.
- [3] K.M. Ruppert, R.J. Kline, and M.S. Rahman. Past, present, and future perspectives of environmental dna (edna) metabarcoding: A systematic review in methods, monitoring, and applications of global edna. *Global Ecology and Conservation*, 17:00547, 2019.
- [4] P. Taberlet. Environmental dna: For biodiversity research and monitoring, 2018.
- [5] J.A. Fellows Yates. *Community-curated and standardised metadata of published ancient metagenomic samples with AncientMetagenomeDir*, volume 8. Scientific Data, 2021.
- [6] L. Orlando. Ancient dna analysis. *Nature Reviews Methods Primers*, 1(1):14, 2021.
- [7] M.W. Pedersen. Ancient and modern environmental dna. *Biol Sci*, 370(1660):20130383, 2015.
- [8] L.H. Armbrrecht. Ancient dna from marine sediments: Precautions and considerations for seafloor coring, sample handling and data generation. *Earth-Science Reviews*, 196:102887, 2019.

- [9] L. Armbrrecht. An optimized method for the extraction of ancient eukaryote dna from marine sediments. *Molecular Ecology Resources*, 20(4):906–919, 2020.
- [10] L. Orlando, M.T.P. Gilbert, and E. Willerslev. Reconstructing ancient genomes and epigenomes. *Nature Reviews Genetics*, 16(7):395–408, 2015.
- [11] M.J.L. Coolen. Combined dna and lipid analyses of sediments reveal changes in holocene haptophyte and diatom populations in an antarctic lake. *Earth and Planetary Science Letters*, 223(1):225–239, 2004.
- [12] Y. Lammers, P.D. Heintzman, and I.G. Alsos. Environmental palaeogenomic reconstruction of an ice age algal population. *Communications Biology*, 4(1):220, 2021.
- [13] Y. Wang. Late quaternary dynamics of arctic biota from ancient environmental genomics. *Nature*, 600(7887):86–92, 2021.
- [14] M.W. Pedersen. Postglacial viability and colonization in north america’s ice-free corridor. *Nature*, 537(7618):45–49, 2016.
- [15] S. Schepper. The potential of sedimentary ancient dna for reconstructing past sea ice evolution. *ISME J*, 13(10):2566–2577, 2019.
- [16] H.H. Zimmermann. Sedimentary ancient dna from the subarctic north pacific: How sea ice, salinity, and insolation dynamics have shaped diatom composition and richness over the past 20,000 years. *Paleoceanography and Paleoclimatology*, 36(4):2020 004091, 2021.
- [17] J. Haile. Ancient dna chronology within sediment deposits: Are paleobiological reconstructions possible and is dna leaching a factor? *Molecular Biology and Evolution*, 24(4):982–989, 2007.

- [18] D. Haouchar. Thorough assessment of dna preservation from fossil bone and sediments excavated from a late pleistocene-holocene cave deposit on kangaroo island, south australia. *Quaternary Science Reviews*, 84:56–64, 2014.
- [19] V. Slon. Neandertal and denisovan dna from pleistocene sediments. *Science*, 356(6338):605–608, 2017.
- [20] E. Willerslev. Ancient biomolecules from deep ice cores reveal a forested southern greenland. *Science*, 317(5834):111–114, 2007.
- [21] E. Willerslev. Diverse plant and animal genetic records from holocene and pleistocene sediments. *Science*, 300(5620):791–795, 2003.
- [22] T.J. Murchie. Optimizing extraction and targeted capture of ancient environmental dna for reconstructing past environments using the palaeochip arctic-1.0 bait-set. *Quaternary Research*, 99:305–328, 2020.
- [23] E. Willerslev. Fifty thousand years of arctic vegetation and megafaunal diet. *Nature*, 506(7486):47–51, 2014.
- [24] R. Dommain. The challenges of reconstructing tropical biodiversity with sedimentary ancient dna: A 2200-year-long metagenomic record from bwindi impenetrable forest, uganda. *Frontiers in Ecology and Evolution*, page 8, 2020.
- [25] Y. Suyama, U. Gunnarsson, and L. Parducci. Analysis of short dna fragments from holocene peatmoss samples. *The Holocene*, 18(6):1003–1006, 2008.
- [26] B.A. Gould. Evidence of a high-andean, mid-holocene plant community: An ancient dna analysis of glacially preserved remains. *American Journal of Botany*, 97(9):1579–1584, 2010.
- [27] T. Jorgensen. A comparative study of ancient sedimentary dna, pollen and macrofossils from permafrost sediments of northern siberia reveals long-term vegetational stability. *Molecular Ecology*, 21(8):1989–2003, 2012.

- [28] J. Pawlowska. Ancient dna sheds new light on the svalbard foraminiferal fossil record of the last millennium. *Geobiology*, 12(4):277–88, 2014.
- [29] M.E. Edwards. Metabarcoding of modern soil dna gives a highly local vegetation signal in svalbard tundra. *The Holocene*, 28(12):2006–2016, 2018.
- [30] M.W. Pedersen. A comparative study of ancient environmental dna to pollen and macrofossils from lake sediments reveals taxonomic overlap and additional plant taxa. *Quaternary Science Reviews*, 75:161–168, 2013.
- [31] C. Warinner. A robust framework for microbial archaeology. *Annual Review of Genomics and Human Genetics*, 18(1):321–356, 2017.
- [32] R. Liang. Genomic reconstruction of fossil and living microorganisms in ancient siberian permafrost. *Microbiome*, 9(1):110, 2021.
- [33] C. Warinner. Ancient human microbiomes. *Journal of Human Evolution*, 79:125–136, 2015.
- [34] M.C. Wibowo. Reconstruction of ancient microbial genomes from the human gut. *Nature*, 594(7862):234–239, 2021.
- [35] E. Capo. Lake sedimentary dna research on past terrestrial and aquatic biodiversity: Overview and recommendations. *Quaternary*, 4(1):6, 2021.
- [36] P. Taberlet. Towards next-generation biodiversity assessment using dna metabarcoding. *Mol Ecol*, 21(8):2045–50, 2012.
- [37] L. Armbrrecht. Paleo-diatom composition from santa barbara basin deep-sea sediments: a comparison of 18s-v9 and diatrbel metabarcoding vs shotgun metagenomics. *ISME Communications*, 1(1):66, 2021.
- [38] R.W. Hagan. Comparison of extraction methods for recovering ancient microbial dna from paleofeces. *American Journal of Physical Anthropology*, 171(2):275–284, 2020.

- [39] J.K. Pearman. Comparing sediment dna extraction methods for assessing organic enrichment associated with marine aquaculture. *PeerJ*, 8:10231, 2020.
- [40] W.D. Orsi. Climate oscillations reflected within the microbiome of arabian sea sediments. *Sci Rep*, 7(1):6040, 2017.
- [41] M.J. Coolen. Evolution of the plankton paleome in the black sea from the deglacial to anthropocene. *Proc Natl Acad Sci U S A*, 110(21):8609–14, 2013.
- [42] M. Hofreiter. Dna sequences from multiple amplifications reveal artifacts induced by cytosine deamination in ancient dna. *Nucleic Acids Research*, 29(23):4793–4799, 2001.
- [43] S. Paabo. Genetic analyses from ancient dna. *Annu. Rev. Genet*, 38:645–679, 2004.
- [44] A. Torti, M.A. Lever, and B.B. J rgensen. Origin, dynamics, and implications of extracellular dna pools in marine sediments. *Marine Genomics*, 24:185–196, 2015.
- [45] A.W. Briggs. Patterns of damage in genomic dna sequences from a neandertal. *Proceedings of the National Academy of Sciences*, 104(37):14616–14621, 2007.
- [46] J. Dabney, M. Meyer, and S. Paabo. Ancient dna damage. *Cold Spring Harb Perspect Biol*, 5:012567, 2013.
- [47] M.-T. Gansauge and M. Meyer. Selective enrichment of damaged dna molecules for ancient genome sequencing. *Genome research*, 24(9):1543–1549, 2014.
- [48] J. Shendure and H. Ji. Next-generation dna sequencing. *Nature Biotechnology*, 26(10):1135–1145, 2008.
- [49] C. Quince. Shotgun metagenomics, from sampling to analysis. *Nature Biotechnology*, 35(9):833–844, 2017.

- [50] E.E. Dormontt. Advancing dna barcoding and metabarcoding applications for plants requires systematic analysis of herbarium collections—an australian perspective. *Frontiers in Ecology and Evolution*, page 6, 2018.
- [51] F. Lejzerowicz. Eukaryotic biodiversity and spatial patterns in the clarion-clipperton zone and other abyssal regions: Insights from sediment dna and rna metabarcoding. *Frontiers in Marine Science*, 8(536), 2021.
- [52] J. Hirai. Dna/rna metabarcoding and morphological analysis of epipelagic copepod communities in the izu ridge off the southern coast of japan. *ICES Journal of Marine Science*, 78(9):3444–3456, 2021.
- [53] O. Laroche. A cross-taxa study using environmental dna/rna metabarcoding to measure biological impacts of offshore oil and gas drilling and production operations. *Mar Pollut Bull*, 127:97–107, 2018.
- [54] C. Pont. Paleogenomics: reconstruction of plant evolutionary trajectories from modern and ancient dna. *Genome Biology*, 20(1):29, 2019.
- [55] M. Schubert. Characterization of ancient and modern genomes by snp detection and phylogenomic and metagenomic analysis using paleomix. *Nature Protocols*, 9(5):1056–1082, 2014.
- [56] M. Leray. A new versatile primer set targeting a short fragment of the mitochondrial coi region for metabarcoding metazoan diversity: application for characterizing coral reef fish gut contents. *Front Zool*, 10:34, 2013.
- [57] B. Lecroq. Ultra-deep sequencing of foraminiferal microbarcodes unveils hidden richness of early monothalamous lineages in deep-sea sediments. *Proc Natl Acad Sci U S A*, 108(32):13177–82, 2011.

- [58] J. Pawłowski and B. Lecroq. Short rdna barcodes for species identification in foraminifera. *J Eukaryot Microbiol*, 57(2):197–205, 2010.
- [59] J. Pawłowska. Ancient dna sheds new light on the svalbard foraminiferal fossil record of the last millennium. *Geobiology*, 12(4):277–288, 2014.
- [60] L. Talas. *Sedimentary Ancient DNA (sedaDNA) Reveals Fungal Diversity and Environmental Drivers of Community Changes throughout the Holocene in the Present Boreal Lake Lielais Svetinu*, volume 9. Microorganisms, Eastern Latvia, 2021.
- [61] S. Ratnasingham and P.D.N. Hebert. The barcode of life data system (<http://www.barcodinglife.org>). *Molecular Ecology Notes*, 7(3):355–364, 2007.
- [62] P. Taberlet. Power and limitations of the chloroplast trn l (uaa) intron for plant dna barcoding. *Nucleic Acids Research*, 35(3):14– 14, 2006.
- [63] K. Deiner. Environmental dna metabarcoding: Transforming how we survey animal and plant communities. *Mol Ecol*, 26(21):5872–5895, 2017.
- [64] L.H. Voldstad. A complete holocene lake sediment ancient dna record reveals long-standing high arctic plant diversity hotspot in northern svalbard. *Quaternary Science Reviews*, 234:106207, 2020.
- [65] S. Huang. Plant sedimentary ancient dna from far east russia covering the last 28,000 years reveals different assembly rules in cold and warm climates. *Frontiers in Ecology and Evolution*, page 9, 2021.
- [66] I. Capua. Metazoan diversity and seasonality through edna metabarcoding at a mediterranean long-term ecological research site. *ICES Journal of Marine Science*, 78(9):3303–3316, 2021.

- [67] N. Leduc. Comparing edna metabarcoding and species collection for documenting arctic metazoan biodiversity. *Environmental DNA*, 1(4):342–358, 2019.
- [68] X. Cao. Sedimentary ancient dna metabarcoding delineates the contrastingly temporal change of lake cyanobacterial communities. *Water Research*, 183:116077, 2020.
- [69] L.S. Epp. New environmental metabarcodes for analysing soil dna: potential for studying past and present ecosystems. *Mol Ecol*, 21(8):1821–33, 2012.
- [70] G. Webster. Assessment of bacterial community structure in the deep sub-seafloor biosphere by 16s rdna-based techniques: a cautionary tale. *Journal of Microbiological Methods*, 55(1):155–164, 2003.
- [71] G.F. Ficetola. Replication levels, false presences and the estimation of the presence/absence from edna metabarcoding data. *Molecular Ecology Resources*, 15(3):543–556, 2015.
- [72] K.A. Ziesemer. Intrinsic challenges in ancient microbiome reconstruction using 16s rrna gene amplification. *Scientific Reports*, 5(1):16498, 2015.
- [73] D.T. Truong. Microbial strain-level population structure and genetic diversity from metagenomes. *Genome Research*, 27(4):626–638, 2017.
- [74] D. Albanese and C. Donati. Strain profiling and epidemiology of bacterial species from metagenomic sequencing. *Nature Communications*, 8(1):2260, 2017.
- [75] C. Quince. Desman: a new tool for de novo extraction of strains from metagenomes. *Genome Biology*, 18(1):181, 2017.
- [76] S. Nurk. metaspades: a new versatile metagenomic assembler. *Genome research*, 27(5):824–834, 2017.
- [77] O. Estrada. Ancient plant dna in the genomic era. *Nature Plants*, 4(7):394–396, 2018.

- [78] L. Schulte. Hybridization capture of larch (*larix mill.*) chloroplast genomes from sedimentary ancient dna reveals past changes of siberian forest. *Molecular Ecology Resources*, 21(3):801–815, 2021.
- [79] M.A. Diroma. New insights into mitochondrial dna reconstruction and variant detection in ancient samples. *Frontiers in Genetics*, page 12, 2021.
- [80] B. Vernot. Unearthing neanderthal population history using nuclear and mitochondrial dna from cave sediments. *Science*, 372(6542):1667, 2021.
- [81] S. Overballe-Petersen, L. Orlando, and E. Willerslev. Next-generation sequencing offers new insights into dna degradation. *Trends in Biotechnology*, 30(7):364–368, 2012.
- [82] J. Binladen. Assessing the fidelity of ancient dna sequences amplified from nuclear genes. *Genetics*, 172(2):733–741, 2006.
- [83] Z. Yin. Computing platforms for big biological data analytics: Perspectives and challenges. *Computational and Structural Biotechnology Journal*, 15:403–411, 2017.
- [84] R.M. Gutaker and H.A. Burbano. Reinforcing plant evolutionary genomics using ancient dna. *Current Opinion in Plant Biology*, 36:38–45, 2017.
- [85] F. Almathen. Ancient and modern dna reveal dynamics of domestication and cross-continental dispersal of the dromedary. *Proceedings of the National Academy of Sciences*, 113(24):6707–6712, 2016.
- [86] M. Meyer. A mitochondrial genome sequence of a hominin from sima de los huesos. *Nature*, 505(7483):403–406, 2014.
- [87] L. Armbricht. Hybridisation capture allows dna damage analysis of ancient marine eukaryotes. *Scientific Reports*, 11(1):3220, 2021.

- [88] M.C. Avila-Arcos. Application and comparison of large-scale solution-based dna capture-enrichment methods on ancient dna. *Scientific Reports*, 1(1):74, 2011.
- [89] J. Dabney. Complete mitochondrial genome sequence of a middle pleistocene cave bear reconstructed from ultrashort dna fragments. *Proceedings of the National Academy of Sciences*, 110(39):15758–15763, 2013.
- [90] J. Enk. Mammuthus population dynamics in late pleistocene north america: Divergence, phylogeography, and introgression. *Frontiers in Ecology and Evolution*, page 4, 2016.
- [91] L. Parducci. Ancient plant dna in lake sediments. *New Phytologist*, 214(3):924–942, 2017.
- [92] L. Kistler. Transoceanic drift and the domestication of african bottle gourds in the americas. *Proceedings of the National Academy of Sciences*, 111(8):2937–2941, 2014.
- [93] S. Schmid. Hyrad-x, a versatile method combining exome capture and rad sequencing to extract genomic information from ancient dna. *Methods in Ecology and Evolution*, 8(10):1374–1388, 2017.
- [94] A. Ginolhac. mapdamage: testing for damage patterns in ancient dna sequences. *Bioinformatics*, 27(15):2153–2155, 2011.
- [95] H. Jonsson. mapdamage2.0: fast approximate bayesian estimates of ancient dna damage parameters. *Bioinformatics*, 29(13):1682–1684, 2013.
- [96] L. Kistler. A new model for ancient dna decay based on paleogenomic meta-analysis. *Nucleic Acids Research*, 45(11):6310–6320, 2017.
- [97] M. Borry. Pydamage: automated ancient damage identification and estimation for contigs in ancient dna de novo assembly. *PeerJ*, 9:11845, 2021.

- [98] T.C. Collin. An open-sourced bioinformatic pipeline for the processing of next-generation sequencing derived nucleotide reads: Identification and authentication of ancient metagenomic dna, 2020.
- [99] W. Xu. An efficient pipeline for ancient dna mapping and recovery of endogenous ancient dna from whole-genome sequencing data. *Ecology and Evolution*, 11(1):390–401, 2021.
- [100] D. Knights. Bayesian community-wide culture-independent microbial source tracking. *Nature Methods*, 8(9):761–763, 2011.
- [101] M. Schubert. Improving ancient dna read mapping against modern reference genomes. *BMC Genomics*, 13(1):178, 2012.
- [102] D.H. Huson. Megan analysis of metagenomic data. *Genome research*, 17(3):377–386, 2007.
- [103] D.H. Huson and N. Weber. Microbial community analysis using megan. *Methods in enzymology*, pages 465–485, 2013.
- [104] B. Cribdon. Pia: More accurate taxonomic assignment of metagenomic data demonstrated on sedadna from the north sea. *Frontiers in Ecology and Evolution*, 8(84), 2020.
- [105] M. Kanehisa. Kegg for integration and interpretation of large-scale molecular data sets. *Nucleic Acids Research*, 40(D1):109– 114, 2011.
- [106] S. Powell. egglog v3.0: orthologous groups covering 1133 organisms at 41 different taxonomic ranges. *Nucleic Acids Research*, 40(D1):284– 289, 2011.
- [107] R. Overbeek. The subsystems approach to genome annotation and its use in the project to annotate 1000 genomes. *Nucleic Acids Research*, 33(17):5691–5702, 2005.
- [108] R.A. Edwards. Real time metagenomics: Using k-mers to annotate metagenomes. *Bioinformatics*, 28(24):3316–3317, 2012.

- [109] K. Prufer. Computational challenges in the analysis of ancient dna. *Genome Biology*, 11(5):47, 2010.
- [110] G.P. Tiley, C. Ane, and J.G. Burleigh. Evaluating and characterizing ancient whole-genome duplications in plants with gene count data. *Genome Biology and Evolution*, 8(4):1023–1037, 2016.
- [111] S.C. Dawson and L.K. Fritz-Laylin. Sequencing free-living protists: the case for metagenomics. *Environmental Microbiology*, 11(7):1627–1631, 2009.
- [112] G. Glockner. The genome of the foraminiferan *reticulomyxa filosa*. *Current Biology*, 24(1):11–18, 2014.
- [113] S. Mukherjee. Genomes online database (gold) v.7: upyears and new features. *Nucleic Acids Research*, 47(D1):649–659, 2018.
- [114] M. Royo-Llonch. Compendium of 530 metagenome-assembled bacterial and archaeal genomes from the polar arctic ocean. *Nature Microbiology*, 6(12):1561–1574, 2021.
- [115] L.A. Arriola, A. Cooper, and L.S. Weyrich. Palaeomicrobiology: Application of ancient dna sequencing to better understand bacterial genome evolution and adaptation. *Frontiers in Ecology and Evolution*, page 8, 2020.
- [116] N. Segata. Metagenomic microbial community profiling using unique clade-specific marker genes. *Nature Methods*, 9(8):811–814, 2012.
- [117] S. Sunagawa. Metagenomic species profiling using universal phylogenetic marker genes. *Nature Methods*, 10(12):1196–1199, 2013.
- [118] I. Domaizon. Dna-based methods in paleolimnology: new opportunities for investigating long-term dynamics of lacustrine biodiversity. *Journal of Paleolimnology*, 58(1):1–21, 2017.

- [119] C. Giguet-Covex. New insights on lake sediment dna from the catchment: importance of taphonomic and analytical issues on the record quality. *Scientific Reports*, 9(1):14676, 2019.
- [120] F. Keck. Assessing the response of micro-eukaryotic diversity to the great acceleration using lake sedimentary dna. *Nature Communications*, 11(1):3831, 2020.
- [121] R. Siano. Sediment archives reveal irreversible shifts in plankton communities after world war ii and agricultural pollution. *Current Biology*, 31(12):2682–2689 7, 2021.
- [122] J.L.A. Shaw. Retrospective edna assessment of potentially harmful algae in historical ship ballast tank and marine port sediments. *Molecular Ecology*, 28(10):2476–2485, 2019.
- [123] M. Meyer. Nuclear dna sequences from the middle pleistocene sima de los huesos hominins. *Nature*, 531(7595):504–507, 2016.
- [124] C.-C. Wang. Ancient human genome-wide data from a 3000-year interval in the caucasus corresponds with eco-geographic regions. *Nature Communications*, 10(1):590, 2019.

Chapter 4

The Arctic carbon cycle: Main factors and winter-summer variability

KAMIL REGINIA

Institute of Oceanology, Polish Academy of Sciences,
Powstańców Warszawy 55, 81-712 Sopot, Poland

4.1 Introduction

From the mid-nineteenth century, an increase in the temperature of the atmospheric air has been observed all over the planet. Anthropogenic climate change not only contributes to the temperature anomaly on land but is also observed in the hydrosphere of the entire globe. Climate change caused by the exploitation of natural fossil fuels, along with increased greenhouse gas emissions including carbon dioxide (CO_2), are no longer just a theoretical presumption but a tangible and perhaps irreversible process. The Arctic is the region with a spectacular response to the climate change that has occurred. Over the past decades, the average temperature in this region has increased by more than 2.5 times compared to the global average [1]. One of the consequences of this influx of heat is the loss of the Arctic ice sheet. Over the past 40 years, the area of sea ice has decreased by about 40% [2]. Thanks to paleo-reconstruction studies enable to prove that the increase in temperature observed today had not occurred before in the last 400 years, and that the global reduction of the Arctic ice sheet exceeded all the negative anomalies of the last millennium [3]. One of the forecasts of climate warming, assuming a temperature increase of 2 degrees [4], suggests about a 15% chance in the summer months for conditions with almost no ice and a reduction in the extent of sea ice by about 20% in the winter in the following decades. A drastic inflow of fresh water may disturb the geochemical [5–7] and biological [8, 9] balance of the Arctic Ocean.

The physical, chemical as well as biological properties of the Arctic Ocean, which are the basis for absorbing heat and buffering acidification reactions with atmospheric CO_2 have limits and may be exceeded. In the annual cycle of sea ice formation and melting, the processes of CO_2 absorption may weaken [10, 11]. As a result of increasing temperature and decreasing the amount of nutrients, the solubility and biological uptake of CO_2 in the ocean may also be inhibited [12, 13]. At present, the seasonal ice cover of the Arctic waters moderates the gas exchange between the atmosphere and the ocean. Arctic ocean absorbs carbon dioxide (CO_2) ranging from -66 to -199 Tg C year⁻¹ (1012 g C), contributing 5-14% to the

global balance of CO₂ sinks and sources [14]. In the near future, further loss of sea ice along with the development of phytoplankton may contribute to increased CO₂ absorption by Arctic surface waters [15]. Extending the growing season of phytoplankton contributes to an increase in primary production by 30-60% over a period of several years [16]. However, further acidification of the Arctic Ocean due to the absorption of atmospheric CO₂ may lead to a reduction in primary production. Carbon dioxide easily diffuses through biological membranes, acidifying fluids outside and inside of the cells. Disturbing the acid-base balance inside the cells has a negative effect on oxygen transport, metabolic rate, calcification, protein synthesis and thus, the survival of the organism. Ionic imbalance in the environment can cause the phenomenon of biological amplification of the effects of acidification. The decomposition of a large amount of organic matter increases the release of CO₂, acidifying the bottom layers. Lowering the pH with increasing $p\text{CO}_2$ reduces the ability of marine species to produce shells and other CaCO₃ structures (aragonite, calcite) in the calcification process. These changes are likely to continue to modify the physics, biogeochemistry and ecology of the Arctic Ocean [17, 18]. The Arctic Ocean has a significant impact on the global carbon cycle, and the Arctic carbon cycle is sensitive to global climate change. As one of the most important processes in the circulation of elements in nature, is crucial for the functioning of aquatic ecosystems. Understanding the differences between the summer and winter seasons in the main processes that characterize the carbon cycle in the Arctic Ocean could answer important questions about the future of the region.

4.2 Characteristics of the Arctic Ocean

The Arctic Ocean is one of the smallest and shallowest oceans in the world, with the center at the North Pole. It has the character of a semi-closed reservoir surrounded by land on all sides. The territory of the Arctic Ocean was divided between the USA, Canada, Norway, Greenland, Iceland and Russia. The Arctic Ocean is crossed by two very important transoceanic routes between East

Asia and Europe along the coast of Russia and the Pacific coast of North America through the Canadian Arctic Archipelago. The distinct seasonality of the region along with the abundant long-term or seasonal ice cover is a unique research place for ecologists and climatologists. Changes caused by global warming pose a concern for the future and fate of the unique Arctic ecosystem.

The Arctic Ocean extends from the North Pole of latitude 90°N to about 60°N to south, covering an area of $14\,090\,000\text{ km}^2$. The average depth of the ocean is 987 m with a maximum value of $5\,527\text{ m}$. The total length of the ocean's coastline is $45\,390\text{ km}$. The water volume of the Arctic Ocean is approx. 18.1 million km^3 , which is only 1.4% of the share in the water volume of all oceans. The central part of the Arctic Ocean is divided into several sub-basins by underwater ocean ridges. The Lomonosov Ridge with an average depth of about $1\,500\text{ m}$, running between the Ellesmera Island and the New Siberian Islands, divides the Arctic Ocean into two parts [19]. These are the Eurasian and Canadian basins, also called the Amerasian Basin [20]. The Eurasian Basin is divided into the Amundsen Basin and the Nansen Basin by the underwater Gakkel Ridge, and the Amerasian Basin to the Canadian basin and the Makarov Basin by the ocean ridge Mandeleev and Alpha (Fig. 4.1). More than half of the surface of the Arctic ocean is occupied by the shelves, which constitute only 5% of the total volume of the Arctic ocean [21]. The ocean includes marginal shelf seas such as the Barents, White, Chukchi, Kara, Lincoln, Laptev, East Siberian seas and Hudson Bay along with the seas of ocean basins such as the Greenland, Beaufort, Baffin Sea, separated by the Arctic Archipelago from the Canadian Basin and the Arctic Sea proper. The largest islands in the Arctic Ocean are Greenland, Novaya Zemlya, Spitsbergen, Ellesmere Island, Victoria Island, Banks Island, Baffin Island, Axel Heiberg Island, and Prince of Wales Island. The shape of the ocean floor is one of the key factors determining the course and direction of ocean currents. Bathymetry affects ocean currents, the circulation of ocean waters, the movement of sediments along the slopes, and above all, the distribution of eternal ice in space [22]. The Arctic ice sheet covers the entire Arctic Ocean in winter and has an average thickness of about 2 m . In winter, maximum range

is reached in March and minimum sea ice in September [23].

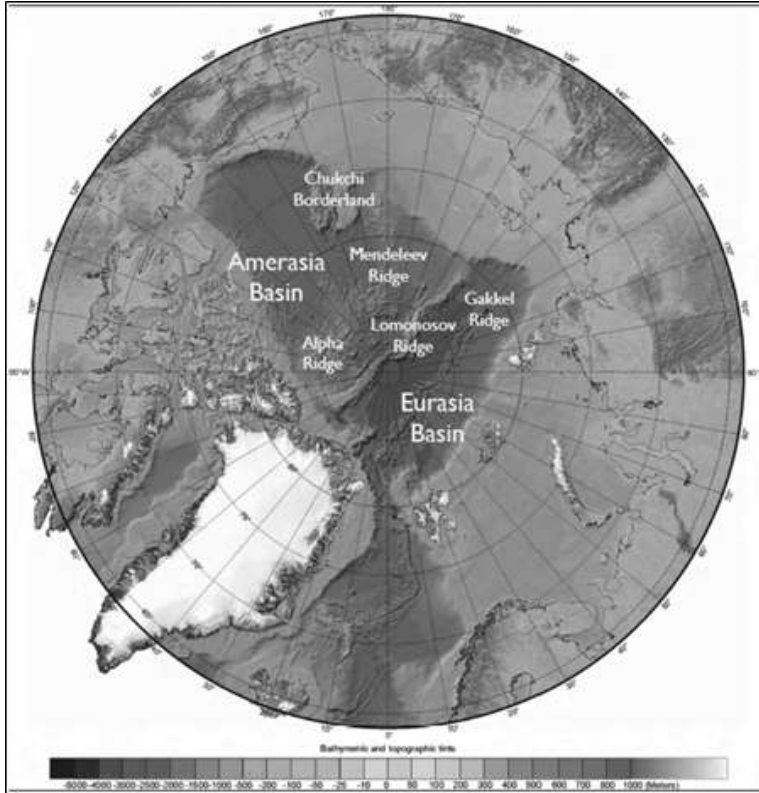


Fig. 4.1: Bathymetry map of Arctic Ocean. Bathymetry from IBCAO 3.0 [24].

The wind blowing on the surface of the ocean along with the difference in temperature and salinity has the greatest impact on the movement of surface waters [25]. The Arctic Ocean is influenced by two major air currents, the ridge of high pressure from Beaufort sea, centered over the Canadian Basin and the ridge of low Icelandic pressure at the ocean's edge. Under the conditions of the weakened Beaufort high and intensified Icelandic low, the ice drifts in the Eurasian Basin, passing from the Laptev Sea towards the Canadian Basin, and then drifting towards the Fram Strait [26]. The mixing rate of warm and cold waters at a low level compared to

non-ice [27] oceans along with weak tidal forces [28] contributes to the maintenance of ice in the Arctic Ocean. The exchange of cold fresh water from the Arctic Ocean and warm salt water from the Atlantic occurs through the Norwegian Sea [29], and more specifically through the Fram Strait and also through the Barents Sea [30]. In turn, the inflow of warm waters from the Pacific follows the only possible route, which is the Bering Strait. From the Arctic, the waters flow in the East Greenland current from the western side of the Fram Strait [31] and the Straits of the Canadian Arctic Archipelago [32]. If the rate of heat exchange between the ocean and the surface layer in contact with the ice increases, it could lead to the complete melting of the ice sheet [33].

4.2.1 Water circulation in the Arctic Ocean

The freshwater cycle, together with the exchange of salt waters and temperature between water bodies, is an important factor in the functioning of the Arctic aquatic ecosystems. The Arctic Ocean receives tributaries from the Atlantic and Pacific Oceans and the northern American and Siberian rivers. Its stratification is primarily determined by salinity (halocline), in which the melting and freezing of sea ice plays a key role in the fresh and salt water cycle [34]. By maintaining the stability of the water column, the halocline isolates surface waters from deep waters. Atlantic water is kept away from direct contact with sea ice, thus reducing ice melting and severe heat loss along with CO₂ emissions to the atmosphere [35].

The warm and salty waters of the Atlantic cross the ridge of Scotland and Greenland entering the Nordic seas guided by the arms of the North Atlantic Gulf Stream (NAC). Then the water masses are transported along the Norwegian Atlantic Current (NWAC) conditioned by the bottom bathymetry [36]. It is divided into the West Spitsbergen Current (WSC) flowing north into the Arctic Ocean through the Fram Strait (Fig. 4.2). It follows the continental slope that splits at the junction of the Yermak plateau and the Spitsbergen continental shelf. Thus, it forms the two arms of Yermak and Svalbard [37]. Part of the WSC orbits westward through the

Fram Strait and mixes with polar waters flowing south [38]. The second branch (NWAC) is the North Cape Current (NCC), which directs the Atlantic waters to the northern shores of Norway, Finland and the Russian Kola Peninsula that make up the Barents Open Sea [39].

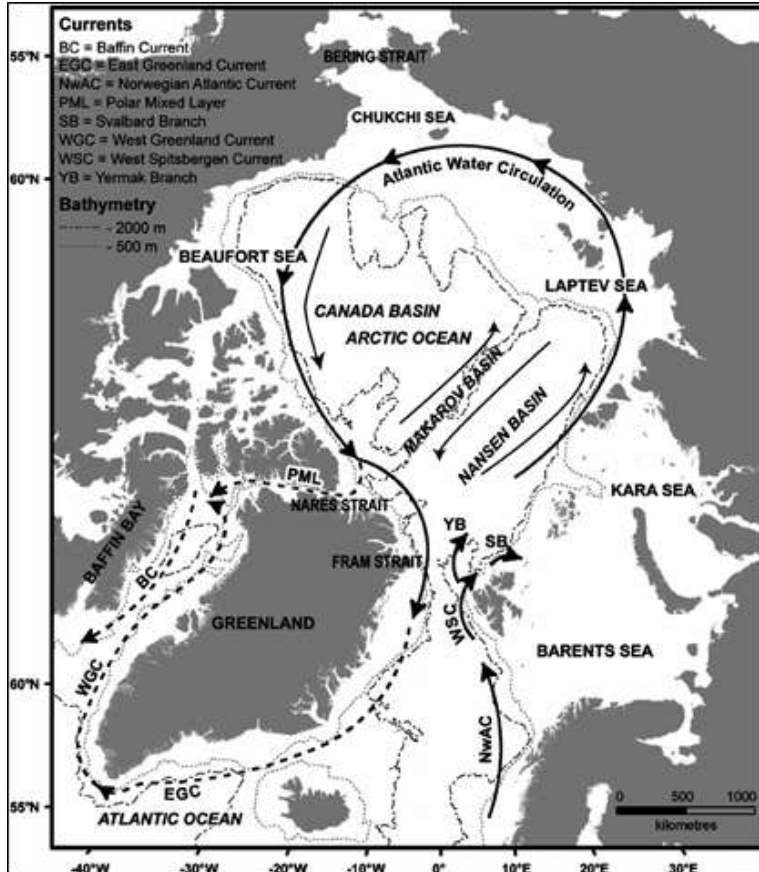


Fig. 4.2: Map showing the major surface currents in the Arctic Ocean. The black arrows correspond to the Atlantic water inflow, which moves counter-clockwise, and the broken arrows show the polar mixed layer (PML) exiting the Arctic Ocean through Fram and Nares straits [40].

The waters leave the Arctic Ocean along the East Greenlandic Cur-

rent (EGC). This current has a significant impact on the export of sea ice, affecting its amount in the Arctic Ocean region. It is estimated that more than 90% of the Arctic Sea ice exported from the Arctic occurs within the East Greenland Current [41]. Maximum ice exports are possible from October to December, and minimum ice exports are from January to March [42]. This seasonal variation is due to the accelerated rate of ice melting, increasing the drifting amount. This results in an increase in the mobility of the ice masses and facilitates transport through the western part of the Fram Strait. During the winter months, the sea ice freezes, thus reducing its drifting amount, while increasing the extent of Arctic sea ice [43].

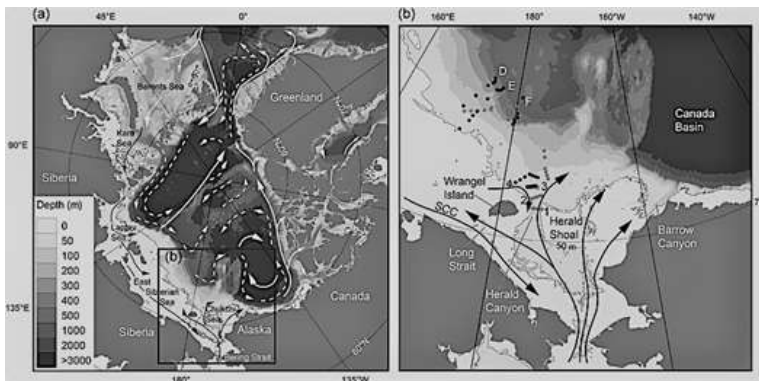


Fig. 4.3: Map of the Arctic Ocean (a) with the mean schematic oceanic circulation illustrated by solid arrow for surface currents, interrupted arrows for intermediate currents, and dotted arrows for deep currents. In panel (b), a close-up of the eastern East Siberian Sea (ESS) and Chukchi Sea (CS), Bathymetry is from the International Bathymetric Chart of the Arctic Ocean (IBCAO) version 4.0 [44, 45].

Another way of water exchange is the Bering Strait, where the Pacific waters flow through the Chukchi Sea and penetrate the depths of the Arctic Ocean [46]. The Pacific waters (PW) exert a strong influence on the Arctic Ocean, providing ocean heat of about one-third of that in the Fram Strait [47]. In addition, PW accounts for

about one-third of the freshwater supply to the Arctic and is also the main source of nutrients [48]. The nutrient-rich water flowing down the Anadyr River flows through the western (Russia) passage of the Bering Strait, while the saltier and colder waters of the Bering Sea flow through the eastern part of the Strait (USA). The influence of the influx from the Pacific is mainly limited to the American Basin [49]. The water masses mix with fresh river waters and are drawn into the Beaufort vortex, held by anti-cyclonal air currents (Fig. 4.3). When the air currents weaken, fresh water leaks from the vortex into the North Atlantic Ocean. This is due to the baroclinic instability. This current variation also affects the Pacific waterways across the Arctic Ocean and ultimately the North Atlantic Ocean.

Both the Bering and Beaufort sea shelves are shallow (<50 m) and subject to high wind influences with the seasonal cycle of sea ice melting/ thawing. The northbound flow of Pacific water is driven by the high pressure that is created by the gradient of salinity. The Pacific waters are much fresher than the Atlantic waters [51], which helps to ventilate the cold halocline inside the Canadian Basin [52]. Pacific water create the gyres which are common in the Canadian Basin [53]. This is probably due to the instability of the Pacific currents along the Chukchi Shelf (Fig. 4.4). Pacific waters leave the Arctic through the Fram Strait and the Canadian Archipelago [54]. The inflow of freshwater from the North Pacific Ocean to the North Atlantic Ocean provides a "short" circuit for the global thermohaline ocean circulation [55]. Both the ventilation and the exchange of freshwater have a significant impact on the carbonate cycle in the ocean and in the global carbon cycle.

4.3 The Carbon Cycle in the Arctic

Carbon is necessary for the existence and functioning of the earth's biosphere, although it is a small fraction of the mass of all the elements of our planet. The transfer of its forms to various internal and external parts of the Earth, along with the processes enabling the maintenance of balance in its individual parts, creates a con-

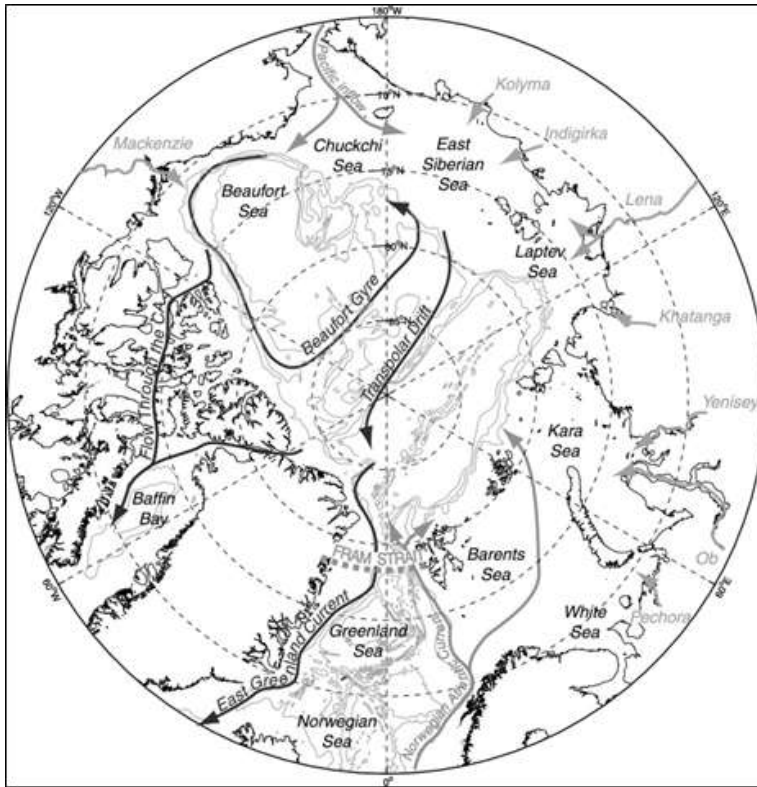
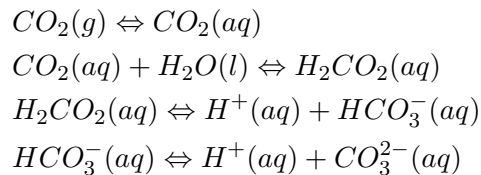


Fig. 4.4: Schematic map showing the surface circulation of the Arctic Ocean and the repeated Fram Strait section. Bathymetric contours are drawn at 1000 m intervals [50].

ceptual model known as the carbon cycle [56]. This cycle in nature includes three major resources, which are ocean and continental waters with sediments, the atmosphere, and the terrestrial and aquatic biosphere. The most abundant form is carbon dioxide (CO_2). This gas has a direct impact on the climate, as a greenhouse gas [57], it affects temperature, but also contributes to the acidification of the oceans [58]. Climate, on the other hand, influences CO_2 concentration through a number of physical, chemical and biological processes and feedback mechanisms. An example of this relationship is the CO_2 solubility modified by the temperature of the oceans. The

higher the temperature of the atmosphere, the warmer the ocean becomes and the solubility of CO_2 decreases. The oceans from all the Earth's carbon stores contain about 39 000 GtC, as opposed to the terrestrial biosphere containing the least 523 GtC. Soils and sediments contain 6 506 GtC and the atmosphere about 829 GtC, but this value is still increasing [59]. The increase in CO_2 concentration in the atmosphere as a result of increased anthropogenic emissions causes a number of changes in the marine carbon cycle and in the Arctic Ocean [60], and, as a result, changes in the biodiversity and spatial distribution of species [61].

The main form of carbon in global bodies of water is dissolved carbon dioxide and its ionic forms. The study of the inorganic carbon cycle in oceans focuses on four parameters such as dissolved inorganic carbon (DIC), total alkalinity (TA), partial pressure of CO_2 ($p\text{CO}_2$), and pH [62]. The main compounds of inorganic carbon in water solution (DIC) are: CO_2 , HCO_3^- , CO_3^{2-} . These ions are formed including by the reaction of atmospheric CO_2 that dissolves in ocean waters to form an unstable, weak carbonic acid (H_2CO_3). On decomposition, it forms a bicarbonate anion (HCO_3^-) and a hydrogen cation H^+ . The HCO_3^- anion dissociates into CO_3^{2-} carbonate anion and H^+ hydrogen cation. The reaction was described by the formula:

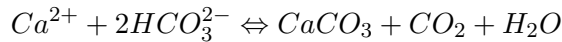


The exchange of CO_2 through the air-sea interface depends on salinity and the difference in CO_2 partial pressures in the water and the atmosphere. This relationship describes Henry's law:

$$p_{\text{CO}_2} = n_{\text{CO}_2} K$$

where, p_{CO_2} – CO_2 partial pressure, n_{CO_2} – number of moles of CO_2 , K – constant of proportionality for CO_2 .

Transport of DIC from the ocean surface to the deep part of the ocean is achieved by the solubility pump. This process is possible due to the coexistence of two important phenomena, which are the inversely proportional solubility of CO_2 to water temperature and the thermohaline circulation caused by changes in sea water density depending on salinity and temperature. Cold deep waters are more saturated with CO_2 than warmer surface waters and therefore CO_2 is pumped into the ocean [63]. Inorganic carbon in water reservoirs is also found in the form of particulate inorganic carbon (PIC) solids of biological and abiotic origin, which are grains of weathered carbonate rocks and the skeletons of calcium-carbonate organisms. Phytoplankton produces particulate inorganic carbon (PIC) in the form of calcium carbonate. Aragonite and calcite (polymorphic forms of calcium carbonates) are used to create crusts and shells, which contributes to an increase in CO_2 concentration in the atmosphere [64]. The reaction to form calcium carbonate is as follows:



This process is called a carbonate pump. Phytoplankton, creating fine limestone plates called coccoliths, has a significant effect on the carbonate chemistry between surface waters and deeper ocean layers by transporting calcium carbonate CaCO_3 down the ocean [65]. In the form of bottom sediments, carbon can be stored for hundreds or even thousands of years [66]. The saturation state with the mineral CaCO_3 (Ω) is defined as the ion product of the carbonate concentrations and the calcium concentration:

$$\Omega = [\text{Ca}^{2+}][\text{CO}_3^{2-}]/K_{sp}^*$$

where, Ω – saturation state, K_{sp}^* – product of stoichiometric solubility.

The stoichiometric solubility product $[K_{sp}^*]$ describes the salinity function together with temperature and pressure [67, 68] expressed

in the unit $[\text{mol}^2/\text{kg}^2]$. The surface waters are generally supersaturated with regard to CaCO_3 . Solution supersaturation can be the driving force for the spontaneous synthesis of inorganic calcium carbonate. However, such a phenomenon occurs sporadically because the spontaneous reaction of calcium Ca^{2+} cations is inhibited by the competing magnesium cation Mg^{2+} against the assumptions resulting from the principles of thermodynamics [69]. Polymorphic forms of calcium carbonate such as stable calcite and metastable aragonite are present due to biological processes taking place in the ocean [70]. The water saturation status for these two minerals is expressed as Ω_{cal} and Ω_{arg} and is a measure of the corrosion potential of organic CaCO_3 structures in marine organisms. In the absence of protective mechanisms, sea water unsaturated with carbonates ($\Omega < 1$) is corrosive to calcifying organisms [71]. In addition, high saturation may also slow down the biological calcification process in saturation states at $\Omega_{arg} = 3.1$ for some organisms such as reef-building corals [72] and classifying phytoplankton [73].

The transfer of inorganic carbon in the form of CO_2 from the atmosphere to the ocean is further dependent on the buffer capacity quantifying the ability of the solution to resist changes in pH by absorbing or desorbing H^+ and OH^- ions. The temperature [T] and the alkalinity of the water [TA] affect the buffer capacity of the solution [74]. Alkalinity, as well as primary production, are the main factors controlling the degree of acidification and hence CO_2 uptake by the waters of the Arctic Ocean. In the mineralisation process, i.e. the formation of calcium carbonate (CaCO_3) minerals from bicarbonate (HCO_3^-) and calcium ions (Ca^{2+}), the abiotic DIC carbon is transferred to the abiotic PIC fraction with the simultaneous release of CO_2 into the water. In the case of biomineralisation, calcium carbonate is produced by calcifying organisms, therefore its production is dependent on the production of organic carbon [75].

Dissolved organic carbon (DOC) occurs in the form of organic compounds of various sizes and molecular weights, from light, simple organic acids to much heavier and more structurally complex compounds. The process that produces dissolved organic carbon is pho-

tosynthesis in the ocean's euphotic zone. Phytoplankton use light, carbon dioxide (DIC) and nutrients available in the first 100 m of the ocean to synthesize many different carbon compounds [76]. During the life cycle of phytoplankton, numerous organic matter (OM) compounds such as carbohydrates, proteins and lipids are formed. These compounds can be transported in the food web and undergo transformations, as a consequence of which new carbon compounds are formed. Stored carbon in the form of, for example, dead organisms, excrement and metabolites is transported to the lower part of the ocean, forming detritus. Incorporated in organisms, CaCO_3 (PIC) is transported to the deep layers of the ocean, where carbon can become part of deep-sea currents and seafloor sediments. Many carbonate components dissolve before reaching the seafloor sediments, releasing CO_2 into deep ocean currents. This process is called a biological pump. This vertical carbon export lowers $p\text{CO}_2$ at the surface and increases CO_2 uptake from the atmosphere.

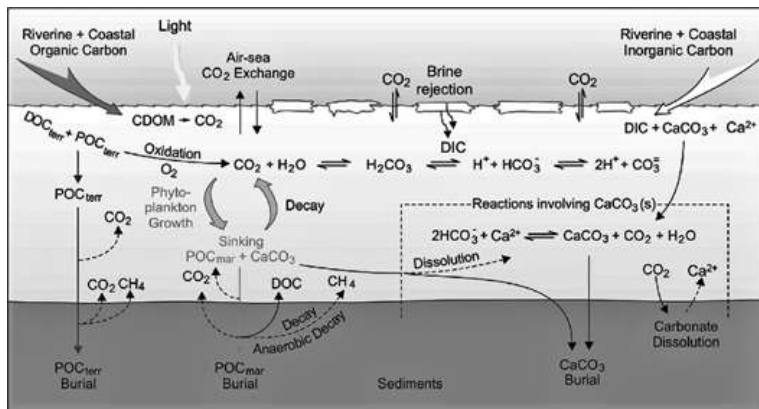


Fig. 4.5: Scheme showing major processes related to the carbon cycle in high-latitude shelf seas [77].

Through aerobic and anaerobic processes under the influence of bacteria, detritus is partially remineralised to forms of inorganic carbon DIC as well as methane CH_4 , which is part of DOC (Fig. 4.5). Dissolved organic carbon can be re-incorporated into particulate or-

ganic carbon (POC) particles consisting of undegraded cells, metabolic excretion products, soft tissues of animal origin sinking in the water column. This process is called a biological pump that affects the storage of carbon in the ocean depths [78].

4.4 Differences between the winter and summer seasons of the selected factors in the carbon cycle

The carbon cycle in the Arctic regions is strongly influenced by the seasonality of this region. Relatively short periods of summer together with a short period of sunlight cause an increase in the temperature of the ocean's surface and the atmosphere at its surface. The temperature of the water surface in summer depends on the amount of solar radiation absorbed by the sea surface. The solar warming of the Arctic Ocean surface is influenced by the rate and extent of melting ice as well as cloud cover with the degree of mixing of the upper layers of the ocean. Of additional significance is the influx of warm waters into the Arctic from the North Atlantic and North Pacific Oceans together with the influx of warm river waters flowing into the marginal shelf seas [79]. In August 2021, the average surface temperatures of the Arctic Ocean ranged from 6°C to 10°C in the south-eastern Chukchi and Barents Seas to around 0°C to 3°C in the East Siberian, Kara Sea, Laptev, Baffin Bay and in ice-free waters east of Greenland [79–81]. During winter, water temperatures in January 2022 for this region ranged from -1.7°C to 7.1°C. The lowest sea temperature measured in this month was -3°C, and the highest was 8.5°C [82]. The halocline stratification in the waters of the Arctic Ocean keeps warm waters from the Atlantic and Pacific Oceans below the surface waters, which explains the January water temperature above 7°C. Ocean waters flowing into the Arctic cool down, increasing the solubility of CO₂. In summer, when the Arctic ice sheet melts, the exposed waters are susceptible to CO₂ uptake and increased exchange with the atmosphere, which promotes acidification of the Arctic Ocean [83]. In addition to temperature, CO₂ exchange between the ocean and the

atmosphere is significantly influenced by the net effect of primary production, the rate of CaCO_3 calcification and dissolution, and brine formation.

One study [84] reported the strongest transfer of CO_2 from the atmosphere in the Greenland/ Norwegian Sea, amounting to $> 15 \text{ mmol}/(\text{m}^2\text{day})$ and the Barents Sea for values $> 12 \text{ mmol}/(\text{m}^2\text{day})$ in the winter season. In the summer season, the greatest transport of CO_2 falls to the Chukchi Sea ($\sim 10 \text{ mmol}/(\text{m}^2\text{day})$). The seasonal variation of CO_2 in the Greenland / Norwegian Sea, the Chukchi Sea and parts of the Barents Sea were determined to be high for a seasonal amplitude value of over $10 \text{ mmol}/(\text{m}^2\text{day})$. For the Chukchi Sea and the Barents Sea, the amplitude of seasonal CO_2 uptake was close to $10 \text{ mmol}/(\text{m}^2\text{day})$. On the other hand, another article [11] compares the long-term data between the Chukchi Shelf and the Canadian Basin. There was a significant increase in $p\text{CO}_2$ on the surface of the Chukchi Sea with negligible ice cover in the southern part of the Canadian Basin. The rate of increase was $4.6 \pm 0.5 \mu\text{atm}/\text{yr}$ for the surface waters of the Chukchi Sea and $1.9 \pm 0.1 \mu\text{atm}/\text{yr}$ for atmospheric CO_2 . The results presented in the study confirmed the fastest $p\text{CO}_2$ increase among other ocean basins [83, 85, 86]. The effect of this change is the halving of the gradient between the atmosphere and the sea ($\Delta p\text{CO}_2$) of $-50 \mu\text{atm}$ in the summer season. Lower $p\text{CO}_2$ is observed in deeper water layers, which may be due to the subduction of higher density Pacific ocean waters under the lower density Canadian basin surface waters. This process is possible due to the increased transport of nutrient-rich waters through the Bering Strait [47]. The nutrient-rich Pacific water keeps $p\text{CO}_2$ low while increasing absorption of atmospheric CO_2 , resulting in increased pump productivity [87]. While productivity alone does not play a direct role in reducing $p\text{CO}_2$ to surface waters, this, in combination with the increased atmospheric currents from the east, may be the basis in this region. Increasing the anti-cyclone flow at Beaufort Gyre resulted in a fresh and shallower surface layer of water in the Canadian Basin (Fig. 4.6). In turn, the accumulation of fresh water weakens the processes of vertical mixing of water. Increased water level movement caused by the disappearance of the ice cover to-

gether with the rapid penetration of atmospheric CO_2 into surface waters leads to $p\text{CO}_2$ equalization between the atmosphere. This process significantly reduces the CO_2 gradient between the atmosphere and surface waters, acting as a kind of barrier, inhibiting further CO_2 uptake in the summer season [88, 89].

The reduction of the ice cover in both summer and winter contributes significantly to changes in the primary production of the Arctic Ocean and the adjacent shelf seas. This process is driven by the melting and retraction of ice in the spring, increasing the availability of sunlight and increased stratification [9]. This leads to an earlier start of matter production in the seasonal cycle taking place in poor light conditions [90]. As observed in [91], the reaction of the primary production of the Arctic Ocean in response to ice retraction varies in space and depends on the season, as in winter the primary production is significantly reduced or does not take place at all. An increased supply of nutrients may also affect overall matter production [92]. As a consequence, the biological activity of, in particular, unicellular eutrophic algae inhabiting the ice and their free-living forms in the water column (phytoplankton) of the euphotic zone increases. In the process of photosynthesis, these organisms convert inorganic carbon into its organic forms. Consequently, primary production is critical to the functioning of the Arctic Ocean's ecosystems by providing energy to various food systems. Chlorophyll a concentrations are used to estimate the total algal biomass [93]. The study [94] presents the results relating to primary productivity above the average in 2020. The research was carried out for the Canadian Basin, it covers the Chukchi Sea, the Beaufort Sea and the Canadian Archipelago region, as well as the Eurasian Basin in the Kara Sea, Laptev and East Siberian Sea regions. Primary productivity was estimated on the basis of chlorophyll a concentration, sea surface temperature, solar radiation and the depth of mixed layers (Tab. 4.1).

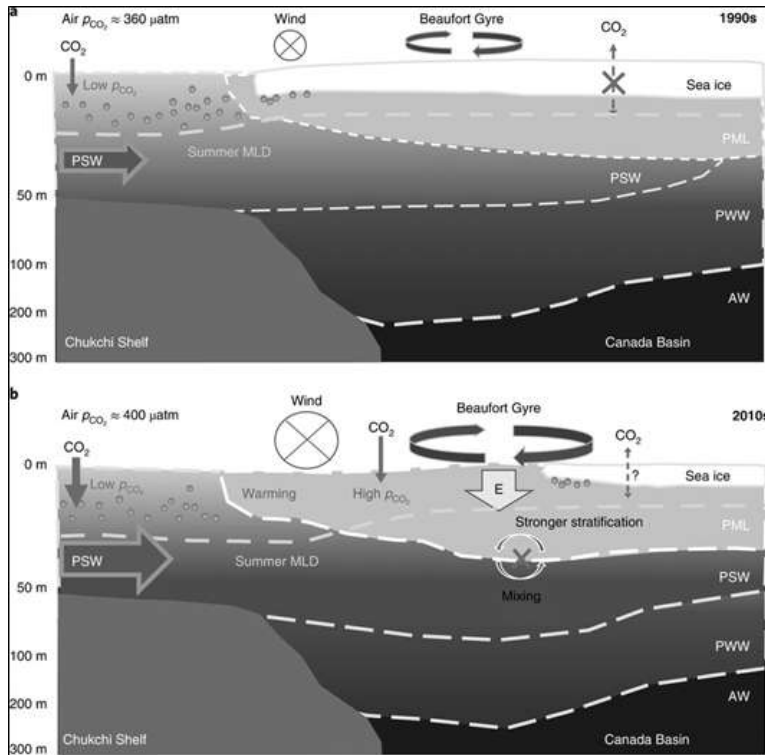


Fig. 4.6: Schematic representation of recent environmental changes in the western Arctic during the ice-melt season. The changes in physical setting in the upper ocean along the Chukchi Shelf to the Canada Basin in the 1990s (a) and 2010s (b). Increased Pacific summer water (PSW) flows through the Chukchi Shelf and subducts into the Beaufort Sea slope and the Canada Basin. The upper water column was depressed and built up a stronger stratification due to the combination of the accumulation of surface ice melt water. Dashed lines indicate the summer mixed layer depth (MLD), which is shallowing from spring to summer and becomes shallower in the basin than on the shelf. PML, polar mixed layer; PWW, Pacific winter water; AW, Atlantic water [11].

Positive trends were statistically significant for the Eurasian Basin: Barents Sea, Greenland Sea, Hudson Bay, Baffin Bay / Labrador

Sea, North Atlantic for the average of all regions. The highest upward of the trend in the period 2003-2020 was found in the Eurasian basin and it amounted to $12.83 \text{ g C/m}^2/\text{yr}/\text{decade}$ with an increase of $\sim 37.7\%$. For the Barents Sea, the trend value was $9.32 \text{ g C/m}^2/\text{yr}/\text{decade}$ with an increase of 21.0% . In the Greenland Sea, the trend was $6.34 \text{ g C/m}^2/\text{yr}/\text{decade}$ and the increase was $\sim 18.7\%$. For primary productivity in the research period 2003-2020, upward trends were observed in all regions of the Arctic Ocean [94].

Tab. 4.1: Linear trends, statistical significance, percent change, and primary productivity anomalies in 2020 (March-September) in the nine regions and overall average [94].

Region	Trend, 2002-20 ($\text{g C/m}^2/\text{yr}/\text{decade}$)	Mann-Kendall p -value	% Change	2020 Anomaly ($\text{g C/m}^2/\text{yr}$) from a 2003-19 reference period	2020 Primary Productivity (% of the 2003-19 average)
Eurasian Arctic	12.83	0.001	37.7	11.74	117.2
Amerasian Arctic	2.21	0.260	10.7	2.90	107.9
sea of Okhotsk	1.22	0.601	2.9	-1.75	97.6
Bering Sea	1.70	0.002	4.7	-0.20	99.7
Barents Sea	9.32	0.004	21.0	2.09	102.5
Greenland Sea	6.34	0.021	18.7	0.98	101.6
Hudson Bay	4.47	0.039	18.9	3.12	107.1
Baffin Bay/ Labrador Sea	4.69	0.007	14.9	0.24	100.4
North Atlantic	4.35	0.001	15.5	1.37	103.8
Average of nine regions	5.24	0.001	16.0	2.28	103.8

Biological processes taking place in the Arctic Ocean, such as photosynthesis or respiration of phytoplankton and zooplankton, may explain the differences in CO_2 concentration and saturation state of CaCO_3 [Ω] between seasons [95, 96]. Zooplankton, which include for example foraminifera, mainly feed on available molecular matter consisting of phytoplankton in the spring and summer seasons and degraded organic material in late fall and winter [97]. This leads to a decrease in the level of nitrates with a decrease in the level of dissolved CO_2 with a simultaneous increase in pH and the level of saturation with calcium carbonates [Ω]. In the autumn, due to the influx of fresh waters from the Atlantic and Pacific oceans, the concentration of dissolved CO_2 increases. During the Arctic winter, ocean carbonate chemistry is characterized by the highest $p\text{CO}_2$, lowest pH and lowest saturation state of CaCO_3 [Ω]. The reason for these changes in the basic parameters of the carbonate cycle may

be the emission of CO_2 generated in the process of respiration and vertical stratification caused by winds [95]. The intensification of the above-mentioned processes leads to a decrease in the saturation state of calcite (Ω_{Ca}) and aragonite (Ω_{Ar}). Increased CO_2 transfer between the atmosphere and the ocean increases the concentration of bicarbonate ions, lowering the degree of CaCO_3 saturation, while increasing the solubility of CaCO_3 minerals [98]. These dependencies are seasonally described in [99]. In turn, another study [100] investigated the distribution of calcium carbonate saturation (Ω) in the Chukchi Sea in the fall of 2012 and the summer of 2013. Aragonite and calcite undersaturation was observed in regions with high biological productivity in the fall season as opposed to the summer season. Comparison with other parameters showed that biological processes such as respiration and photosynthesis are factors that control the variability of Ω over time and space. The carbonate saturation in the bottom waters of the Chukchi Sea ranged from 0.3 to 2.0 for aragonite and from 0.5 to 3.2 for calcite in autumn, and in summer it was from 1.1 to 2.8 for aragonite and from 1.7 to 4.4 for calcite. A decrease in the Ω value was observed in late summer and winter, and an increase in spring and early summer. The calculations performed in the study indicated the possibility of aragonite insufficiency of bottom waters and extension of the period of undersaturation twice [100].

4.5 Conclusion

The discussed factors characterizing and influencing the carbon cycle in the Arctic Ocean show a strong seasonal dependence. The presence of an ice cover as a physical barrier is one of the factors limiting the access of atmospheric CO_2 to the surface waters of the Arctic Ocean. A number of positive feedback processes related to the increase in CO_2 concentration in the atmosphere lead to the loss of the ice barrier and to the disruption of seasonal processes responsible for maintaining the geochemical balance and the entire carbon cycle. Further research into the effects of ice loss, along with increased uptake of CO_2 from the waters of the Arctic Ocean and marginal shelf seas, is essential to forecast future changes.

Bibliography

- [1] V.A. Semenov, T. Martin, L.K. Behrens, and M. Latif. Arctic sea ice area in cmip3 and cmip5 climate model ensembles—variability and change. *Cryo-sphere Discuss*, 9:1077–1131, 2015.
- [2] J. Overpeck, K. Hughen, D. Hardy, R. Bradley, R. Case, M. Douglas, B. Finney, K. Gajewski, G. Jacoby, A. Jennings, S. Lamoureux, A. Lasca, G. MacDonald, J. Moore, M. Retelle, S. Smith, A. Wolfe, and Zielinski. Arctic environmental change of the last four centuries. *Science*, 278(5341):1251–1256, 1997.
- [3] C. Kinnard, C.M. Zdanowicz, D.A. Fisher, E. Isaksen, A. Vernal, and L.G. Thompson. Reconstructed changes in arctic sea ice over the past 1450 years. *Nature*, 2011.
- [4] A.L. Niederdrenk and D. Notz. Arctic sea ice in a 1.5 °C warmer world. *Geophys. Res. Lett*, 45:1963–1971, 2018.
- [5] M. Yamamoto-Kawai, F.A. McLaughlin, E.C. Carmack, S. Nishino, K. Shimada, and N. Kurita. Surface freshening of the Canada basin, 2003–2007: River runoff versus sea ice meltwater. *J. Geophys. Res*, 114:00 05,, 2009.
- [6] M. Yamamoto-Kawai, F. McLaughlin, and E. Carmack. Ocean acidification in the three oceans surrounding northern North America. *J. Geophys. Res. Oceans*, 118:6274–6284,, 2013.

- [7] F.A. McLaughlin and E.C. Carmack. Nutricline deepening in the canada basin, 2003-2009, *geophys. Res. Lett*, 37, L24602, 2010.
- [8] S. Pabi, G.L. Dijken, and K.R. Arrigo. Primary production in the arctic ocean. *J. Geophys. Res*, 113:08005,, 2008.
- [9] K.R. Arrigo and G.L. Dijken. Secular trends in arctic ocean net primary production. *J. Geophys. Res*, 116:09011,, 2011.
- [10] M. Manizza, M.J. Follows, S. Dutkiewicz, D. Menemenlis, C.N. Hill, and R.M. Key. Changes in the arctic ocean co2 sink (1996-2007): a regional model analysis. *Global Biogeochem. Cycles*, 27:1108–1118, 2013.
- [11] Z. Ouyang, D. Qi, L. Chen, T. Takahashi, W. Zhong, and M.D. DeGrandpre. Sea-ice loss amplifies summertime decadal co2 increase in the western arctic ocean. *Nat. Clim. Chang*, 10:678–684, 2020.
- [12] W.J. Cai, L. Chen, B. Chen, Z. Gao, S.H. Lee, and J. Chen. Decrease in the co2 uptake capacity in an ice-free arctic ocean basin. *Science*, 329:556–559, 2010.
- [13] P.E. Land, J.D. Shutler, R.D. Cowling, D.K. Woolf, P. Walker, and H.S. Findlay. Climate change impacts on sea-air fluxes of co2 in three arctic seas: a sensitivity study using earth observation. *Biogeosciences*, 10:8109–8128, 2013.
- [14] N.R. Bates and J. Mathis. T.: The arctic ocean marine carbon cycle: evaluation of air-sea co2 exchanges, ocean acidification impacts and potential feedbacks. *Biogeosciences*, 6:2433–2459,.
- [15] L.G. Anderson and S. Kaltin. Carbon fluxes in the arctic ocean - potential impact by climate change. *Polar Res*, 20(2):225–232,, 2001.
- [16] K.R. Arrigo, G.L. Dijken, and S. Pabi. The impact of a shrinking arctic ice cover on marine primary production, *geophys. Res. Lett*, 35, L19603.

- [17] R.W. Buddemeier, J.A. Kleypas, and R. Aronson. B.: Coral reefs and global climate change: Potential contributions of climate change to stresses on coral reef ecosystems, 44. Technical report. download report at:.
- [18] Royal society: Ocean acidification due to increasing atmospheric carbon dioxide, the clyvedon press, 2005.
- [19] J.R. Cochran, M.H. Edwards, and B.J. Coakley. Morphology and structure of the lomonosov ridge, arctic ocean. *Geochemistry, Geophysics*, 2006. Geosys1343 tems, 7 (5).
- [20] Göran Björk, Martin Jakobsson, Bert Rudels, James H Swift, Leif Anderson, Dennis A Darby, Jan Backman, Bernard Coakley, Peter Winsor, Leonid Polyak, et al. Bathymetry and deep-water exchange across the central lomonosov ridge at 88–89 n. *Deep Sea Research Part I: Oceanographic Research Papers*, 54(8):1197–1208, 2007.
- [21] M. Jakobsson. Hypsometry and volume of the arctic ocean and its constituent seas. *Geochem. Geophys. Geosyst*, 3(5), 2002.
- [22] Igor Florinsky, S. Filippov, A. Abramova, Yulia Zarayskaya, and E.V. Selezneva. Towards geomorphometric modelling of the topography of the arctic ocean floor, 2018.
- [23] F. Fetterer, K. Knowles, W. Meier, M. Savoie, and A. Windnagel. *Updated daily Sea Ice Index version 3*. National Snow and Ice Data Center, Boulder Colorado USA. NSIDC, 2017.
- [24] M. Jakobsson and L. Mayer. The international bathymetric chart of the arctic ocean (ibcao) version 3.0. *geophysical research letters*, 39, l12609, 2012.
- [25] A Balasubramanian. The ocean currents, 2014.
- [26] R. Kwok, G. Spreen, and S. Pang. Arctic sea ice circulation and drift speed: Decadal trends and ocean currents. *Journal of Geophysical Research: Oceans*, 118(5):2408–2425, 2013.

- [27] E.A. D'Asaro and J.H. Morison. Internal waves and mixing in the arctic ocean. deep sea research part a. *Oceanographic Research Papers*, 39(2):459–484, 1992.
- [28] Z. Kowalik and A.Y. Proshutinsky. Diurnal tides in the arctic ocean. *Journal of Geophysical Research: Oceans*, 98(C9):16449–16468, 1993.
- [29] B. Dickson, J. Meincke, and P. Rhines. Arctic-subarctic ocean fluxes: defining the role of the northern seas in climate. In R.R. Dickson, J. Meincke, and Rhines, editors, *P.(Eds.), Arctic-Subarctic Ocean Fluxes. Springer, the Netherlands*, pages 1–13. 2008.
- [30] J. Blindheim and S. Osterhus. The nordic seas, main oceanographic features. In Helgeange In, T. Dokken, T. Furevik, R. Gerdes, and W. Berger, editors, *The Nordic Seas: An Integrated Perspective*, pages 11–37. American Geophysical Union, 2005.
- [31] R.A. Woodgate, E. Fahrbach, and G. Rohardt. Structure and transports of the east greenland current at 75 n from moored current m. *Journal of 1957 Geophysical Research: Oceans*, 104(C8):18059–18072, 1999.
- [32] A. Munchow, H. Melling, and K.K. Falkner. An observational estimate of volume and freshwater flux leaving the arctic ocean through nares strait. *Journal of Physical Oceanography*, 36(11):2025–2041, 2006.
- [33] G.A. Maykut and N. Untersteiner. Some results from a time-dependent thermodynamic model of sea ice. *Journal of Geophysical Research*, 76(6):1550–1575, 1971.
- [34] S. Pivovarov, R. Schlitzer, and A. Novikhin. River runoff influence on the water mass formation in the kara sea. In R. Stein, K. Fahl, D.K. FÄLttterer, E.M. Galimov, and O.V. Stepanets, editors, *Siberian river run-off in the Kara*

- Sea: characterisation, quantification, variability, and environmental significance*, volume 6, pages 9–26, Amsterdam, The Netherlands, 2003. Elsevier.
- [35] M. Steele and T. Boyd. Retreat of the cold halocline layer in the arctic ocean. *Journal of Geophysical Research*, 103(C5):10419–10435, 1998.
- [36] K.A. Orvik and P. Niiler. Major pathways of atlantic water in the northern north atlantic and nordic seas toward arctic. *Geophysical Research Letters*, 29(19):2–1, 2002.
- [37] K. Aagaard and E.C. Carmack. The role of sea ice and other fresh water in the arctic circulation. *Journal of Geophysical Research*, 94(C10):14485–14498,, 1989.
- [38] R.H. Bourke and R.P. Garrett. Sea ice thickness distribution in the arctic ocean. *Cold Regions Science and Technology*, 13(3):259–280, 1987.
- [39] J. Karstensen, P. Schlosser, D.W.R. Wallace, J.L. Bullister, and J. Blindheim. Water mass transformation in the greenland sea during the 1990s. *J. Geophys. Res*, 110, C07602, 2005.
- [40] David Ledu, Andre Rochon, de Vernal Anne, and Guillaume St-Onge. Palynological evidence of holocene climate change in the eastern arctic: a possible shift in the arctic oscillation at the millennial time scale this article is one of a series of papers published in this special issue on the theme polar climate stability network. *Canadian Journal of Earth Sciences*, 45:1363–1375, 2008.
- [41] Rebecca A. Woodgate, Eberhard Fahrbach, and Gerd Rohardt. Structure and transports of the east greenland current at 75°N from moored current m”. *Journal of Geophysical Research*, 104(C8):18059–18072, 1999.
- [42] T. Martin and P. Wadhams. Sea-ice flux in the east greenland current”. *Deep-Sea Research Part II: Topical Studies in Oceanography*, 46(6-7):1063, 1999.

- [43] T. Vinje, N. Nordlund, and A. Kvambekk. Monitoring ice thickness in fram strait. *Journal of Geophysical Research*, 103(C5):10,437–10,450, 1998.
- [44] M. Jakobsson, L.A. Mayer, and C. Bringensparr. The international bathymetric chart of the arctic ocean version 4.0. *Sci Data*, 7:176, 2020.
- [45] Jaclyn Clement Kinney, Karen M Assmann, Wieslaw Maslowski, Göran Björk, Martin Jakobsson, Sara Jutterström, Younjoo J Lee, Robert Osinski, Igor Semiletov, Adam Ulfsbo, et al. On the circulation, water mass distribution, and nutrient concentrations of the western chukchi sea. *Ocean Science*, 18(1):29–49, 2022.
- [46] E. Watanabe and H. Hasumi. Pacific water transport in the western arctic ocean simulated by an eddy-resolving coupled sea ice-ocean model. *Journal of Physical Oceanography*, 39(9):2194–2211, 2009.
- [47] R.A. Woodgate, T.J. Weingartner, and R. Lindsay. Observed increases in bering strait oceanic fluxes from the pacific to the arctic from 2001 to 2011 and their impacts on the arctic ocean water column. *Geophysical Research Letters*, 39(24):6,, 2012.
- [48] M. Serreze and J. Francis. The arctic amplification debate. *Climate Change*, 76:241–264,, 2006.
- [49] B.A. Bluhm, K.N. Kosobokoba, and E.C. Carmack. A tale of two basins: An integrated physical and biological perspective of the deep arctic ocean. In *Progress in Oceanography*, doi. 2015.
- [50] The freshwater composition of the fram strait outflow derived from a decade of tracer measurements. *Journal of Geophysical Research*, 117:11005, 2012.
- [51] R. Huang and R. Schmitt. The goldsbrough-stommel circulation of the world oceans. *J. Phys. Oceanogr*, 23:1277–1284, 1993.

- [52] Robert S Pickart, Thomas J Weingartner, Lawrence J Pratt, Sarah Zimmermann, and Daniel J Torres. Flow of winter-transformed pacific water into the western arctic. *Deep Sea Research Part II: Topical Studies in Oceanography*, 52(24-26):3175–3198, 2005.
- [53] M. Timmermans, J. Toole, A. Proshutinsky, R. Krishfield, and A. Plueddemann. Eddies in the canada basin, arctic ocean, observed from ice-tethered profilers. *J. Phys. Oceanogr*, 38:133–145, 2008.
- [54] J.-E. Tremblay, Y. Gratton, J. Fauchot, and N.M. Price. Climatic and oceanic forcing of new, net, and diatom production in the north water. *Deep-Sea Res*, 49:4927–4946, 2002.
- [55] S.E. Wijffels, R.W. Schmitt, H.L. Bryden, and A. Stigebrandt. Transport of freshwater by the oceans. *J. Geophys. Res.*,22:155– 162,, 1992.
- [56] F. Mackenzie and Abraham Lerman. Brief overview of carbon on earth, 2006.
- [57] J. Orr, V. Fabry, and O. Aumont. Anthropogenic ocean acidification over the twenty-first century and its impact on calcifying organisms. *Nature*, 437:681–686, 2005.
- [58] John Tyndall. The bakerian lecture-on the absorption and radiation of heat by gases and vapours. In *and on the physical connexion of radiation, absorption, and conduction* *Proc. R. Soc*, Lond.11, 1862. 100-104.
- [59] P. Ciais, Sabine Chris, Balasubramanian Govindasamy, Laurent Bopp, V. Brovkin, J. Canadell, Abha Chhabra, Ruth Defries, James Galloway, and Martin Heimann. Carbon and other biogeochemical cycles. *Climate Change*, pages 465–570, 2013.
- [60] N.R. Bates and J. Mathis. T.: The arctic ocean marine carbon cycle: evaluation of air-sea co2 exchanges, ocean acidification impacts and potential feedbacks. *Biogeosciences*, 6:2433–2459,.

- [61] Victoria J. Fabry, Brad A. Seibel, Richard A. Feely, and James C. Orr. Impacts of ocean acidification on marine fauna and ecosystem processes. *ICES Journal of Marine Science*, 65(ue 3):414–432, 2008-04.
- [62] A.G. Dickson, C.L. Sabine, and J.R. Christian. Guide to best practices for ocean co2 measurements, sidney, british columbia, north pacific marine science organization. *PICES Special Publication*, 3, 2007.
- [63] J.A. Raven and P.G. Falkowski. Oceanic sinks for atmospheric co2. *Plant Cell Environ*, 22:741–755, 1999.
- [64] Steven Emerson. *Chemical Oceanography and the Marine Carbon Cycle*. Cambridge University Press, United Kingdom, 2008.
- [65] Björn Rost and Ulf Riebesell. Coccolithophores and the biological pump: responses to environmental changes. In *Coccolithophores: from molecular processes to global impact*, pages 99–125. Springer, 2004.
- [66] K.L. Denman. *Couplings between changes in the climate system and biogeochemistry*. In: *Climate Change 2007: The Physical Science Basis. Contribution of Working Group I to the Fourth Assessment Report of the Intergovernmental Panel on Climate Change*. Cambridge University Press, Cambridge, United Kingdom and New York, NY, USA, 2007.
- [67] F.J. Millero. Thermodynamics of the carbon dioxide system in the oceans. *Geochim. Cosmochim. Acta*, 59:661– 677, 1995.
- [68] A. Mucci. The solubility of calcite and aragonite in seawater at various salinities, temperatures and 1 atmosphere total pressure. *Am. J. Sci*, 238:780– 799, 1983.
- [69] A.I. Rushdi, R.M. Pytkowicz, E. Suess, and C.T. Chen. The effects of magnesium-to-calcium ratios in artificial seawater, at different ionic products, upon the induction time, and the mineralogy of calcium carbonate: a laboratory study. *Geologische Rundschau*, 81:21571–21578,, 1992.

- [70] Melissa Chierici and Agneta Fransson. Calcium carbonate saturation in the surface water of the arctic ocean: Undersaturation in freshwater influenced shelves. *Biogeosciences*, 6:10 5194–6–2421–2009, 2009.
- [71] B.H. Corliss and S. Honjo. Dissolution of deep-sea benthonic foraminifera. *Micropaleontology*, 27:356–378, 1981.
- [72] J.A. Kleypas, R.W. Buddemeier, D. Archer, J.P. Gattuso, C. Langdon, and B.N. Opdyke. Geochemical consequences of increased atmospheric carbon dioxide on coral reefs. *Science*, 284:118–20, 1999.
- [73] U. Riebesell, I. Zondervan, B. Rost, P.D. Tortell, R. Zeebe, and F.M.M. Morel. Reduced calcification of marine plankton in response to increased atmospheric co₂. *Nature*, 407:364–367,, 2000.
- [74] S. Jutterstrom and L.G. Anderson. The saturation of calcite and aragonite in the arctic ocean. *Marine Chem*, 94(1-4):101–110.
- [75] V. Brovkin, J. Bendtsen, M. Claussen, A. Ganopolski, C. Kubatzki, V. Petoukhov, and A. Andreev. Carbon cycle, vegetation, and climate dynamics in the holocene: Experiments with the climber-2 model. *Global Biogeochem Cycles*, 16:1139, 2002.
- [76] Nathaëlle Bouttes, Didier M. Roche, V. Mariotti, and L. Bopp. Including an ocean carbon cycle model into iloveclim (v1.0). geoscientific model development. *European Geosciences Union*, 8(5):1563 – 1576, 2015.
- [77] David Capelle, Zou Zou Kuzyk, Tim Papakyriakou, Celine Gueguen, Lisa Miller, and Robie Macdonald. Effect of terrestrial organic matter on ocean acidification and co₂ flux in an arctic shelf sea. *Progress in Oceanography*, 185:102319, 2020.

- [78] N. Bouttes, D. Paillard, D.M. Roche, V. Brovkin, and L. Bopp. Last glacial maximum CO_2 and $\delta^{13}\text{C}$ successfully reconciled. *Geophys. Res. Lett.*, 38:02705, 2011.
- [79] Mary-Louise Timmermans and Z Labe. Arctic report card 2020: sea surface temperature. 2020.
- [80] R.W. Reynolds, N.A. Rayner, T.M. Smith, D.C. Stokes, and W. Wang. An improved in situ and satellite SST analysis for climate. *J. Climate*, 15:1609–1625, 2002.
- [81] R.W. Reynolds, T.M. Smith, C. Liu, D.B. Chelton, K.S. Casey, and M.G. Schlax. Daily high-resolution-blended analyses for sea surface temperature. *J. Climate*, 20:5473–5496, 2007.
- [82] Des clics nomades/seatemperatu.re 2015-2022 – all right reserved. <https://www.seatemperatu.re/seas-and-oceans/arctic-ocean/january/>.
- [83] B.I. McNeil and R.J. Matear. Southern ocean acidification: a tipping point at 450-ppm atmospheric CO_2 . *Proc. Natl. Acad. Sci. USA*, 105:18860–18864, 2008.
- [84] Sayaka Yasunaka, Akihiko Murata, Eiji Watanabe, Melissa Chierici, Agneta Fransson, Steven Heuven, Mario Hoppema, Masao Ishii, Truls Johannessen, Naohiro Kosugi, Siv K. Lauvset, Jeremy T. Mathis, Shigeto Nishino, Abdirahman M. Omar, Are Olsen, Daisuke Sasano, Taro Takahashi, and Rik Wanninkhof. Mapping of the air-sea CO_2 flux in the arctic ocean and its adjacent seas: Basin-wide distribution and seasonal to interannual variability. *Polar Science, Volume*, 10(ue 3), 2016.
- [85] T. et al Takahashi. Climatological mean and decadal change in surface ocean pCO_2 , and net sea-air CO_2 flux over the global oceans. *Deep Sea Res*, 2 56:554–577, 2009.
- [86] T. et al Takahashi. Climatological distributions of pH , pCO_2 , total CO_2 , alkalinity, and CaCO_3 saturation in the global surface ocean, and temporal changes at selected locations. *Mar. Chem*, 164:95–125, 2014.

- [87] J.M. Grebmeier. Ecosystem characteristics and processes facilitating persistent macrobenthic biomass hotspots and associated benthivory in the pacific arctic. *Prog. Oceanogr*, 136:92–114, 2015.
- [88] K.A. Giles, S.W. Laxon, A.L. Ridout, D.J. Wingham, and S. Bacon. Western arctic ocean freshwater storage increased by wind-driven spin-up of the beaufort gyre. *Nat. Geosci*, 5:194–197, 2012.
- [89] C. Peralta-Ferriz and R.A. Woodgate. Seasonal and interannual variability of pan-arctic surface mixed layer properties from 1979 to 2012 from hydrographic data, and the dominance of stratification for multiyear mixed layer depth shoaling. *Prog. Oceanogr*, 134:19–53, 2015.
- [90] A. Randelhoff and Coauthors. Arctic mid-winter phytoplankton growth revealed by autonomous profilers. *Sci. Adv*, 6:2678, 2020.
- [91] Global and regional drivers of nutrient supply, primary production and co2 drawdown in the changing arctic ocean. *Prog. Oceanogr*, 139:171–196 2, 2015.
- [92] S.F. Henley, M. Porter, L. Hobbs, J. Braun, R. Guillaume-Castel, E.J. Venables, E. Dumont, and F. Cottier. Nitrate supply and uptake in the atlantic arctic sea ice zone: seasonal cycle, mechanisms and drivers. *Philos. Trans. Royal Soc. A*, 378:20190361, 2020.
- [93] M.J. Behrenfeld and E. Boss. Beam attenuation and chlorophyll concentration as alternative optical indices of phytoplankton biomass. *J. Mar. Res*, 64:431–451, 2006.
- [94] Karen E. Frey, J.C. Comiso, L.W. Cooper, J.M. Grebmeier, and L.V. Stock. Arctic report card 2020: Arctic ocean primary productivity: The response of marine algae to climate warming and sea ice decline, united states. *National Oceanic and Atmospheric Administration. Office of Oceanic and Atmospheric Research*, 2020.

- [95] A. Fransson, M. Chierici, I. Skjelvan, A. Olsen, P. Assmy, and A.K. Peterson. Effects of sea-ice and biogeochemical processes and storms on under-ice water f_{CO_2} during the winter-spring transition in the high arctic ocean: implications for sea-air CO_2 fluxes. *J. Geophys. Res. Oceans*, 122:5566–5587, 2017.
- [96] E. Tynan, J.S. Clarke, M.P. Humphreys, M. Ribas-Ribas, M. Esposito, and V.M.C. Rerolle. Physical and biogeochemical controls on the variability in surface pH and calcium carbonate saturation states in the atlantic sectors of the arctic and southern oceans 2016. *deep sea res*, 2016.
- [97] C. Gannefors, M. Boer, G. Kattner, G. Graeve, K. Eiane, and B. Gulliksen. The arctic sea butterfly limacina helicina: lipids and life strategy. *Mar. Biol*, 147:169–177.
- [98] R. Zeebe and D. Wolf-Gladrow. *CO₂ in Seawater: Equilibrium, Kinetics, Isotopes*. Elsevier Oceanography Series. Elsevier, Amsterdam, 2001.
- [99] Katarzyna Zamelczyk, Agneta Fransson, Melissa Chierici, Elizabeth Jones, Julie Meilland, Griselda Anglada-Ortiz, and Helene Lodemel. Distribution and abundances of planktic foraminifera and shelled pteropods during the polar night in the sea-ice covered northern barents sea, 2021. 10.3389/fmars.2021.644094.
- [100] M. Yamamoto-Kawai, T. Mifune, T. Kikuchi, and S. Nishino. Seasonal variation of ω_{CO_3} saturation state in bottom water of a biological hotspot in the chukchi sea. *Arctic Ocean, Biogeosciences*, 13:6155–6169,.

Chapter 5

The seasonal variations in the thermohaline structure of the Arctic Fjords in a changing climate: A comparison between Kongsfjorden, Isfjorden and Hornsund

PAVANI VITHANA MADUGETA VIDANAMESTRIGE

Institute of Oceanology, Polish Academy of Sciences,
Powstańców Warszawy 55, 81-712 Sopot, Poland

5.1 Introduction

Climate change severely affects the Arctic environment [1]. Several studies have revealed that the Arctic warming rate is twice as high as the world average due to rapid sea ice loss, a phenomenon known as Arctic amplification [1, 2]. Sea ice gets thinner as it melts, making it more vulnerable to melting. When the ice melts completely, ocean surfaces can absorb more solar energy, resulting in extra heating. Changes observed in the Arctic are likely to have far-reaching consequences.

Consequences of the Arctic amplification are especially pronounced in fjords due to the melting of marine-terminating glaciers. The warming-induced glacier melting is the major contributor to global mean sea-level rise [3]. The contribution of glaciers and ice sheets to global mean sea-level rise was 42% in 1971-2018. The contribution of the Greenland ice sheet was 12.6% to the global mean sea level rise in same period [3]. The rising sea levels are potentially dangerous due to coastal floodings. Moreover, the freshwater delivery from melting glaciers and ice sheets largely modifies marine ecosystems on different levels. Most importantly, freshening of the ocean influences the distribution of the water masses that control other components of the ecosystem; this includes chemical properties, biological life and different physical processes. Therefore, studying the thermohaline structure of Arctic fjords in a changing climate is critical. The present review concerns this issue.

The main goal of this overview is to discuss the seasonal variability of the thermohaline structure of the Arctic fjords as an effect of different internal and external physical processes. Here we focus on three fjords located in the Svalbard archipelago: Kongsfjorden, Isfjorden and Hornsund (See Fig. 5.1). The monograph is structured as follows. First, the study sites are presented in details (Sec. 5.2). Then, seasonal trends in the thermohaline structure of the Arctic fjords are discussed (Sec. 5.3). During the last section (Sec. 5.4), we discuss current observation and future perspectives of Kongsfjorden, Isfjorden and Hornsund in a warming climate.

5.2 Locations and characteristic features of fjords

Spitsbergen (between $76^{\circ}30'$ - 80° N and 10° - 22° E) is the largest island of the Svalbard archipelago (Fig. 5.1). Several significant features of West Spitsbergen fjords distinguish them from other Arctic fjords and questioning the applicability of established fjord theories [4]. For instance, sills are absent at the entrance of fjords [5–7]. Moreover, the West Spitsbergen shelf is located at the convergence of two water currents: warm West Spitsbergen Current (WSC) and cold Spitsbergen Polar Current (SPC) (Fig. 5.1) [8, 9]. In this review, we focus on three West Spitsbergen fjords: Kongsfjorden, Isfjorden and Hornsund (Fig. 5.1).

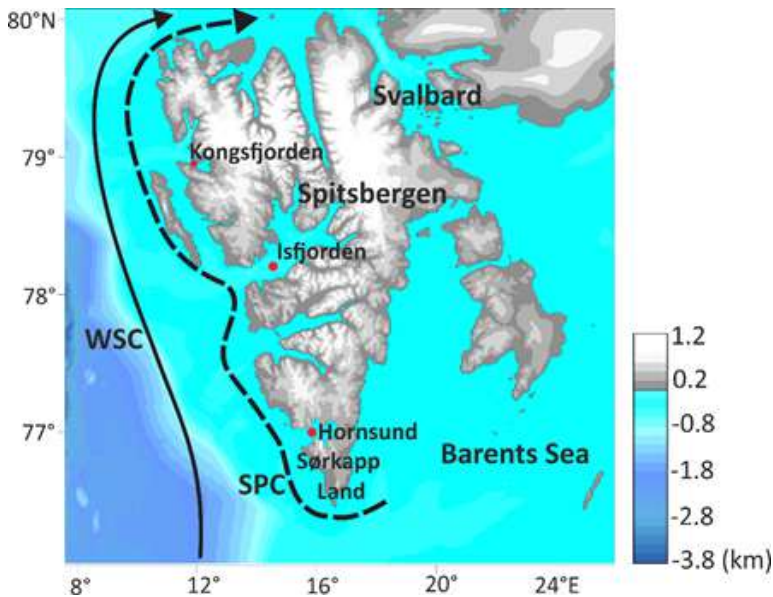


Fig. 5.1: Map of the Svalbard Archipelago with dominating current systems. West Spitsbergen Current (WSC) is shown by black solid arrow, and Spitsbergen Polar Current (SPC) is shown by black dashed arrow.

5.2.1 Kongsfjorden

Kongsfjorden is located in the northern part of the West Spitsbergen coast. It is 20-25 km long and 4-10 km wide (Fig. 5.1) [10, 11]. The Kongsfjorden is oriented Southeast to Northwest at about $78^{\circ}50'N$ and $11^{\circ}-12^{\circ}E$. The characteristic landmarks of Kongsfjorden are Blomstrandhalvøya island, Brandalpynten cape, Lovénøyane archipelago and Dyrevika and Raudvika bays (Fig. 5.2).

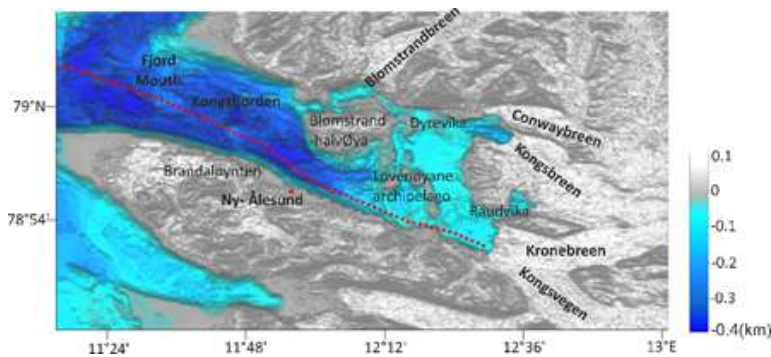


Fig. 5.2: Bathymetry map of Kongsfjorden with characteristic landmarks and tidewater glaciers. The red dot shows the location of Ny-Ålesund. The red dashed line shows Kongsfjorden Transect from outer end to the inner end of the fjord is advected from Tverberg *et al.* [12].

Kongsfjorden is about 350 m deep at the mouth and became shallow towards the inland with typical depths less than 100 m in regions east of Ny-Ålesund [13]. The absence of the sill at the fjord mouth allows for exchanging the fjord and shelf waters [7]. The submarine sills are outstretched from the Lovénøyane islands to northward and southward, creating a barrier between the outer fjord and inner fjord [14].

Seven tidewater glaciers terminate in the northern, eastern and southeastern regions of the Kongsfjorden. Blomstrandbreen, Conwaybreen, Kongsbreen, and Kronebreen are few examples (Fig. 5.2) [14].

Kongsfjorden's climate is relatively less oceanic compared to Horn-

sund [15]. The mean annual air temperature and mean annual precipitation were as follow -4.2°C and 415.5 mm in 1969-2013 at Ny-Ålesund [16]. In Ny-Ålesund, southeastern wind flows along Kongsfjorden, transporting cold and dense air from the Kongsvegen glacier [17, 18].

5.2.2 Isfjorden

Isfjorden is the most extensive fjord system of the western Spitsbergen, located in between 78° - $78^{\circ}50'$ N and 13° - $17^{\circ}30'$ E (Fig. 5.1). Along the Isfjorden, the mean width is 24 km and length about 100 km [19]. In the shelf of Isfjorden, a trough (Isfjordrenna) of about 250 m depth extends from the shelf edge to the mouth of Isfjorden [5, 20]. As a result, Isfjorden is closely linked to the West Spitsbergen Shelf and slope region, allowing the flow of warm Atlantic water from the West Spitsbergen Current into the fjord.

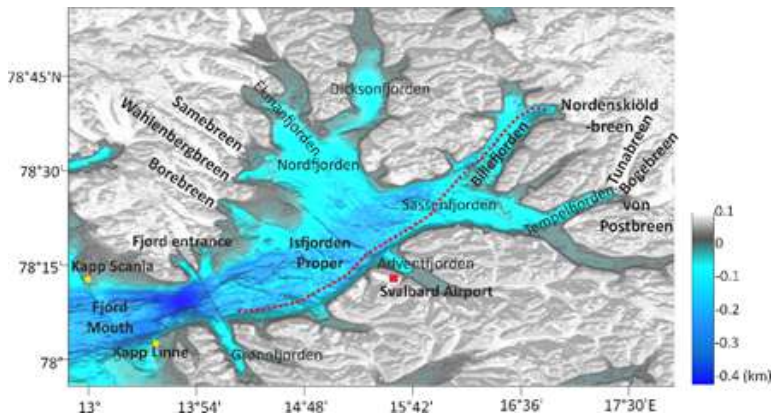


Fig. 5.3: Bathymetry map of Isfjorden with side fjords and prominent glaciers. The black line defines the fjord entrance [5]. The red dashed line shows Kongsfjorden Transect from the entrance to the inner end of the Billefjorden is advected from Skogseth *et al.* [19].

The Isfjorden mouth is 10 km wide and about 455 m deep; it is located between Kapp Scanja and Kapp Linne (Fig. 5.3) [5]. Isfjorden has no distinct sill at the mouth. Therefore, influences from external waters (Ex. Atlantic Water and Arctic Water) on the fjord occur

year-round. The Isfjorden proper is the main basin, 70 km long and 200-300 m deep, oriented to Northeast (at about $78^{\circ}10'N$) with about 60° clockwise angle in regard to the North [5]. The Isfjorden proper contains four main side fjords: Nordfjorden on the northern side, Sassenfjorden on the Eastward and Grønfyorden and Adventfjorden on the southern side (Fig. 5.3). In addition, Nordfjorden heads to Dicksonfjorden and Ekmanfjorden and Sassenfjorden lead to Tempelfjorden, and Billefjorden (Fig. 5.3). Billefjorden is the only side fjord with the sill in the Isfjorden system [5].

Isfjorden has ten tidewater glaciers in northern, eastern and north-eastern regions. Borebreen, Wahlenbergbreen, Samebreen, Nordenskiöldbreen, Tunabreen, Bogebreen and von Postbreen are few examples (Fig. 5.3) [21, 22].

The climate of Isfjorden may be less oceanic than Hornsund (similar conditions as Kongsfjorden [15]). In Isfjorden, the mean annual precipitation is 196 mm at Svalbard Airport in 1971-2000 [23]. In addition, the mean annual air temperature of the Svalbard Airport area was $-5.9^{\circ}C$ in the same period. During winter, the average wind direction shifted from Northeasterly to Southeasterly during 1987-2017 period [19]. The higher winter air temperatures are characterised by strong Southeasterly and Easterly winds, while North-easterly winds drive lower winter air temperatures. Moreover, this could be related to the winter cyclones around the Svalbard region.

5.2.3 Hornsund

In comparison to Kongsfjorden and Isfjorden, Hornsund is a comparatively small; it is located between $76^{\circ}56'-76^{\circ}94'N$ and $15^{\circ}45'-15^{\circ}78'E$ in the southernmost part of the West Spitsbergen (Fig. 5.1). The fjord is approximately 30 km long and 2-12 km wide [24].

The entry to Hornsund, which is located between the capes of Worcesterpynten on the northern coast and Palffyodden on the southern coast (Fig. 5.4) is very flat and shallow, with a maximum depth of only 150 m [6]. The lack of a prominent entrance sill allows shelf water to pour in from the outside. Moreover, the ba-

thymetry map of Hornsund shows a deep sill of about 50 m, which separates the main basin and inner basin of the fjord [6]. The main basin of the fjord has a maximum depth of about 230 m [6]. The inner basin is called Brepollen; it is about 13 km long and 1.7-15 km wide [24] (Fig. 5.4). The maximum depth of the Brepollen is about 140 m [24]. The glacier dynamics directly influences the shape and size of Hornsund [25]. The average annual retreat of glaciers in Hornsund was 70 m in 2000-2010 [26]. Apart from Brepollen, several glacial bays were created by the glacier retreat; examples include Western Burgerbukta and Eastern Burgerbukta and Samarinvågen (Fig. 5.4).

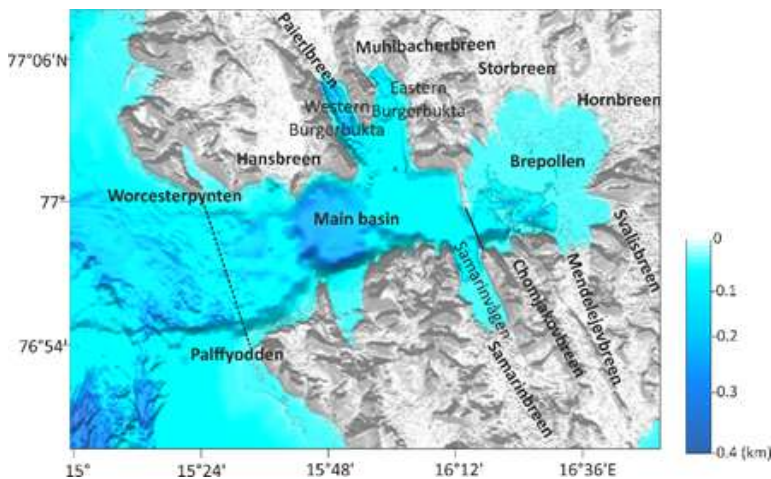


Fig. 5.4: Bathymetry map of Hornsund with glacial bays and tide-water glaciers. The black dashed line separating the outer part and main basin represents the fjord mouth. The black solid line separate the main basin and Brepollen.

The majority of Hornsund is covered by glaciers (67% of total drainage basins) [26]. Hornsund has about fifteen tidewater glaciers. Hansbreen, Paiarlbreen, Mühlbacherbreen, Storbreen, Hornbreen, Svalisbreen, Mendelejev breen, Chomjakovbreen, and Samarinbreen are examples of tidewater glaciers that terminate into Hornsund (Fig. 5.4).

The climate of the Hornsund region is comparatively oceanic, in

comparison to Kongsfjorden and Isfjorden [15]. The mean annual air temperature and precipitation in Hornsund were -3.7°C and 478 mm in 1979-2018 [27]. In addition, the majority of the winds come from the East [26].

5.2.4 Comparison of Kongsfjorden, Isfjorden and Hornsund

Here, the special characteristic features of the three fjords are compared (Tab. 5.1).

Tab. 5.1: Comparison of specific features of Hornsund, Isfjorden and Kongsfjorden.

	Features	Kongsfjorden	Isfjorden	Hornsund
1	Location	78°50'-79°05'N 11°20'-12°40'E	78°-78°50'N 13°-17°30'E	76°56'-76°94'N 15°45'-15°78'E
2	Length [km]	20-25 [10, 11]	100 [19]	30 [24]
3	Width [km]	4-10 [10, 11]	24 [19]	2-12 [24]
4	Depth at the fjord mouth [m]	350 [13]	455 [5]	150 [6]
5	Presence of sill	No [7]	Yes – between Isfjorden Proper and Billefjorden [5]	Yes – between Main Basin and Brepollen [6]
6	Secondary bays/ Side fjords	2	7	4
7	Tidewater glaciers	7	10	15
8	Time period of meteorological observations	1969-2013 (Ny-Ålesund)	1971-2000 (Svalbard Airport)	1979-2018
a	Mean annual air temperature ($^{\circ}\text{C}$)	-4.2 [16]	-5.9 [23]	-3.7 [27]
b	Mean annual precipitation	415.5 [16]	196 [23]	478 [27]
9	Prominent wind	Southeasterly [17]	Southeasterly and Northeasterly [19]	Easterly [26]

Comparison of Kongsfjorden, Isfjorden and Hornsund demonstrated that:

- Kongsfjorden is the Northernmost fjord, while Hornsund is the southernmost fjord of the West Spitsbergen.
- Isfjorden is the largest fjord among these three fjords.

- The fjord mouths are deeper in Kongsfjorden and Isfjorden while shallower in Hornsund. The impact of West Spitsbergen Current is stronger in Kongsfjorden and Isfjorden. The impact of the Spitsbergen Polar Current is stronger in Hornsund. (The Spitsbergen Polar Current is the surface current, and West Spitsbergen Current is the Intermediate current).
- The absence of a sill at the mouth is common for all three fjords. This facilitates the flow of water from the shelf into the fjords. However, Hornsund and Isfjorden show inner basins, Brepollen and Billefjorden, respectively. Isfjorden records a higher number of side fjords compared to the other two fjords.
- Hornsund has more tidewater glaciers than Kongsfjorden and Isfjorden.
- The periods of meteorological observations, for which mean air temperature and precipitation are available in the publications, were different for three considered fjords. Therefore, it is not possible to compare directly these two parameters for different fjords.
- The Kongsfjorden is more pronounced with Southeasterly wind while Hornsund – with Easterly wind. In contrast, Isfjorden experience both Southeasterly and Northeasterly winds.

5.3 Seasonal trends in the thermohaline structure of the Arctic fjords

5.3.1 Internal and external factors affecting the thermohaline structure

The stratification of Arctic fjords changes on a seasonal and inter-annual scale. The layering of water masses is controlled by a series of internal and external processes, which could be related to each other. The processes are presented in Fig. 5.5 [18, 28]. Fig. 5.5 also shows the typical pattern of the thermohaline structure of Arctic fjords during summer, which is detailed in the next Sec. 5.3.2.

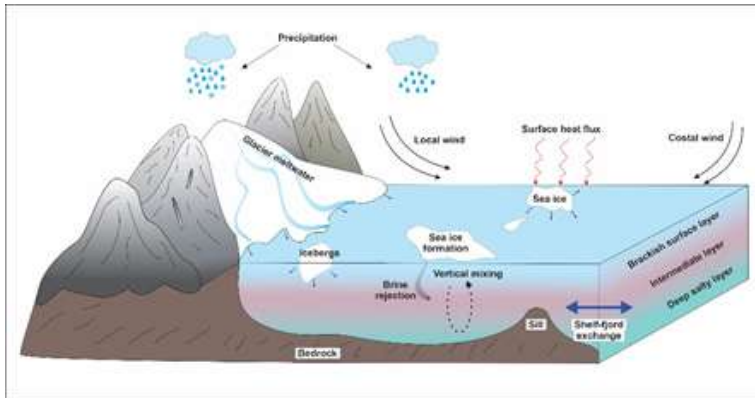


Fig. 5.5: Schematic illustration of the classical arrangement of the water layers in the Arctic fjord (Brackish surface layer, Intermediate layer and Deep salty layer) [4]. The internal and external processes affecting the stratification are also shown [18, 28]. The blue spiral arrows show the melting of sea ice, icebergs and glaciers.

The internal processes acting within the fjord include: cryogenic freshwater influx (melting of glaciers, icebergs and sea ice), precipitation, surface heat flux, local wind forces, tidal motion, sea ice formation and brine rejection [18, 28]. The melting of glaciers and icebergs enhances the freshwater influx to the surface layer of the fjords [28]. This is an example of stratification driven by salinity rather than temperature (see ‘brackish surface layer’ in Fig. 5.5). In cloudless days during summer, surface layer outside of glacial bays forms also as a result of the increased solar radiation [7, 18]. In contrast, the heat loss during winter and related sea ice formation with brine release to the water below drive convection movements [18].

The main external process influencing the stratification is the exchange between fjord and external water masses (fjord-shelf exchange). The water masses brought by the West Spitsbergen Current and Spitsbergen Polar Current drives this exchange. These currents are presented in Fig. 5.1. The West Spitsbergen Current is topographically steered along the continental slope of the West Spitsbergen. It brings warm and salty Atlantic Water [29, 30]. The

Spitsbergen Polar Current carries colder and comparatively fresher Arctic Water as well as it can bring sea ice from the Barents Sea [31]. The Atlantic Water meets the Arctic Water via the West Spitsbergen Shelf. The Spitsbergen Polar Current is a surface current that often acts as a barrier between West Spitsbergen Current and fjords [32, 33]. Different external factors determine the possibility of advection of Atlantic Water from West Spitsbergen Current to the shelf (e.g., coastal winds and eddy overturning) [18, 30, 34] and then to the fjord (e.g., geostrophic control) [5, 7, 35]. For instance, the heat loss from the surface layer will drive eddy overturning across the shelf edge and keep the light water above dense water. When the northerly winds are prominent, the surface water layer moves away from the shelf towards the ocean. As a result, Atlantic Water advection is occurred in intermediate or deeper levels of the shelf. The Atlantic Water in the shelf intrudes into the fjord when the water exchange barrier (geostrophic control) breaks down due to the low-density differences between shelf water and fjord water [12]. The inflow of the cold water from the Spitsbergen Polar Current into the fjords has also been observed [36].

The variations of the thermohaline structure of fjords are the result of interactions between the above mentioned internal and external factors.

5.3.2 Characteristic features of the thermohaline structure of the West Spitsbergen Fjords

Types of Water Masses

Understanding the spatial distribution of the water masses in fjords is crucial for understanding the seasonal variations of the thermohaline structure of fjords. Different types of water masses found in fjords of the West Spitsbergen can be classified as follows:

- external: Atlantic Water (AW) and Arctic Water [37–39]
- internal: Surface Water masses (SW), Local Water (LW) and Winter Cooled Water (WCW) [18]
- mixed: Transformed Atlantic Water (TAW), Intermediate Water (IW) and Cooled Atlantic Water (CAW) [18, 40].

AW from the West Spitsbergen Current and Arctic Water from the Spitsbergen Polar Current originate outside the fjord and bring warm and cold water to the fjords, respectively. Moreover, the distribution of water masses in the summer is different in comparison to the winter [18, 40].

Tab. 5.2: Temperature and salinity ranges of water masses common for Hornsund, Isfjorden and Kongsfjorden as adapted from Svendsen *et al.* [18], Nilsen *et al.* [5] and Promińska *et al.* [31].

Water mass	Potential temperature [°C]	Salinity [psu]
Atlantic Water (AW)	$T > 3$	$S > 34.9$
Surface Water (SW)	$T > 1$	$S < 34$
Transformed Atlantic Water (TAW)	$T > 1$	$34.7 < S < 34.9$
Intermediate Water (IW)	$T > 1$	$34 < S < 34.7$
Local Water (LW)	$T < 1$	
Winter Cooled Water (WCW)	$T < -0.5$	$S > 34.4$

Tab. 5.3: Temperature and salinity ranges of Arctic Water for Hornsund (defined from the shelf) [31] and Isfjorden (defined from Barents sea) [19], and Cooled Atlantic Water (CAW) for Kongsfjorden [40].

Fjord	Water mass	Potential temperature [°C]	Salinity [psu]
Hornsund	Arctic Water	$-1.5 < T < 2$	$34 < S < 34.5$
Isfjorden	Arctic Water	$T < 0$	$34.3 < S < 34.8$
Kongsfjorden	Cooled Atlantic Water	$1 < T < 3$	$S > 34.9$

Temperature and salinity ranges of major water masses common for Kongsfjorden, Isfjorden and Hornsund as adapted from Svendsen *et al.* [18], Nilsen *et al.* [5] and Promińska *et al.* [31] are shown in Tab. 5.2. Nevertheless, ranges of temperature and salinity for Arctic Water, observed only in Hornsund and Isfjorden, differ from

each other (Tab. 5.3.) [19, 31]. Apart from that, temperature and salinity ranges for Cooled Atlantic Water, which is observed only in Kongsfjorden, is stated in Tab. 5.3 [40].

General features of the thermohaline structure of the West Spitsbergen fjords

According to Farmer and Freeland [4], silled fjords have a typical summer thermohaline structure with three layers: surface, intermediate, and deep. However, some studies reported that non-silled Hornsund [41], Isfjorden [5] and Kongsfjorden [7] also display this three layer arrangement during summer. Svendsen *et al.* [18] explained the three layer structure with the arrangement of water masses in summer, common for the West Spitsbergen fjords. Accordingly, in the summer (July-September), freshwater from melting glaciers and sea ice and river influx enhances the freshwater content of the Surface Water. The intermediate layer, observed beneath the surface layer, is a transition layer comprising Intermediate Water or Transformed Atlantic Water [5, 18]. Intermediate Water is formed by the combination of Surface Water and the subsurface water below (Atlantic Water, Transformed Atlantic Water or Local Water) via the heat exchange and mixing processes [5, 18]. Transformed Atlantic Water is formed as a combination of Atlantic Water and Arctic Water [18]. The deep layer below the intermediate layer is comprised of old winter water, which could be produced e.g., from brine release during the sea ice formation and winter heat loss to the atmosphere or due to the Atlantic Water advection into the fjord [12, 18]. In the late summer, the stratification can be broken down due to the surface cooling and starting of convection [41].

Generally, in winter (January-May), the fjord water is substantially cooled at the surface layer due to heat loss to the atmosphere. The surface cooling increases the water density and promotes convection. As a result, Local Water is produced [18]. In addition, when the Local Water reaches its freezing point, the sea ice formation releases brine [5]. This causes deep winter convection that can penetrate the fjord bottom, producing the Winter Cooled Water [18].

Common features of the thermohaline structure of Kongsfjorden and Isfjorden

Generally, the advection of Atlantic Water is expected to be occurred only during summer [18, 28]. However, the studies of Kongsfjorden and Isfjorden have revealed that the Atlantic Water advection can be occurred during winter also [12, 19]. Accordingly, three types of winter scenarios have been identified for Isfjorden [19] and Kongsfjorden [12] with the probability of Atlantic Water inflow: Winter Deep, Winter Intermediate and Winter Open (Fig. 5.6a-c)). In the same figure (Fig. 5.6), three types of summer distributions of water masses are also presented: Summer Deep, Summer Intermediate and Summer Open (Fig. 5.6d-f)).

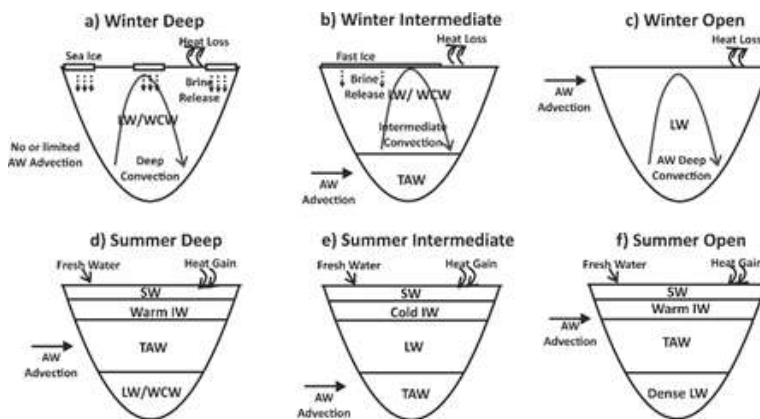


Fig. 5.6: Illustration of the water mass structure in a) Winter Deep, b) Winter Intermediate, c) Winter Open, d) Summer Deep, e) Summer Intermediate, and f) Summer Open common for Kongsfjorden and Isfjorden. Modified from Fig. 21 of Skogseth *et al.* [19] and mean temperature-salinity graphs of summers following winters types in Tverberg *et al.* [12] and De Rovere *et al.* [42].

Accordingly, **Winter Deep** scenario (Fig. 5.6a)) are distinguished by winter convection in the fjord which reaches the bottom of the water column, with either none or strongly limited winter Atlantic Water advection into the fjord. The deep convection occurs as a consequence of effective sea ice formation, triggering brine re-

lease, and strong heat loss to the cold atmosphere. It drives the production of dense bottom water in the fjord (LW and WCW).

Unlike the previous winter scenario (Fig. 5.6a)), the **Winter Intermediate** scenario (Fig. 5.6b)) is characterised by intermediate depth limited winter convection, along with winter advection of Atlantic Water into the deepest layer of the fjord. And the less effective sea ice formation is occurred due to the less heat flux to cold atmosphere. Less dense LW/WCW occur above dense Transformed Atlantic Water.

Winter Open scenario (Fig. 5.6c)) are distinguished by Atlantic Water advection into the surface layer of the fjord, and the winter convection of this Atlantic Water is extended to the bottom. This situation is common during winters significantly different from the previous two types, presented in (Fig. 5.6a)) and (Fig. 5.6b)), and there is no sea ice is formed due to the inflow of Atlantic Water. The deep Atlantic Water convection forms cold and high salinity Local Water.

In addition, winter types impact on the following summer thermo-haline structures. Accordingly, the key effect of the winter types on the summer water mass stratification is the depth of summer Atlantic Water advection (Fig. 5.6d-f)). Moreover, the depth of the summer Atlantic Water advection is strongly influenced by the density of the old winter water [12].

In the following summer of Winter Deep scenario (**Summer Deep**, Fig. 5.6d)), Atlantic Water advection occurs at a certain intermediate depth. The surface layer contains brackish Surface Water. The inflowing Atlantic Water converts to Transformed Atlantic Water over the depth above the remaining cold and dense LW/WCW, produced in winter. Furthermore, as a result of the mixing of Surface Water and Transform Atlantic Water, the warm Intermediate Water layer occurs.

In the following summer of Winter Intermediate scenario (**Summer Intermediate**, Fig. 5.6e)) the Atlantic Water advection occurs at a deeper layers compared with the Summer Deep scenario. The surface layer is colder and less saline in this case due to the warm

and saline Atlantic Water intrude into deep layer, is not significantly affect the surface layer. Unlike the Summer Deep case, the Intermediate Water is cold due to the mixing of Surface Water and Local Water below.

In the summer of Winter Open (**Summer Open**, Fig. 5.6f) condition, the advection of Atlantic Water may be incredibly shallow as a result of relatively dense winter water produced from the Winter Open compared to the Winter Deep. The Surface Water and warm Intermediate Water occur above the Transformed Atlantic Water with dense Local Water in the deepest part.

The internal and external factors discussed in Sec. 5.3.1 differently affect the thermohaline structure of the fjords in different seasons. Moreover, the impact of density differences between the fjord water and adjacent shelf water on the Atlantic Water advection vary during summers and winters; for example, the water exchange barrier may occur or not (geostrophic control) [7, 35]. This causes significant variations in temperature-salinity profiles of the fjord by modification of water mass distribution and variability of Atlantic Water advection. Therefore, in some circumstances, the water mass distribution and so the thermohaline structure of the fjords show some deviations from the typical structure.

Kongsfjorden – deviations from common schemes

Although Kongsfjorden has winter types as shown in Fig. 5.6a)-c), some deviations from the common pattern can be observed [12]. Here onwards, we discuss those deviations which are specific only for Kongsfjorden.

The deviations of the Winter scenarios (from the diagrams presented in Fig. 5.6a)-c)) are the followings:

1. **Winter Deep** – The entire water column is filled only with Winter Cooled Water ($T < -1.5^{\circ}\text{C}$; $S > 34.7$ psu) (See Fig. 3.13 Winter temp. 2002 and Winter sal. 2002 in Tverberg *et al.* [12]).
2. **Winter Intermediate** – Only Local Water is present from surface to intermediate depth (See Fig. 3.13 Winter temp. 2004 and Winter sal. 2004 in Tverberg *et al.* [12]).

3. **Winter Open** – The entire water column is filled with Cooled Atlantic Water ($1.5 < T < 3^{\circ}\text{C}$; $S > 35$ psu) (See Fig. 3.13 Winter temp. 2007 and Winter sal. 2007 in Tverberg *et al.* [12]).

In some circumstances, the summer types following winters show some water mass modification unique only for Kongsfjorden, despite common summer patterns in Fig. 5.6d)-f).

The deviation of the Summer Types (from the diagrams presented in Fig. 5.6d)-e)) are the followings:

1. **Summer Deep** – Warm and thin surface layer ($T > 5^{\circ}\text{C}$). Local Water is prominent in the deeper layer ($T < 1^{\circ}\text{C}$) (See Fig. 3.13 Summer temp. 2002 and Summer sal. 2002 in Tverberg *et al.* [12]) . In some cases, Transformed Atlantic Water occurs in the deeper layer [42].
2. **Summer Intermediate** – Thick Surface Water layer is present (See Fig. 3.13 Summer temp. 2004 and Summer sal. 2004 in Tverberg *et al.* [12]).
3. **Summer Open** – Cooled Atlantic Water is prominent in the deeper layer below Atlantic water (See Fig. 3.13 Summer temp. 2007 and Summer sal. 2007 in Tverberg *et al.* [12]) or Transformed Atlantic Water.

Accordingly, pure Atlantic Water from the West Spitsbergen Current can be also observed in Kongsfjorden during summer [12]. Furthermore, the densest water of Kongsfjorden is not Winter Cooled Water but Cooled Atlantic Water [12, 40].

Notably, the Winter Deep and Winter Intermediate winters were pronounced before mid of 2000, and Winter Open winters were pronounced following years [12, 42]. Accordingly, Kongsfjorden was gradually warming recently due to the active role of Atlantic origin waters. As a result, Kongsfjorden has been transformed from the Arctic to the Atlantic type over the last decade [12, 42].

Isfjorden – deviations from common schemes

When considering Isfjorden, researchers focused on Isfjorden Proper and Billefjorden (See Fig. 5.3; [5, 19]). The Isfjorden proper has no

sill at the mouth [5]. In contrast, the situation of the Billefjorden is different because Billefjorden is the only side fjord with the sill in the Isfjorden system [5].

The Isfjorden Proper shows winter types, see Fig. 5.6a)-c); however, some deviations from the typical structure could be observed [19]:

1. **Winter Deep** – Patches of Local Water are found in intermediate depths ($T > -0.5^{\circ}\text{C}$) (See Fig. 7a and Fig. 7b in Skogseth *et al.* [19]).
2. **Winter Intermediate** – Low salinity Winter Cooled Water ($S < 34.5$ psu) is above high salinity Local Water ($34.5 < S < 34.7$ psu) (See Fig. 7d and Fig. 7e in Skogseth *et al.* [19]).
3. **Winter Open** – Water column is filled with cooled Transformed Atlantic Water ($T < 1^{\circ}\text{C}$; $34.7 > S < 34.9$ psu) (See Fig. 7g and Fig. 7h in Skogseth *et al.* [19]).

In some circumstances, the summer types following winters (Fig. 5.6d)-f)) show water mass deviations unique only for Isfjorden, despite common summer types.

The deviations of summer types are following:

1. **Summer Deep** – Local Water is prominent in the deeper layer ($T < 1^{\circ}\text{C}$) (See Fig. 7j and Fig. 7k in Skogseth *et al.* [19]).
2. **Summer Intermediate** – Patches of Local Water are presented in intermediate depths ($T < 1^{\circ}\text{C}$) (See Fig. 7m and Fig. 7n in Skogseth *et al.* [19]).
3. **Summer Open** – Cooled Transformed Atlantic Water ($1 < T < 1.5^{\circ}\text{C}$) can be found in the deep layer (See Fig. 7p and Fig. 7q in Skogseth *et al.* [19]).

The differences in winter structure between Billefjorden and Isfjorden Proper are following:

1. The water column of Billefjorden is filled only with the Winter Cooled Water ($T < -0.5^{\circ}\text{C}$; $S > 34.4$ psu) for all winter types (See Fig. 7a, Fig. 7b, Fig. 7g, and Fig. 7h in Skogseth *et al.* [19]).
2. The winter type shown in Billefjorden is similar to **Winter**

Deep (See Fig. 5.6a)).

The differences in summer structure between Billefjorden and Isfjorden Proper are following:

1. **Summer Deep** – Winter Cooled Water ($T < -0.5^{\circ}\text{C}$; $S > 34.7$ psu) is prominent in the deeper layer (See Fig. 7j and Fig. 7k in Skogseth *et al.* [19]). Transformed Atlantic Water is absent.
2. **Summer Open** – Winter Cooled Water ($T < -0.5^{\circ}\text{C}$; $S > 34.8$ psu) is prominent in the deeper layer (See Fig. 7p and Fig. 7q in Skogseth *et al.* [19]).

Recently, the Isfjorden system has been warming gradually in the winter due to the increased Atlantic Water Advection [19, 30]. As a result, Winter Open winters were more pronounced in the last decade, while Winter Deep and Winter Intermediate winters were pronounced before 2011 [19]. Accordingly, Isfjorden has been transformed from the Arctic to the Atlantic dominance in winter over the last decade.

Hornsund – deviations from common schemes

Southernmost Hornsund does not show all winter types as Kongsfjorden and Isfjorden [31].

The deviations from typical winter types are the following:

1. The water column of Hornsund is filled with Local Water and Winter Cooled Water (Fig. 5.7a)).
2. The winter type shown in Hornsund is similar to **Winter Deep** (See Fig. 5.6a)).

Considering the summer type of stratification in Hornsund, the two basins should be considered separately – Main Basin and Inner Basin (Brepollen) (See Fig. 5.4). These two regions differ in terms of the water mass structure during summer [31].

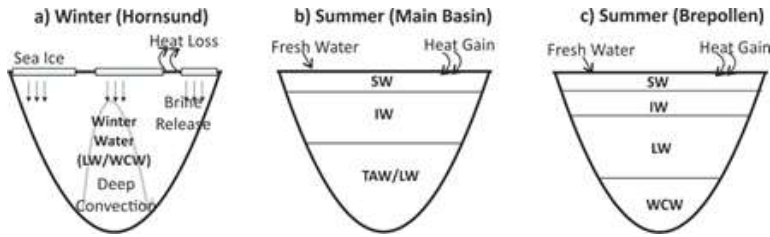


Fig. 5.7: Illustration of the winter and summer water mass stratification in Hornsund, a) Winter (Modified from Cottier *et al.* [28]), b) Main Basin in summer and c) Brepollen in summer [31].

Deviations of summer structure in the Main Basin are the following:

1. Local Water is present in the deep layer when Atlantic Water is absent on the shelf (Fig. 5.7b)) (See Fig. 4 in Promińska *et al.* [31]).
2. Transformed Atlantic Water is present in the deep layer when Atlantic Water is found on the shelf (Fig. 5.7b)) (See Fig. 4 in Promińska *et al.* [31]).
3. In some exceptional cases Intermediate Water is found below the Surface Water, filling the entire basin towards the bottom when less Transform Atlantic Water is at the bottom of the shelf (See Fig. 4 in Promińska *et al.* [31]).

Accordingly, the thermohaline structure of the Main Basin may depend on the waters on the shelf rather than the remains of previous winter water [31].

The difference in the summer structure in Brepollen in comparison with Main Basin is the following:

1. The deep layer is characterized by Winter Cooled Water below Local Water (Fig. 5.7c)).
2. In rare cases, the Atlantic Water can pass the sill and reach Brepollen, resulting in the presence of Transformed Atlantic Water at the intermediate depth (e.g. summer 2014; Promińska *et al.* [31]).

Notably, Hornsund received large ice packs from the Barents sea in addition to Arctic Water from Spitsbergen Polar Current [31].

Therefore, the reason behind Hornsund remains as a more Arctic dominance fjord is the significant influence of Spitsbergen Polar Current than Atlantic Water from West Spitsbergen Current [6, 15].

5.3.3 Comparison of seasonal variations of the thermohaline structure in Kongsfjorden, Isfjorden and Hornsund

The comparison of seasonal variations of the thermohaline structure in Kongsfjorden, Isfjorden and Hornsund is presented in Tab. 5.4.

Tab. 5.4: Comparison of winter and summer variations of thermohaline structure in Kongsfjorden, Isfjorden and Hornsund.

Seasonal variations	Kongsfjorden	Isfjorden	Hornsund
WINTER			
Prominent water inflow from the shelf	Atlantic Water [12]	Atlantic Water [19]	Arctic water and ice packs from the Barents Sea [31]
Winter scenarios	Three winter scenarios [12]	Three winter scenarios [19]	Winter Deep [31]
Prominent water masses in winter	TAW and CAW	Low dense WCW, Cooled TAW in Isfjorden Proper and WCW in Billefjorden	WCW
SUMMER			
Main freshwater influx	Glacier meltwater runoff [18]	Glacier meltwater runoff [43]	Glacier meltwater runoff [44]
Prominent water inflow from the shelf	Atlantic Water [12]	Atlantic Water [19]	Arctic water and Antlatic Water [31]
Summer scenarios	Three summer scenarios [12]	Three summer scenarios [19]	–
Prominent water masses in summer	CAW	Cooled TAW in Isfjorden Proper dense WCW in Billefjorden	LW/TAW in Main Basin and WCW in Brepollen

In Tab. 5.4, the winter variations thermohaline structure of Kongsfjorden, Isfjorden and Hornsund are presented in 1, 2 and 3 rows. The summer variations of thermohaline structure are presented in rows 4, 5, 6 and 7.

Analysis of Tab. 5.4 demonstrates that the main difference in winter and summer scenarios is between Kongsfjorden, and Isfjorden from one side and Hornsund from the other side. It includes:

1. The impact of Arctic water is specific, mainly in Hornsund.

2. Only one winter scenario is typical of Hornsund, while for Kongsfjorden and Isfjorden – the three winter and summer types
3. There is also a difference in the types of water masses, e.g., WCW is observed only in Hornsund and was not registered in Kongsfjorden, and the Isfjorden Proper.
4. The glacier meltwater runoff is the main freshwater contributor in three fjords.

Notably, there are differences in winter and summer scenarios of Kongsfjorden and Isfjorden also. In the Kongsfjorden, the intensity of Atlantic type water is higher (Cooled Atlantic Water) than Isfjorden (Cooled Transform Atlantic Water).

5.4 Kongsfjorden, Isfjorden and Hornsund in a warming climate: current observation and future perspectives

Changes that occur in the atmospheric and oceanic circulation patterns due to climate change enhance the influence of warm and saline Atlantic Water in the Arctic region; this mechanism is called ‘Atlantification’ [45, 46]. Therefore, an increased advection of the Atlantic Water from the West Spitsbergen Current to the West Spitsbergen Fjords is observed [35, 47]. The Atlantic Water influx is linked with the temperature and salinity variations of the water layers in Kongsfjorden, Isfjorden and Hornsund.

During the last decade, Kongsfjorden and Isfjorden have been gradually warming due to the increased advection of Atlantic Waters in the fjords. As a result, Kongsfjorden and Isfjorden have been transformed from the Arctic dominance to the Atlantic dominance fjords over the last decade [12, 19, 42]. In addition, the presence of Atlantic origin water (Atlantic Water or Transform Atlantic Water) in Hornsund has increased during the last decade [36]. However, Hornsund has preserved its Arctic dominance due to the regulating effect of Arctic Water, delivered by the Spitsbergen Polar Current [36]. Spitsbergen Polar Current acts as a barrier between the West Spits-

bergen Current and Hornsund. Notably, continuing Atlantification of the Arctic ocean may diminish the role of the Spitsbergen Polar Current on the Hornsund. If this happens, Hornsund will be more sensitive to the influence of the West Spitsbergen Current and may warm rapidly. However, a different scenario is also possible.

The warming-induced glacier melting is pronounced in Arctic fjords. For instance, the retreat of tidewater glaciers in Hornsund is accelerating in last few decades from warming in Svalbard [26]. The accelerated retreat of glaciers cause fjord freshening. Long-term freshening of fjords may cease the shelf-fjord water exchange due to the creation of density barriers. Consequently, I hypothesize that Hornsund may stay isolated from the influence of the Atlantic Water, at least to a certain extent. Moreover, due to fast retreating of Hornbreen terminus (See Fig. 5.4), Hornsund may transform to a strait, which will separate the most southern part of the Spitsbergen (Sørkapp Land, See Fig. 5.1) from the other part of the island in the future [48]. The opening of such strait, which is related to warming, would change the thermohaline structure of Hornsund dramatically.

In conclusion, the West Spitsbergen fjords are sensitive to the Atlantification of the Arctic. The variability of the thermohaline structure of fjords may play an important role as an indicator of the ocean sensitivity to the global climate shifts.

Acknowledgement

I would like to give my heartiest gratitude to my supervisors Prof. Natalia Gorska from the Institute of Oceanology and Dr. Oskar Glowacki from the Institute of Geophysics, for their immense support in preparing the manuscript and encouragement.

Bibliography

- [1] Judah Cohen, James A Screen, Jason C Furtado, Mathew Barlow, David Whittleston, Dim Coumou, Jennifer Francis, Klaus Dethloff, Dara Entekhabi, James Overland, et al. Recent arctic amplification and extreme mid-latitude weather. *Nature geoscience*, 7(9):627–637, 2014.
- [2] Mark C Serreze and Roger G Barry. Processes and impacts of arctic amplification: A research synthesis. *Global and planetary change*, 77(1-2):85–96, 2011.
- [3] Valérie Masson-Delmotte, Panmao Zhai, Anna Pirani, Sarah L Connors, Clotilde Péan, Sophie Berger, Nada Caud, Y Chen, L Goldfarb, MI Gomis, et al. Climate change 2021: the physical science basis. *Contribution of working group I to the sixth assessment report of the intergovernmental panel on climate change*, 2(1):2391, 2021.
- [4] David M Farmer and Howard J Freeland. The physical oceanography of fjords. *Progress in oceanography*, 12(2):147–219, 1983.
- [5] Frank Nilsen, Finlo Cottier, Ragnheid Skogseth, and S Mattsson. Fjord–shelf exchanges controlled by ice and brine production: the interannual variation of atlantic water in isfjorden, svalbard. *Continental Shelf Research*, 28(14):1838–1853, 2008.
- [6] Agnieszka Promińska, Małgorzata Cisek, and Waldemar Walczowski. Kongsfjorden and hornsund hydrography–

- comparative study based on a multiyear survey in fjords of west spitsbergen. *Oceanologia*, 59(4):397–412, 2017.
- [7] Finlo Cottier, Vigdis Tverberg, Mark Inall, Harald Svendsen, Frank Nilsen, and Colin Griffiths. Water mass modification in an arctic fjord through cross-shelf exchange: The seasonal hydrography of kongsfjorden, svalbard. *Journal of Geophysical Research: Oceans*, 110(C12), 2005.
- [8] Bjørn Helland-Hansen and Fridtjof Nansen. *The Norwegian Sea: its physical oceanography based upon the Norwegian researches 1900-1904*, volume 2. Det Mallingske bogtrykkeri, 1909.
- [9] Ursula Schauer, Eberhard Fahrback, Svein Osterhus, and Gerd Rohardt. Arctic warming through the fram strait: Oceanic heat transport from 3 years of measurements. *Journal of Geophysical Research: Oceans*, 109(C6), 2004.
- [10] John A Howe, Katrine Husum, Mark E Inall, James Coogan, Adrian Luckman, Riccardo Arosio, Colin Abernethy, and David Verchili. Autonomous underwater vehicle (auv) observations of recent tidewater glacier retreat, western svalbard. *Marine Geology*, 417:106009, 2019.
- [11] Olga Pavlova, Sebastian Gerland, and Haakon Hop. Changes in sea-ice extent and thickness in kongsfjorden, svalbard (2003–2016). *The ecosystem of kongsfjorden, svalbard*, pages 105–136, 2019.
- [12] Vigdis Tverberg, Ragnheid Skogseth, Finlo Cottier, Arild Sundfjord, Waldemar Walczowski, Mark E Inall, Eva Falck, Olga Pavlova, and Frank Nilsen. The kongsfjorden transect: seasonal and inter-annual variability in hydrography. *The Ecosystem of Kongsfjorden, Svalbard*, pages 49–104, 2019.
- [13] Laura Halbach, Mikko Vihtakari, Pedro Duarte, Alistair Everett, Mats A Granskog, Haakon Hop, Hanna M Kauko, Svein Kristiansen, Per I Myhre, Alexey K Pavlov, et al. Tidewater glaciers and bedrock characteristics control the phytoplankton

- growth environment in a fjord in the arctic. *Frontiers in Marine Science*, 6:254, 2019.
- [14] Katharina Streuff, Matthias Forwick, Witold Szczuciński, Karin Andreassen, and Colm Ó Cofaigh. Submarine landform assemblages and sedimentary processes related to glacier surging in kongsfjorden, svalbard. *arktos*, 1:1–19, 2015.
- [15] Małgorzata Cisek, Przemysław Makuch, and Tomasz Petelski. Comparison of meteorological conditions in svalbard fjords: Hornsund and kongsfjorden. *Oceanologia*, 59(4):413–421, 2017.
- [16] JI López-Moreno, J Boike, A Sanchez-Lorenzo, and JW Pomeroy. Impact of climate warming on snow processes in ny-ålesund, a polar maritime site at svalbard. *Global and Planetary Change*, 146:10–21, 2016.
- [17] HJ Beine, S Argentini, A Maurizi, G Mastrantonio, and A Viola. The local wind field at ny-å lesund and the zeppelin mountain at svalbard. *Meteorology and Atmospheric Physics*, 78(1):107–113, 2001.
- [18] Harald Svendsen, Agnieszka Beszczynska-Møller, Jon Ove Hagen, Bernard Lefauconnier, Vigdis Tverberg, Sebastian Gerland, Jon Børre Ørbæk, Kai Bischof, Carlo Papucci, Marek Zajaczkowski, et al. The physical environment of kongsfjorden–krossfjorden, an arctic fjord system in svalbard. *Polar research*, 21(1):133–166, 2002.
- [19] Ragnheid Skogseth, Léa LA Olivier, Frank Nilsen, Eva Falck, N Fraser, Vigdis Tverberg, Anna Birgitta Ledang, Anna Vader, Marius Opsanger Jonassen, Janne Søreide, et al. Variability and decadal trends in the isfjorden (svalbard) ocean climate and circulation—an indicator for climate change in the european arctic. *Progress in Oceanography*, 187:102394, 2020.
- [20] Neil J Fraser, Ragnheid Skogseth, Frank Nilsen, and Mark E Inall. Circulation and exchange in a broad arctic fjord using glider-based observations. *Polar research*, 37(1):1485417, 2018.

- [21] Matthias Forwick, Tore O Vorren, Morten Hald, Sergei Korsun, Yul Roh, Christoph Vogt, and Kyu-Cheul Yoo. Spatial and temporal influence of glaciers and rivers on the sedimentary environment in sassenfjorden and tempelfjorden, spitsbergen. *Geological Society, London, Special Publications*, 344(1):163–193, 2010.
- [22] Marek W Ewertowski, David JA Evans, David H Roberts, and Aleksandra M Tomczyk. Glacial geomorphology of the terrestrial margins of the tidewater glacier, nordenskiöldbreen, svalbard. *Journal of Maps*, 12(sup1):476–487, 2016.
- [23] Inger Hanssen-Bauer, EJ Førland, Hege Hisdal, Stephanie Mayer, Anne Brit Sandø, and Asgeir Sorteberg. Climate in svalbard 2100. *A knowledge base for climate adaptation*, 470, 2019.
- [24] Mateusz Moskalik, Piotr Grabowiecki, Jarosław Tęgowski, and Monika Żulichowska. Bathymetry and geographical regionalization of brepollen (hornsund, spitsbergen) based on bathymetric profiles interpolations. *Polish Polar Research*, (1):1–22, 2013.
- [25] L Kolondra. Satellite orthophotomap of a part of south spitsbergen, svalbard. *University of Silesia, Sosnowiec*, 2010.
- [26] Małgorzata Błaszczyk, Jacek Adam Jania, and Leszek Kolondra. Fluctuations of tidewater glaciers in hornsund fjord (southern svalbard) since the beginning of the 20th century. *Polish Polar Research*, 34(4), 2013.
- [27] Tomasz Wawrzyniak and Marzena Osuch. A 40-year high arctic climatological dataset of the polish polar station hornsund (sw spitsbergen, svalbard). *Earth System Science Data*, 12(2):805–815, 2020.
- [28] FR Cottier, F Nilsen, R Skogseth, V Tverberg, J Skarðhamar, and H Svendsen. Arctic fjords: a review of the oceanographic environment and dominant physical processes. *Geological Society, London, Special Publications*, 344(1):35–50, 2010.

- [29] Robert Osinski, Wieczorek Piotr, Agnieszka Beszczynska-Moeller, and Ilona Goszczko. Adcp-referenced geostrophic velocity and transport in the west spitsbergen current. *Oceanologia*, 45:425–435, 2003.
- [30] Frank Nilsen, Ragnheid Skogseth, Juni Vaardal-Lunde, and Mark Inall. A simple shelf circulation model: intrusion of atlantic water on the west spitsbergen shelf. *Journal of Physical Oceanography*, 46(4):1209–1230, 2016.
- [31] Agnieszka Promińska, Eva Falck, and Waldemar Walczowski. Interannual variability in hydrography and water mass distribution in hornsund, an arctic fjord in svalbard. *Polar Research*, 37(1):1495546, 2018.
- [32] Vigdis Tverberg, Ole Anders Nøst, Christian Lydersen, and Kit M Kovacs. Winter sea ice melting in the atlantic water subduction area, svalbard norway. *Journal of Geophysical Research: Oceans*, 119(9):5945–5967, 2014.
- [33] R Skogseth, PM Haugan, and M Jakobsson. Watermass transformations in storfjorden. *Continental Shelf Research*, 25(5-6):667–695, 2005.
- [34] Finlo R Cottier, Frank Nilsen, ME Inall, Sebastian Gerland, Vigdis Tverberg, and Harald Svendsen. Wintertime warming of an arctic shelf in response to large-scale atmospheric circulation. *Geophysical Research Letters*, 34(10), 2007.
- [35] John M Klinck, James J O’Brien, and Harald Svendsen. A simple model of fjord and coastal circulation interaction. *Journal of Physical Oceanography*, 11(12):1612–1626, 1981.
- [36] Agnieszka Strzelewicz, Anna Przyborska, and Waldemar Walczowski. Increased presence of atlantic water on the shelf south-west of spitsbergen with implications for the arctic fjord hornsund. *Progress in Oceanography*, 200:102714, 2022.
- [37] B Rudels, R Meyer, Eberhard Fahrbach, VV Ivanov, S Østerhus, D Quadfasel, Ursula Schauer, V Tverberg, and

- RA Woodgate. Water mass distribution in Fram Strait and over the yermak plateau in summer 1997. In *Annales Geophysicae*, volume 18, pages 687–705. Springer Verlag Göttingen, Germany, 2000.
- [38] James H Swift. The arctic waters. In *The Nordic Seas*, pages 129–154. Springer, 1986.
- [39] Tom Sawyer Hopkins. The gin sea—a synthesis of its physical oceanography and literature review 1972–1985. *Earth-Science Reviews*, 30(3-4):175–318, 1991.
- [40] Arild Sundfjord, J Albretsen, Yoshi Kasajima, Ragnheid Skogseth, J Kohler, C Nuth, J Skarðhamar, Finlo Cottier, Frank Nilsen, Lars Asplin, et al. Effects of glacier runoff and wind on surface layer dynamics and atlantic water exchange in kongsfjorden, svalbard; a model study. *Estuarine, Coastal and Shelf Science*, 187:260–272, 2017.
- [41] Sławomir Swerpel. The hornsund fiord: water masses. *Polish Polar Research*, pages 475–496, 1985.
- [42] Francesco De Rovere, Leonardo Langone, Katrin Schroeder, Stefano Miserocchi, Federico Giglio, Stefano Aliani, and Jacopo Chiggiato. Water masses variability in inner kongsfjorden (svalbard) during 2010–2020. *Frontiers in Marine Science*, 9:741075, 2022.
- [43] Ánund Killingtveit, Lars-Evan Pettersson, and Knut Sand. Water balance investigations in svalbard. *Polar Research*, 22(2):161–174, 2003.
- [44] Małgorzata Błaszczuk, Dariusz Ignatiuk, Aleksander Uszczyk, Katarzyna Cielecka-Nowak, Mariusz Grabiec, Jacek A Jania, Mateusz Moskalik, and Waldemar Walczowski. Freshwater input to the arctic fjord hornsund (svalbard). *Polar Research*, 2019.
- [45] Igor V Polyakov, Andrey V Pnyushkov, Matthew B Alkire, Igor M Ashik, Till M Baumann, Eddy C Carmack, Ilona Goszczko, John Guthrie, Vladimir V Ivanov, Torsten Kanzow,

- et al. Greater role for atlantic inflows on sea-ice loss in the eurasian basin of the arctic ocean. *Science*, 356(6335):285–291, 2017.
- [46] Sigrid Lind, Randi B Ingvaldsen, and Tore Furevik. Arctic warming hotspot in the northern barents sea linked to declining sea-ice import. *Nature climate change*, 8(7):634–639, 2018.
- [47] Eirik J Fjørland, Rasmus Benestad, Inger Hanssen-Bauer, Jan Erik Haugen, and Torill Engen Skaugen. Temperature and precipitation development at svalbard 1900–2100. *Advances in meteorology*, 2011(1):893790, 2011.
- [48] Mariusz Grabiec, Dariusz Ignatiuk, Jacek Adam Jania, Mateusz Moskalik, Piotr Głowacki, Małgorzata Błaszczyk, Tomasz Budzik, and Waldemar Walczowski. Coast formation in an arctic area due to glacier surge and retreat: The hornbreen–hambergbreen case from spistbergen. *Earth Surface Processes and Landforms*, 43(2):387–400, 2018.

Chapter 6

The behaviour of fish (*Baltic herring*) with particular emphasis on spatial orientation in various conditions

ALEKSANDER ŻYTKO

Institute of Oceanology, Polish Academy of Sciences,
Powstańców Warszawy 55, 81-712 Sopot, Poland

6.1 Introduction

Biomass measurements, so important for the proper assessment of the ecosystem condition and planning of the fishery management, are carried out using mainly acoustic techniques. These techniques are used because of their undoubted advantages, such as their long range in water, the ability to study a large area at once, and being non-invasive. But, one of the disadvantages of the acoustic methods is their sensitivity to changes in the behaviour of the fish [1–4]. To convert echo signals into useful information on fish biomass, the mean backscattering cross-section or the mean target strength is needed [5–7]. The backscattering cross-section provides a measure to quantify the returning echo intensity after a transmitted acoustic pulse encounters an object and is scattered in the backward direction, while the target strength (TS) is its logarithmic representation [7]. The accuracy of the fish biomass estimation depends therefore on the accuracy of the measured TS value. How individual fish scatters the sound back towards the sonar depends primarily on the morphology of the fish, the sound frequency used (echosounder frequency), the orientation of fish in the water relative to the incident sound wave [8, 9], and also on the depth – the swimbladder changes its volume depending on the pressure [9–11].

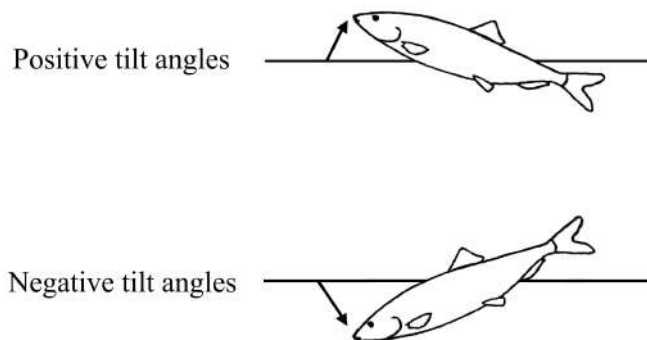


Fig. 6.1: Positive and negative tilt angles.

The tilt angle, which can be defined as the angle between the cent-

ral axis of a fish (imaginary line going through fish from its tail to jaws) and a horizontal line, determines the angle at which an incident acoustic wave hits the fish. Due to the fact that scattering by many fish species is highly directional, the target strength could be described as a function of fish tilt angle [8–10, 12, 13]. The orientation angle of the fish in the school is therefore a very important factor that should be taken into account when estimating their biomass. Here we use a convention that when the fish heads up, its tilt angle is positive, and when it heads down, its tilt angle is negative (Fig. 6.1). The tilt angle distribution of herring depends on their behaviour, which may be a typical pattern related to the time of day and is subject to regular diel/seasonal variations, or may be disturbed by predators or human activities. In particular, the tilt angle distribution of herring will vary between foraging, schooling, and vertical migration [14, 15]. The approach taken in this chapter is to review the recent literature on measuring herring tilt angles, observing its patterns of behaviour, and deviations from them, such as avoidance of vessels, and have a discussion comparing the results and different methodologies.

6.2 Herring swimming patterns and buoyancy

Herring, as a physostomous, are not able to secrete gas into their swimbladders to increase buoyancy, they must take air from the surface [9, 16, 17]. Therefore, since the volume of the bladder changes with depth according to Boyle's law [15, 18, 19], their buoyancy also changes with depth. If the fish stay at a depth for a long time, another factor appears; the gas is lost by diffusion through the water bladder wall and the buoyancy may be reduced even further [9]. At the depths where the herrings remain neutral buoyant there is no need for any special swimming technique and they usually swim horizontally [20]. Close to the surface they may have high positive buoyancy, and to compensate for this they swim with negative tilt angles (head down, see Fig. 6.1). When diving to deeper depths herring can downward glide [15, 20, 21]. To reach the greater depth

(e.g. defense response against predators), herring are known to release gas from swimbladder when descending [22, 23]. Air bubbles releasing changes fish buoyancy and they descend rapidly to greater depths. The changes of buoyancy have to be compensated by the way of swimming – they may increase speed or introduce a correction angle [15, 24]. Since herring is a constant swimmer [15, 24], no herring is observed at a very low swimming speed or hovering. However, observations do not support the expectation that an increase in swimming speed for herring at depths should be observed in order for them to compensate for negative buoyancy [15]. On the contrary, the observed trace velocities were slower at greater depths. Rather than increasing swimming speed, the herring adjusts the tilt angle, as this strategy is energetically advantageous. To maintain a constant depth while being negatively buoyant, herrings also use a technique in which they alternately swim upward with greater speeds (greater than body length per second) and then slowly sink/glide down. This is called the rise and glide technique [15, 21].

In addition to the properties of swimbladders, tissue density is also a factor that influences buoyancy. He & Wardle (1986) [25] conducted a study of mackerel and found the tilt angle to be positively correlated with fish body density. Atlantic herring has a higher body fat content than Baltic herring, which may partially compensate for the negative buoyancy effect at depths (the depth of neutral buoyancy will vary depending on the body fat content of the fish and thus the tissue density) [9, 11]. This may be the reason why the orientation angle distributions would change seasonally [20], which would be associated with a decrease in lipid reserves during the wintering period [1], hence resulting in an increase in fish tissue density.

Main conclusions – herring swimming strategies depends on buoyancy and could be as follows:

- in the neutral buoyancy range, herring will swim more or less horizontally,
- outside the neutral buoyancy range, herring will swim with a correction angle,

- outside the neutral buoyancy range, herring occasionally swim up and then descends (rise and glide technique).

6.3 Diel variation

Let us now discuss how the behaviour of fish changes during the diurnal cycles and how this will affect the orientation of the fish. These changes result from predator avoidance, foraging, and energy conservation strategies [1, 15, 20].

6.3.1 Schooling behaviour during day – impact on fish orientation

A school of fish can be simply defined as a dense group of fish swimming together [26]. Fish can disperse and swim individually, or they can aggregate into interacting groups - for example during feeding and spawning - and some species can swim in large, dense schools during the day time [3]. This type of behaviour is also typical for herring – herring could gather together when the lighting is above a certain level [17]. During the day they could remain at greater depths, concentrated in dense schools. Swimming in schools is considered to be an effective form of underwater movement and is beneficial to individuals. It allows for a greater probability of surviving predator attacks, more effective foraging, hydrodynamic advantages, and easier migration than for a single individual [3, 27]. One of the main reason that herring aggregate in schools during the day in deeper waters is to avoid predators guided mainly by the sense of sight during hunting, mainly cod (*Gadus morhua*), saithe (*Pollachius virens*) and killer whales (*Orcinus orca*) [20]. The more densely packed the fish school is, the more consistent their orientation angles become and the more movements of the fish are coordinated (the standard deviation of the school tilt angle decreases). Different orientation angles only occur at the periphery of the school where the fish density is lower.

6.3.2 Night-time shoaling behaviour – impact on fish orientation

At night, the schools of fish often disperse and spread into looser clusters and layers [3, 15, 17, 20]. Apart from the fact that there are a large number of fish in some area, such groups do not show any coordination between individuals. To distinguish them from schools, Pitcher (1983) [28] proposes that such fish aggregations be termed 'shoals'. When the schools of Norwegian spring-spawning herring disperse into layers and shoals at night, the fish stocking density can drop by two orders of magnitude from an average of about 1-2 fish/ m^3 to 0.02 fish/ m^3 [3]. The behaviour of fish schools is different at night from that during the day as described in the previous subsection. It is because as dusk sets in, the risk of attack by visual predators is lowered. A large portion of fish population then migrates vertically to the upper water layers. The main purpose of this ascent could be to reduce swimming energy consumption and refill swimbladder. Closer to the surface, fish swimbladders are more inflated and have a greater volume, so the fish do not need to spend as much energy to overcome sinking as at greater depths [15]. Additionally, Huse & Korneliussen (2000) [20] observed that for overwintering Atlantic herring towards midnight there was an upward movement of the deeper layers, and then a subsequent slow sinking again until reaching the daytime level at dawn. The function of this ascent during the night was interpreted as energy conservation - one firm upward movement in the middle of the night is energetically more beneficial than frequent alternating upward swimming and gliding [21]. This behaviour may only be unique to overwintering since herring barely feed during this period, and must limit their energy expenditure.

The rise and glide technique used at night will cause herring angles to vary greatly. This can be observed during acoustic measurements where the lower TS values obtained during night could be explained by widening the distribution of angles [20]. Since there is no coordination in shoaling as there is in schooling during the day, the orientation angle distribution will be much wider. An additional factor that may explain the lower TS values recorded at

night is that fish closer to the surface are more susceptible to vessel avoidance [29–31], which may cause tilting as well as swimming out of acoustic detection range. A more detailed discussion of this phenomenon will be provided in the following sections.

6.3.3 Diel vertical migration

During the day, herring swim at deeper depths in tight schools, at night they move closer to the surface and spread into looser layers. In between these two behaviours, there is a transition stage when herring carry out vertical migration at dawn and dusk. The movement of herring schools during the migration impacts on its target strength. In some studies, particularly low TS values were recorded at dusk and partly at dawn [20], which were related to the tilt angles that herring need to maintain during vertical migration. The tilt angles during dawn and dusk migrations may differ from each other, which could be indirectly verified by different TS values in these two periods. The recorded TS minima measured during dawn migrations were less pronounced than the minima measured during dusk migrations due to some of the herring descending to daily depth during the night. This may be due to the fact that the herring does not have to change its spatial orientation as it sinks, it can simply release air from the swimbladder, so the angle distribution may be completely different when herring swim up or descend.

6.4 Diel variation in behaviour – measurements of herring orientation angles

6.4.1 Research methodologies

Measuring the spatial orientation of fish is often very challenging. Acoustic measurement methods, despite their enormous advantages, such as being much less invasive and also providing a much larger sample volume, are more difficult to be implemented and their data are hard to interpret [32, 33]. Therefore, more direct optical methods are used most often.

The method includes lowering the camera into the fish school, along with a reference point against which the orientation angle of the fish can be measured. The problem of such an approach is its limited visibility in seawater and its lighting, so the method can only be performed on a small scale (sample volume and number of observed individual fish). Due to this fact, some measurements were carried out only during the day, with good visibility and at shallow depths [24, 34]. Some of the measurements were carried out with artificial lighting [35], or with far-red light used to minimally disturb the animals (visible light may cause fish to react significantly disrupting the measurements) [36]. Some of the measurements were carried out on natural schools, for example, during herring wintering in Norwegian fjords [15, 20], and some on fish enclosed in artificially built experiment pens [10, 24, 34]. The swimming speed and direction (orientation) of individual herring were meanwhile measured with the target tracking method [15, 24].

6.4.2 Measuring tilt angles – results

This section will discuss the results of experiments carried out to estimate the orientation angles of fish.

Comparison of the parameters of orientation distribution measured in various experiments [14, 15, 24, 34, 35] described in this section is presented in Tab. 6.1. Here $\bar{\gamma}$ – mean value (third column) and S_{γ} – standard deviation (fourth column) of the measured orientation distribution, assuming a Gaussian distribution. A positive value of the angle indicates a head up position of the fish, while a negative value means head down position (Fig. 6.1). The second column contains references to the source publications, and the last one contains comments about the conditions of the experiment.

Tab. 6.1: Synthetic comparison of herring orientation angles measured in various experiments.

Reference	$\bar{\gamma}$ [°]	S_γ [°]	Remarks
Radakov <i>et al.</i> , 1959 [35]	app. 0	-	visual observation from the submarine at a depth of 80-100 m
Beltestad, 1973 [14]	3.8	6.0	for herring individuals observed during the day
	0.2	11.9	for herring individuals observed during the night
	-3.9	12.8	for 1819 individuals of herring at a depth of 1.5 m
Ona, 1984 [34]	-3.2	13.6	for 898 individuals of herring at a depth of 4 m
	0.2	11.9	for for 874 individuals of herring at a depth of 30 m
	0	10	for aggregation of herring at night at 62 m
Ona <i>et al.</i> , 1996 [15]	-10.0	5.0	for aggregation of herring at day at 200-260 m
	40.0	10.0	for aggregation of herring at night at depths of 330-360 m
	30.0/-30.0	-	bimodal distribution with both positive and negative modes, daytime at depths of 330-360 m
Ona, 2001 [24]	-1.1	10.0	for a single adult herring observed for 30 h in a pen close to the surface
	-3.1	14.2	for 943 herring individuals in the pen at depths up to 30 m

The first attempts to estimate the orientation angle of herring by direct observation were made by Radakov and Solovjev (1959) [35] (first row in Tab. 6.1), who visited the wintering areas of Norwegian spring-spawning herring in a submarine. The herring were observed both visually in artificial light and acoustically with an echo sounder. It was observed that at a depth of 80–100 m, angles of orientation were mostly horizontal in the evening, but with a predominant negative tilt around dawn. The depths of these observations were not accurately recorded, ranging from 80 to 100 meters. If this observation is correct, it could mean that the herring at this depth had neutral buoyancy, which is contradicted by later meas-

urements [15]. No other later experiment obtained similar results, however, their results are questionable due to their use of artificial light. Betelstad (1973) [14] (second row in Tab. 6.1) investigated the dependence of angle distributions on fish behaviour, in particular the feeding at night and schooling during the day. Photographically, it has been estimated that the probability density function (PDF) had a mean daytime tilt angle of 3.8° , with standard deviation of 6.0° . For herring individuals observed during the night it was -3.2° of the mean with 13.6° standard deviation. The next experiments were carried out in pens and artificial reservoirs. Ona (1984) [34] (third row in Tab. 6.1) conducted optical measurements during the day in net pens with a volume of 100 m³, placed in a fjord. In a net pen approximately 6-7 fish / m³ was placed, at several adaptation depths. Although some extreme orientation angles of up to 50 degrees were observed, the mean orientation angle of fish swimming close to the surface was close to a level with a slightly negative mean value. His photographic measurements showed that for herring at depths of 1.5 and 4 m, the tilt angle distributions were -3.9° (S.D. = 12.8°) and 0.2° (S.D. = 11.9°), respectively. He also noticed that at a depth of about 30 meters, the herring clearly acquired negative buoyancy, and began to swim at a higher speed and inclined at a certain angle (the head was up in relation to the tail, see Fig 6.1). This was reflected in the frequency distribution of the tilt angle – then the herring’s mean orientation angle was 6 to 11 degrees, heads up. Ona (1984) [34] conducted research only to a depth of 30 meters because this was depth sunlight reached, allowing observations using the optical method (with no artificial light necessary), therefore data from greater depths cannot be compared. However, even from measurements at a depth of 30 meters, it was concluded that the herring had a negative buoyancy at greater depths and that positive orientation angles should be expected to compensate for it [34]. Huse & Ona (1996) [15] (fourth row in Tab. 6.1) conducted research in which a frame with a sonar transducer and camera connected with cables was lowered into the herring schools, while the research vessel was drifting. He observed the impact of buoyancy on fish orientation: orientation angles close to the horizontal were recorded at shallow depths, and a change in the tilt angle

was noticeable when the herring achieved negative buoyancy while descending. At great depths (330 m) at night, large angles, up to 40 degrees, with the head upwards were recorded. The following values can be read from figures 2 and 3 of Huse (1996) [15]: at night at 62 meters, average tilt angle was 0° , and during the day at a depth of 200-260 m, average tilt angle was -10° . At greater depths, in the order of 330-360 meters mean tilt angle was 40° at night, while a bimodal distribution with both positive and negative mode during the day. Ona (2001) [24] (fifth row in Tab. 6.1) observed that while the mean values of the tilt angles at 20, 25, 30, and 40 m were close to zero or slightly head-up, near the surface (at a depth of 5 m) there was a slightly negative average head-down posture, -1.61° . The herring thus compensated for the positive buoyancy caused by the slight compression of the swim bladders. The angles were also close to the level, head up by day, head down at night (Fig. 6.1). Ona (2001) [24] observed an individual adult herring that was swimming freely in the experimental pen for a period of 30 hours. The target tracking method, combined with additional optical (camera) observations, was used. The camera determined the angle of their orientation, and the transducer following their movements was lowered into the school for better resolution (the degree of accuracy in estimating the herring swimming angle depends on the resolving power). Measurements were carried out with no artificial lights – natural light conditions only.

The herring, swimming mainly at shallow depths in the pen, passed through the transducer beam at a mean angle that was almost horizontal (-1.1° and -0.7°) with a standard deviation of about 10° . These distribution parameters are similar to the photographically estimated distributions of the herring tilt angle under similar conditions. The resultant estimated average swimming speed of herring was 35 cm per second or about 1.1 body lengths per second.

Ona (2001) [24] investigated the difference between the swimming angle of an individual fish and the actual orientation angle comparing results of the target tracking method and optical one.

Comparison of data from 5 depth intervals, from 5 to 40 m, showed that the herring generally swam straight with respect to its body

axis, and the difference between the actual tilt angle and the swimming angle was small at all depths [24]. However, the data were analysed only up to a depth of 40 m, and at greater depths this difference may increase.

6.5 Disturbances in fish behaviour

6.5.1 Predator avoidance behaviour

Having an open swimbladder for herring has the advantage of being able to perform rapid vertical movements in response to predation [37]. Nottestad (1998) [23] studied the behaviour of the school when interacting with predators, with an emphasis on releasing gas bubbles when changing depth. In his study the ship was constantly hovering over the target herring school that was observed with a down-looking sonar, looking for a predator to attack the fish school. When the predator attacked, the herring from the school released some of the air from their swimbladders. This was visible on the sonar and a foam formation was observed on the surface. The release of the gas made the herring school a sudden downward movement and in all cases ended the predator-prey interaction [23].

Fast downward swimming appears to be a common and effective response against predators in schools of herring [37]. In addition, the active release of gas from their swimbladders can be an effective contributor to avoiding predators by scattering light and thus reducing the range of vision of predators, especially near the surface during the day. It has also been suggested that gas bubbles can confuse orcas biological sonar by scattering sound [38].

6.5.2 Vessel avoidance

The mere presence of a research vessel may cause a reaction among the fish that disrupts their measurement. Three factors can influence fish behaviour: vessel lighting, vessel noise, and the hydrodynamic pressure field generated by the vessel. We will consider the influence of these factors in turn. A vessel-induced fish reaction can be defined simply as a change in behaviour in response to the

approach of a moving survey vessel [4]. Changing behaviour most often involves trying to move away from the source of the stimulus. Common reactions are escaping to the deeper water or sideways and changes in the distribution of tilt angles in the school [2, 7]. Ship avoidance can be interpreted as predator avoidance behaviour [39]. Fish are known to be attracted to or avoid light and visual stimuli from ships [40], but visual stimuli are unlikely to cause a long-range response, especially during the day [3, 4]. The underwater sound emitted by vessels is believed to be the most likely trigger for a long-range response, as ships generate high levels of noise in the fish hearing frequency range that propagates fast and far away from the vessel [2, 31, 41]. However, it does not have to be the only factor [42]. Olsen *et al.* (1982) [41] proposed a model that described vessel avoidance behaviour as a function of the pressure gradient of the propeller noise. The extent of the vessel avoidance reaction was strongly dependent on the depth at which the fish were staying. The biggest change in the behaviour of fish is when they are close to the surface [29, 39, 41]. When the herring is in the depths (>250 m) the reaction is not noticeable every time [43]. The effect also varied depending on the time of day and was much more pronounced at night, but this is most likely related to the depth of the fish. Vabø *et al.* (2002) [39] stated that the effect of avoidance reactions for herring faded out below 100 m, and was not observed below 150 m at night. The absence of avoidance reaction during the day could be explained with the fact that during the day the main part of the biomass was distributed below 150 m. However, Olsen *et al.* (1983) [29] stated that the reaction of the fish was similar both during the day and at night, based on measurements for various species of fish, including those that did not migrate. Despite the different conditions, all species reacted by changing behaviour in response to the ship's approach. The greatest reaction – polar cod – was observed up to 150 m from the ship [29]. Mitson & Knudsen (2003) [31] also studied the reactions of fish to the approaching vessel to assess the responsible factors for disturbing the fish. They showed that avoidance behaviour by a herring school was shown to result from a noisy vessel, by contrast, there was an example of no reaction of herring to a noise-reduced vessel. Their observations

of echo energy from schools were made from a downward-looking echo sounder transducer submerged at 12 m when the survey vessel approached and passed it at close range. In opposition to this, Ona *et al.* (2007) [42] studied how the reaction of fish changes depending on the 'quiet class' of the research vessel. It turned out that silent research vessels using modern solutions to suppress noise pollution generated a significant response in the school anyway. The behaviour of herring was stimulated by two research vessels: designed with and without reduced radiated noise standards. Both ships generated a reaction pattern, but contrary to expectations, the response initiated by the silent ship was not weaker, but sometimes even stronger and longer than that triggered by a conventional noisy ship. A similar experiment was carried out by De Robertis & Wilson (2010) [44]. Their results indicate that the reaction of the fish to the noise-reduced vessel is weaker than the reaction to the conventionally constructed vessel, but still clearly visible.

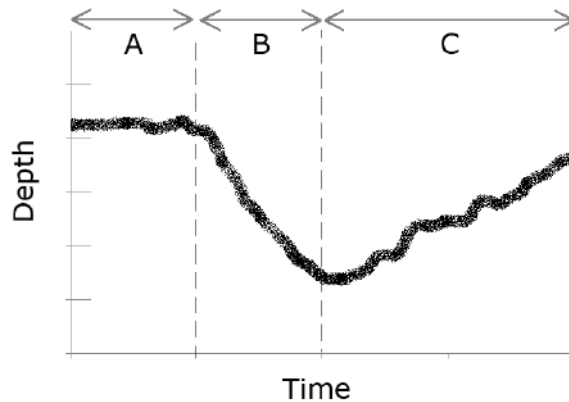


Fig. 6.2: Schematic echogram of the reaction of fish to a passing vessel. The black line is the median depth distribution of the fish school. One can distinguish three phases: undisturbed swimming (A), avoidance reaction (B), recovery (C).

A schematic representation of the record of the herring's reaction to the incoming ship is shown in Fig. 6.2. The fish remain at their natural habitat depth (A) until a stimulus from the approaching

vessel reaches them (B). They then begin their escape until the ship is exactly above them and passes them. After the vessel passed by, the school returns to the setting of the original undisturbed depth (C).

The extent of the vessel avoidance reaction was strongly dependent on the depth at which the fish were staying. The biggest change in the behaviour of fish was when they were close to the surface [29, 39, 41]. When the herring were at the deeper depths (>250 m) the reaction is not noticeable every time [43]. The effect also varied depending on the time of day and was much more pronounced at night, which was most likely related to the depth of the fish. Vabøet *et al.* (2002) [39] stated that the effect of avoidance reactions for herring faded out below 100 m, and was not observed below 150 m at night. The absence of avoidance reaction during the day could be explained by the fact that during the day the main part of the biomass was distributed below 150 m.

6.6 Vessel avoidance – measurements of herring orientation angles

6.6.1 Research methodologies

The vessel avoidance research requires the acoustic transducer to be mounted outside the surveying vessel causing the studied response. The experiments were conducted in various configurations:

- a submerged and stationary transducer the oncoming ship passed exactly over it. During the passage of the vessel, the change of echo from the fish under the transducer was examined [29],
- a smaller vessel equipped with an echosounder placed in the path of the surveying vessel [39],
- a bottom-moored, upward-looking echosounder: the research vessel passed over [42].

The transducer depths from the experiments described here ranged from 10 to 137 m [43].

6.6.2 Measuring tilt angles – results

This section will discuss the orientation angles of fish received as a result of observing fish vessel avoidance behaviour. Some of the orientation parameters were estimated because not all of the described experiments focused on obtaining exact tilt angle values.

Tab. 6.2 presents a comparison of the parameters of orientation distribution measured during vessel avoidance in various experiments [29, 31, 43]. Similar to Tab. 6.1, $\bar{\gamma}$ – mean value (third column) and S_γ – standard deviation (fourth column) of the measured orientation distribution assuming Gaussian distribution. The second column contains references of the sources, and the last one contains comments about the conditions of the experiment.

Tab. 6.2: Synthetic comparison of herring orientation angles measured in various vessel avoidance experiments.

Reference	$\bar{\gamma}$ [°]	S_γ [°]	Remarks
Olsen <i>et al.</i> , 1983 [29]	-27.5	5.0	for the herring individuals observed at a depth of 40 - 50 m during their reaction response to a passing vessel
Mitson <i>et al.</i> , 2003 [31]	-15	-	estimated value from Fig 6 [31] for the herring individuals observed at a depth of 60 - 75 m during their reaction in response to a passing vessel
Hjellvik <i>et al.</i> , 2008 [43]	-20	-	estimated value from Fig 2 [43] for the herring individuals observed at a depth of 200 - 250 m during their reaction in response to a passing vessel

Tilt angle measurements of herring individuals observed at a depth of 40-50 m during their response to a passing vessel by Olsen *et al.* (1983) [29] (first row in Tab. 6.2), resulted in a mean tilt angle of 27.5° with a standard deviation of 5.0°. Most of the experiments were not focused on tilt angle measurements. However, from the echograms showing the reaction of the fish and knowing the swimming speed of the fish, it was possible to estimate the angle at which the fish fled down (the angle at which the center of gravity of the school moved), as in the target tracking method. Thus, based on

Fig. 6 of Mitson & Knudsen (2003) [31], which showed the change in mean depth of the recorded echo energy due to the passage research vessel, the average speed of the herring escape into the deep could be estimated. The center of gravity of the school sank approximately 15 m per minute, which resulted in a vertical component of the velocity vector approximately 0.25 m/s. Assuming that the maximum speed of the herring was approximately 1 m/s [45], the calculated minimum angle of escape of the herring into the depths was about 15° (second row in Tab. 6.2). The tilt angle could be greater if the herring were escaping at a slower speed. Performing analogous calculations based on Fig. 2 of Hjellvik *et al.* (2008) [43], which showed example echograms from the echosounder when a vessel passed by, the minimum value of the tilt angle was approximately 20° (third row in Tab. 6.2). It can be seen that the values given in Tab. 6.2 are significantly larger than those shown in Tab. 6.1.

6.7 Discussion

Behaviour of fish is a very important factor that can affect the accuracy of the TS measurements in various ways, where orientation and depth of fish have significant impact on the TS. Target Strength is a conversion factor that converts a hydroacoustic quantity to a biological quantity, i.e. number of fish. Therefore, the sensitivity of the TS to fish orientation can provide the knowledge of fish orientation and is critical for a reliable fish abundance/biomass estimation.

6.7.1 Comparison of various methodologies for measuring fish orientation

The experiments described in this chapter dealt with different aspects of herring behaviour and fish orientation were performed under different conditions. Some of the measurements on orientation of individuals were carried out in net pens (*ex situ* measurements) and in herrings' natural environment (*in situ* research). Both methods have their own advantages and disadvantages.

***Ex situ* measurements**

Cage fish experiments are much easier to perform than fish orientation measurements in natural marine conditions but lead to uncertainty as to whether the behaviour of caged fish can ever be the same as that of wild fish [10]. Even when there are more fish in the cage, they have no room for their natural behaviour - experiments with caged fish place a small population of fish in an alien environment. They are forced to swim in a relatively small volume of water at a certain depth. These conditions cannot be considered natural, and whether fish will ever adopt truly natural patterns of behaviour in a small experimental cage is debatable [10]. Such measurements provide reliable results only for the physiognomy of the bladder, buoyancy, and changes in target strength and allow us to understand the swimming physics of herring, which is believed to be the same regardless of the circumstances, but on their basis, it is not possible to conclude about the behaviour of fish in their natural environments, such as diurnal cycles and larger vertical migration distance, etc.

***In situ* measurements**

Only *in situ* research allows us to study the actual behaviour of fish in their natural environments. Moreover such research enables fish behaviour observations and fish orientation measurements to be performed at depths spanning much larger depth range as compared to those performed in net pens. On the other hand, these measurements are very susceptible to disturbances in the form of fish avoidance of vessels which should be taken into account when designing the experiment. To avoid vessel avoidance reaction, measurements should be carried out from the ship in a drift or through a measuring buoy suspended in the water column.

Impact of vessel avoidance

One of the important questions regarding the fish orientation measurements is: how accurately can the real herring tilt angles be measured experimentally?

Fish have the largest tilt angles when they escape from a vessel (up to 27.5° , recorded by Olsen, 1983 [29]). The estimated fish orientations due to vessel avoidance are presented in Tab. 6.2 and confirm this thesis. However, these are by no means the angles at which the undisturbed herring would swim naturally. Something similar to the uncertainty principle appears here, where the very act of measuring disturbs the state of the system (at least for the fish schools at shallow depths). Therefore, it is challenging to develop a reliable method for measuring the spatial orientation of a fish in its natural environment. The matter is even more complicated by the fact that there is no understanding of the reasons for vessel avoidance by fish. Mitson and Knudsen (2003) [31] argued that it was merely due to the vessel-induced noise and could be effectively overcome by using a noise-reduced vessels. However, experiments conducted by Ona (2007) *et al.* [42] and De Robertis and Wilson (2010) [44] indicated that even ships meeting the modern noise standards could still induce unexpected fish responses, so the use of such technologies could not completely solve the problem completely. As the vessel avoidance reaction only diminishes at depths deeper than 100 meters [39], it should be regularly taken into account while interpreting results from shallow waters (for example in the Baltic Sea) where the depth does not often exceed 100 m. However, in hydroacoustic biomass estimation, general information about the "natural" angle distribution of herring may not be necessary. Fish orientation distribution estimated directly at the time of measurement should be sufficient even if it is contaminated by the vessel avoidance. Information about the actual fish tilt angle could be introduced for an appropriate correction to fish biomass estimates.

6.7.2 Fish orientation and their behaviour – comparison

In this subsection we would like to summarize the results of herring orientation measurements on their natural behaviour, described earlier in this chapter. The experiments complement each other and result in a consistent picture.

Ex situ experiments have shown the behaviour and the swimming patterns of fish at shallow depths. It is the case where *in situ* measurements would not be easily made due to vessel avoidance. *In situ* measurements confirmed the diurnal changes in the behaviour. The main conclusion is that fish behaviour and fish orientation angles are dependent on lighting and buoyancy, including the followings:

- Herrings swim horizontally when their buoyancy is close to neutral, in shallow depths (0 to at least 60 m) regardless of time of the day (second and third rows in Tab. 6.1).
- At medium depths (around 100-200 m), where there seems to be enough light in the middle of the day for schooling, herring float horizontally during the period with sufficient lighting, and at lower light levels (at night) they swim with an upward tilt or alternating between swimming up and gliding down (fourth row in Tab. 6.1).
- In deep waters (300-400 m), where even daytime lighting does not seem to be sufficient for schooling, herring either swims with positive tilt angles or alternately swim up and glide down (fourth row in Tab. 6.1).
- At night, in loose herring aggregations different tilt angles occur for maneuvering and maintaining appropriate depths. It is expressed in a much larger standard deviation of the tilt angle distribution than when fish are schooling (second row in Tab. 6.1). The tilt angle distributions of fish in schools are narrower than those obtained for loose aggregations.
- Herring do not have to change their angle of orientation to descend deeper, it is enough for them to release air from the bladder. This can be seen during the dawn migration. When there is a need for a sudden change of depth (running away from a predator or a source of noise), they change their swimming angle by mowing quickly, and by releasing gas to provide an additional acceleration for descending.

In summary, differences in buoyancy at different depths can affect the width (standard deviation) of tilt angle distribution. When fish are neutral buoyant they will all likely swim horizontally, but when

they are negative buoyant there are several methods to compensate for this and hence may react differently.

Two reported results (first and fourth rows in Tab. 6.1) have different patterns than those summarized above: observations of Radakov and Solovjev (1959) [35] and Huse (1996) [15]. Radakov and Solovjev (1959) demonstrated that herring at depth of 100 meters had neutral buoyancy, which contradicted the later measurements. The odd tilt angle of about -10 degrees for herring, was observed during the day at a depth of 200 m by Huse (1996). This angle is unusual for herring schools at such a depth. Other measurements demonstrated positive orientation angles [15, 34]. A plausible explanation of such observations could be that it was the school's response to a predator or other unidentified sources of disturbances.

As mentioned in this chapter, fish behaviour could have a dramatic impact on acoustic abundance estimates. The target strength of fish is strongly influenced by the orientation of the fish and their behaviour. Currently, this variability has not been taken into account in conventional acoustic research and fish abundance/biomass estimates.

Acknowledgement

Author would like to thank his supervisors, Natalia Gorska from Institute of Oceanology PAS, and Dezhang Chu from NOAA, USA, for help with the preparation of the manuscript, first reviews and all support.

Bibliography

- [1] I. Røttingen, K. G. Foote, I. Huse, and E. Ona. Acoustic abundance estimation of wintering norwegian spring spawning herring, with emphasis on methodological aspects. ICES, 1994.
- [2] R.B. Mitson. Underwater noise of research vessels: review and recommendations. *ICES Cooperative Research Report*, 209 pp. 61, 1995.
- [3] Fréon P. and Misund O. A. *Dynamics of pelagic fish distribution and behaviour: effects on fisheries and stock assessment*. Fishing News Books. Blackwell Science, Oxford, 1999.
- [4] A. De Robertis and N. O. Handegard. Fish avoidance of research vessels and the efficacy of noise-reduced vessels: a review. *ICES Journal of Marine Science*, 70(1):34–45, 2013.
- [5] P. Degnbol, H. Lassen, and K.J. Staehr. In-situ determination of target strength of herring and sprat at 38 and 120 khz. *Dana*, 5:45–54, 1985.
- [6] T. Didrikas and S. Hansson. In situ target strength of the baltic sea herring and sprat. *ICES Journal of Marine Science*, 61(3):378–382, 2004.
- [7] J. Simmonds and D.N. MacLennan. *Fisheries Acoustics: Theory and Practice*. 2nd Ed. Blackwell Publishing, London, 2005.
- [8] O. Nakken and K. Olsen. Target strength measurements of fish. *Rapports et Proces-Verbaux des Reunions*, 70:52–69, 1977.

- [9] Blaxter J.H.S. and Batty R.S. Swimbladder "behaviour" and target strength. *Rapports et Proces-verbaux des Reunions du Conseil International pour l'Exploration de la Mer*, 189:233–244, 1990.
- [10] J.I. Edwards, F. Armstrong, A.E. Magurran, and T.J. Pitcher. Herring, mackerel and sprat target strength experiments with behavioural observations. ICES CM 1984. Technical report, B:34, 1984.
- [11] Egil Ona. In situ observations of swimbladder compression in herring. ICES, 1984.
- [12] K. Olsen. Orientation measurements of cod in Lofoten ofoten obtained from underwater photographs and their relation to target strength. ICES C.M.1971/ B:17. 8 pp., 1971.
- [13] K. G. Foote. Effect of fish behaviour on echo energy: the need for measurements of orientation distributions1. *ICES Journal of Marine Science*, 39(2):193–201, 1980.
- [14] A. K Beltestad. Feeding behaviour and vertical migration in 0-group herring (*Clupea harengus L.*) in relation to light intensity. *Candidata realium thesis, University of Bergen, Norway (in Norwegian).*, 1973.
- [15] I. Huse and E. Ona. Tilt angle distribution and swimming speed of overwintering Norwegian Spring spawning Herring. *ICES Journal of Marine Science*, 53:863–873, 1996.
- [16] G. Fahlen. Morphological aspects on the hydrostatic function of the gas bladder of clupea harengus l. *Acta Univ. Lund*, II:1–49, 1967.
- [17] J. H. S. Blaxter and Hunter J. R. S. The biology of the clupeoid fishes. *Advances in Marine Biology*, 20:1–223, 1982.
- [18] N. Gorska and E. Ona. Modelling the effect of swimbladder compression on the acoustic backscattering from herring at normal or near-normal dorsal incidences. *ICES Journal of Marine Science*, 60(6):1381–1391, 2003.

- [19] S. M. M. Fässler, P. G. Fernandes, S. I. K. Semple, and A. S. Brierley. Depth-dependent swimbladder compression in herring *clupea harengus* observed using magnetic resonance imaging. *Journal of Fish Biology*, 74(1):296–303, 2009.
- [20] I. Huse and R. Korneliussen. Diel variation in acoustic density measurements of overwintering herring (*Clupea harengus* L.). *ICES Journal of Marine Science*, 57(4):903–910, 2000.
- [21] D. Weihs. Mechanically efficient swimming techniques for fish with negative buoyancy. *Journal of Marine Research*, 31:194–209, 1973.
- [22] R. E. Thorne and G. L. Thomas. Acoustic observations of gas bubble release by pacific herring (*clupea harengus pallasi*). *Canadian Journal of Fisheries and Aquatic Sciences*, 47(10):1920–1928, 1990.
- [23] L. Nøttestad. Extensive gas bubble release in Norwegian spring-spawning herring (*Clupea harengus*) during predator avoidance. *ICES Journal of Marine Science*, 55(6):1133–1140, 1998.
- [24] E. Ona. Herring tilt angles, measured through target tracking. *Herring: Expectations for a New Millennium*, pages 509–519, 2001.
- [25] P. He and C. Wardle. Tilting behavior of the atlantic mackerel, *scomber scombrus*, at low swimming speeds. *Journal of Fish Biology*, 29:223 – 232, 1986.
- [26] D. V. Radakov. *Schooling in the Ecology of Fish*. John Wiley and Sons; New York, 1973.
- [27] T.J. Pitcher. *Functions of Shoaling Behaviour in Teleosts*, pages 294–337. Croom Helm, London and Sydney, 1986.
- [28] T. J Pitcher. Heuristic definitions of fish shoaling behaviour. *Animal Behaviour*, 31(2):611–613, 1983.

- [29] K. Olsen, J. Angel, F. Pettersen, A. Løvik, O. Nakken, S.C. Venema, et al. Observed fish reactions to a surveying vessel with special reference to herring, cod, capelin and polar cod. *FAO Fisheries Report*, 300:131–138, 1983.
- [30] K. Olsen. Fish behaviour and acoustic sampling. *Rapports et Procès-verbaux des Réunions du Conseil International pour l'Exploration de la Mer*, 189:147–158, 1990.
- [31] R. B. Mitson and H. P. Knudsen. Causes and effects of underwater noise on fish abundance estimation. *Aquatic Living Resources*, 16(3):255–263, 2003.
- [32] T. Stanton, D. Reeder, and J. Jech. Inference of fish orientation from broadband acoustic echoes. *Ices Journal of Marine Science*, 60:524–531, 2003.
- [33] J. Jaffe and P. Roberts. Estimating fish orientation from broadband, limited-angle, multiview, acoustic reflections. *The Journal of the Acoustical Society of America*, 129:670–80, 2011.
- [34] E. Ona. Tilt angle measurements on herring. ICES C.M. 1984/B:19, 1984.
- [35] P.V. Radakov and B.S. Solovjev. The first experiences with the use of a submarine for observation of the behaviour of herring. *Rybnoe chozjajstvo*, 7:16–21, 1959.
- [36] Misund O.A. Beltestad, A.K. Behaviour of norwegian spring spawning herring in relation to underwater light. Technical report, ICES FTFB Working Group 1988/04/18-19, Ostende., 1988.
- [37] J. H. S. Blaxter. The herring: A successful species? *Canadian Journal of Fisheries and Aquatic Sciences*, 42:21–30, 1985.
- [38] L.G. Barrett-Lennard, J.K.B. Ford, and K.A. Heise. The mixed blessing of echolocation: differences in sonar use by fish-eating and mammal-eating killer whales. *Animal behaviour*, 51(3):553–565, 1996.

- [39] R. Vabø, K. Olsen, and I. Huse. The effect of vessel avoidance of wintering norwegian spring spawning herring. *Fisheries Research*, 58:59–77, 2002.
- [40] J. J. Lévénez, F. Gerlotto, and D. Petit. Reaction of tropical coastal pelagic species to artificial lighting and implications for the assessment of abundance by echo integration. *Rapports et Proces-Verbaux des Réunions du Conseil International pour l'Exploration de la Mer*, 189:128–134, 1990.
- [41] K. Olsen. Quantitative estimations of the influence of fish behaviour on acoustically determined fish abundance. *FAO Fish. Rep.*, 300:139–149, 1982.
- [42] E. Ona, O. R. Godø, N. O. Handegard, V. Hjellvik, R. Patel, and G. Pedersen. Silent research vessels are not quiet. *The Journal of the Acoustical Society of America*, 121(4):145–150, 2007.
- [43] V. Hjellvik, N. O. Handegard, and E. Ona. Correcting for vessel avoidance in acoustic-abundance estimates for herring. *ICES Journal of Marine Science*, 65:1036–1045, 2008.
- [44] A. De Robertis and C. D. Wilson. Silent ships sometimes do encounter more fish. 2. Concurrent echosounder observations from a free-drifting buoy and vessels. *ICES Journal of Marine Science*, 67(5):996–1003, 2010.
- [45] H. C. Boyar. Swimming speed of immature atlantic herring with reference to the Passamaquoddy Tidal Project. *Transactions of The American Fisheries Society*, 90:21–26, 1961.